IRE Transactions

on Microwave Theory and Techniques

Volume MTT-5 JANUARY, 1957 Number 1

In This Issue

For complete Table of Contents, see page 1.

PUBLISHED BY THE
Professional Group on Microwave Theory and Techniques

IRE TRANSACTIONS®

on Microwave Theory and Techniques

Published by the Institute of Radio Engineers, Inc., for the Professional Group on Microwave Theory and Techniques, at 1 East 79th Street, New York 21, New York. Responsibility for the contents rests upon the authors, and not upon the IRE, the Group, or its members. Price per copy: IRE PGMTT members, $1.75; IRE members, $2.60; nonmembers, $5.25. Annual subscription price: IRE members, $8.50; colleges and public libraries, $12.75; nonmembers, $17.00.

Address all manuscripts to Kiyo Tomiyasu, General Electric Company, Palo Alto, Calif.

IRE Transactions on Microwave Theory and Techniques

Published by the Professional Group on Microwave Theory and Techniques

Volume MTT-5 JANUARY, 1957 Number 1

TABLE OF CONTENTS

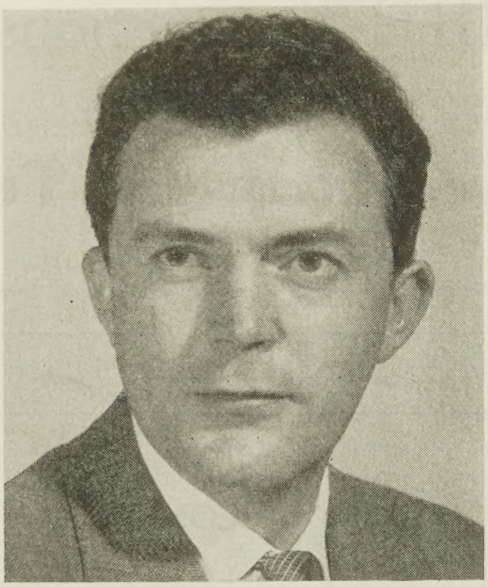

J. R. Whinnery

John R. Whinnery was born on July 26, 1916 in Read, Colo. He received the B.S. degree in electrical engineering from the University of California in 1937, and immediately went to work for the General Electric Company in Schenectady, N. Y.

At the General Electric Company, Mr. Whinnery entered the three-year Advanced Engineering Program, and following that, supervised the high-frequency part of that program for two years. He then worked in the Electronics Laboratory and the Research Laboratory on problems in velocity-modulation tubes, traveling-wave tubes, and disk-seal triodes. In 1945–1946 he was also part-time lecturer in Union College.

In 1946, Mr. Whinnery returned to the University of California to teach electrical engineering and to complete work on his Ph.D. degree. He is now professor of electrical engineering there and chairman of the Electrical Engineering Division. During summer periods he has worked at Stanford University, the Hughes Aircraft Company, and the Ramo-Wooldridge Corporation, and during an industrial leave in 1951–1952 he was head of the Microwave Section of the Hughes Electron Tube Laboratory.

Mr. Whinnery is co-author with Simon Ramo of the text "Fields and Waves in Modern Radio," and is also author of several journal papers on waveguide discontinuities, antenna problems, and microwave tubes.

Mr. Whinnery became an associate member of the IRE in 1941, a senior member in 1944, and received the Fellow award in 1952. He held offices in the San Francisco Section from 1948 to 1954, becoming chairman in 1953, and has been active in WESCON and on many national IRE committees. He is now a director-at-large of the IRE.

The Next Problem in Engineering Education

JOHN R. WHINNERY
University of California, Berkeley, California

We have read very much in the past few years of the need for more engineers, so I shall not repeat the arguments here. Many of you have taken part in the very excellent programs designed to acquaint high school students with the opportunities in an engineering career, and I should first like to point out how successful these programs have been. This fact, I believe, is not generally realized. To use our own school as an example, enrollments during the past two years for the university as a whole have risen about 14 per cent, using the same standards of admitting only those among the upper 15 per cent of high school graduates. This rise reflects very nearly the increased birth rate at the end of the depression and the population growth of this area. During this same period, enrollment in engineering has increased about 50 per cent, and in electrical engineering 80 per cent. Although we do not break down the fields of interest further in the early undergraduate years, I believe the proportion of those interested in the microwave field is remaining nearly constant in spite of the competition from several newer fields.

Now that there is success in this first step of stimulating interest in engineering among new students, we must pass to the next one and ask, "What do we do with them?"

All who have thought about the problem know that we must be concerned with quality as much or more than quantity. If we start to measure our success by the number of engineering degrees compared with some carefully estimated quota, or with those from a competitor in the cold war, we are lost.

Our technology continues to become more complicated, and it is recognized that the quality and level of instruction must be improved. However, there exist many pressures toward downgrading, for as numbers of entrants increase, the difficulties of keeping a first-quality staff in the face of the fierce industrial competition also increase. This is of course not the fault of the industries, for they only recognize a real situation. Strictly speaking, it is up to the universities also to recognize it, even though it is difficult within the relatively inelastic educational budgets. The problem has been solved in a few schools, but I believe it is correct to say that in a majority of them, including many of the fine small ones, it is getting worse.

Both government and industry now help the universities in a very large way through sponsored research programs, fellowships, grants-in-aid, and cooperative programs. Many, in recognizing the seriousness of the problem, have felt that government and industry as a whole should do something more drastic, on a larger scale, and at once. If such emergency steps are taken, they must be taken with great wisdom so that the "shock wave" does not destroy the system it is planned to save. In any event the seriousness of the problem should be recognized and all possible solutions debated. We in schools will in the meantime need the continued support and advice from our friends in government and industry.

Broad-Band Balanced Duplexers*

CLARENCE W. JONES†

Summary—Balanced duplexer circuits are described and a comparison is made between the two principal configurations employing gaseous switching devices. The balanced tr duplexer is limited in power-handling ability, while the balanced atr duplexer has slightly greater received-signal insertion loss. An analysis is made of the reflecting properties of an atr array, and the practical upper limit of the number of array elements is determined.

A DUPLEXER, in the language of radar, is a switching device which disconnects the transmitter from the receiver, usually by means of gaseous discharge tubes called tr's and atr's. There are at least three principal types of duplexers, each of which may have several variations dependent upon the specific application, power level to be handled, or bandwidth required. These types are: 1) branching duplexer, 2) polarization-twist duplexer, and 3) balanced duplexer. This classification does not cover all of the possible configurations of duplexers which employ gaseous discharge switches, nor does it include the duplexers employing ferrite-switching elements, although a large percentage of these ferrite devices could be included under categories 2) and 3).

The bandwidth of a duplexer is determined by both the bandwidths of the switching tubes, tr's and atr's, and the circuit configuration. The branching duplexer is the simplest configuration but is not inherently broad band. Its performance near the band edges is greatly influenced by the transmitter impedance. Both the polarization-twist and the balanced-duplexer characteristics are unaffected by the transmitter impedance within the useful pass band. The balanced duplexer is inherently capable of the greatest bandwidth, in principle being limited only by the waveguide bandwidth.

Balanced duplexers can take on many physical shapes. They may be built in coaxial line with ring hybrids or quarter-wave coaxial hybrids,[1] in slab line using circuits equivalent to the coaxial circuits, or in waveguide with ring hybrids,[2] directional couplers, or magic tees.[2] The switching circuits may employ either narrow-band or broad-band tr and atr elements of waveguide or coaxial construction. It is also possible to mix the waveguide and coaxial construction if this has an advantage in a particular application.

* Original manuscript received by the PGMTT, April 2, 1956. The research in this document was supported jointly by the U. S. Army, Navy, and Air Force under contract with Mass. Inst. Tech., Cambridge, Mass.

† Lincoln Lab., M.I.T., Lexington, Mass.

[1] C. G. Montgomery, R. H. Dicke, and E. M. Purcell, M.I.T. Rad. Lab. Ser., McGraw-Hill Book Co., Inc., New York, N. Y., vol. 8, ch. 12, 1948.

[2] L. D. Smullin and C. G. Montgomery, "Microwave Duplexers," M.I.T. Rad. Lab. Ser., McGraw-Hill Book Co., Inc., New York, N. Y., vol. 14, ch. 8, 1948.

It is the purpose of this paper to analyze the operation of balanced duplexers, in particular the configurations employing directional coupler hybrid junctions. The analysis is best carried out through use of the scattering matrix.

Scattering Matrix Representation of Microwave Circuits

The scattering matrix representation[3] lends itself admirably to a large number of microwave problems, and will be used here in so far as practical to describe the behavior of balanced duplexers. The scattering matrix relates the waves traveling outward at a set of n terminals to those waves traveling inward at the set of terminals. $\mathbf{S}$ will be used to designate a scattering matrix, with subscripts added where appropriate in order to avoid confusion. Thus we may write

$$\begin{bmatrix} E_{01} \\ E_{02} \\ \cdot \\ \cdot \\ E_{0n} \end{bmatrix} = \begin{bmatrix} S_{11} & S_{12} \cdots S_{1n} \\ \cdot \quad \cdot \quad \cdot \quad \cdot \quad \cdot \quad \cdot \quad \cdot \\ S_{n1} \cdot \quad \cdot \quad \cdot \quad S_{nn} \end{bmatrix} \begin{bmatrix} E_{i1} \\ E_{i2} \\ \cdot \\ \cdot \\ E_{in} \end{bmatrix}. \tag{1}$$

The terms on the major diagonal, S_{11}, S_{22}, $\cdots$, etc., are the reflection coefficients that would be measured if all other terminals were terminated with a match. All other matrix elements are transfer terms, again applying to the case where the terminals are reflectionless.

In order to solve the duplexer problem represented by Fig. 1, it is necessary to obtain the scattering matrices for the switching elements and the hybrids. The switching element is a two-terminal device and can be represented by

$$\mathbf{S}_s = \begin{bmatrix} S_{11} & S_{12} \\ S_{12} & S_{11} \end{bmatrix}. \tag{2}$$

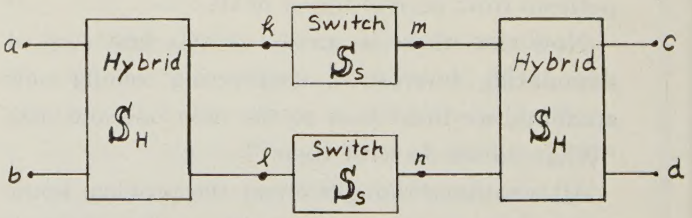

Fig. 1—Balanced duplexer.

The matrix is completely symmetrical because the reflection and transfer characteristics are the same when viewed from either terminal. The switch is a passive bi-

[3] Montgomery, Dicke, and Purcell, *op. cit.*, ch. 5.

lateral device which has two operating conditions. S_{11} and S_{12} have two sets of values, one during the time the transmitter is on, and the other during the time the radar is receiving. More will be said about this in a later section.

The hybrid is a four-terminal device which ideally has the property that power supplied to a given terminal is equally divided between two of the three remaining terminals and nothing is coupled to the fourth terminal. It is possible to build hybrids which have a high degree of isolation and acceptable balance over a very wide band. For example, a multiple slot hybrid can have a directivity of 40 db and a deviation from 3 db coupling of 0.3 db over the 40 per cent waveguide band. If one properly numbers the terminals, the scattering matrix for an ideal directional coupler hybrid may be written

$$S_H = \frac{1}{\sqrt{2}} \left[\begin{array}{cc|cc} 0 & 0 & 1 & j \\ 0 & 0 & j & 1 \\ \hline 1 & j & 0 & 0 \\ j & 1 & 0 & 0 \end{array}\right]. \tag{3}$$

The term S_{12} is zero by definition for a perfect hybrid and so small in a practical unit that it can be set equal to zero without appreciable error. It can be proved[4] that for $S_{12}=0$, $S_{11}=0$ also. In general the hybrids cannot be considered perfect, but for the case of the directional coupler hybrid, of either the multi-slot or the short-slot type, it has been found that calculations are sufficiently accurate if it is assumed that only the power split departs from ideal. The scattering matrix for this case may be written

$$S_H = \left[\begin{array}{c|c} 0 & \boldsymbol{H} \\ \hline \boldsymbol{H} & 0 \end{array}\right], \tag{4}$$

where $\boldsymbol{H}$ is a submatrix which contains the terms describing the power split. Eq. (4) applies to all types of hybrid circuits whose isolation is sufficiently good that S_{12} may be neglected. The form of $\boldsymbol{H}$ is different for directional coupler hybrids than for magic tee and ring hybrids and, as a result, the circuit configurations vary with the type of hybrid or combinations of hybrids used. Fig. 2 illustrates this. The scattering matrix for ideal ring hybrids or magic tees (5) may be compared to the scattering matrix for the ideal directional-coupler hybrid (3).

$$S_T = \frac{1}{\sqrt{2}} \left[\begin{array}{cc|cc} 0 & 0 & 1 & 1 \\ 0 & 0 & -1 & 1 \\ \hline 1 & -1 & 0 & 0 \\ 1 & 1 & 0 & 0 \end{array}\right]. \tag{5}$$

The directional-coupler hybrid provides the duplexer circuit with the highest degree of symmetry, which would lead one to believe that this configuration should

[4] *Ibid.*, ch. 9.

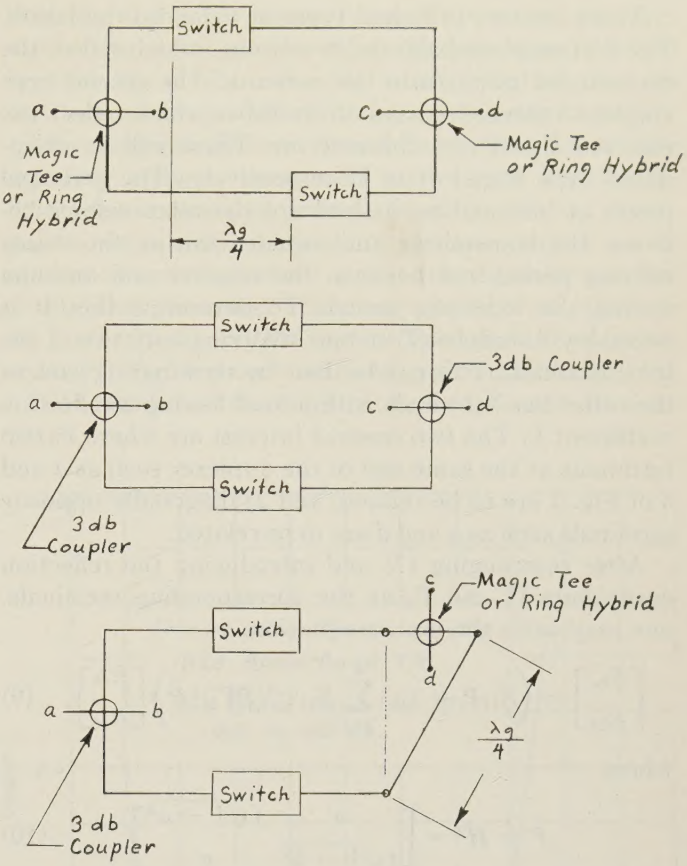

Fig. 2—Several possible balanced-duplexer configurations.

be capable of the greatest bandwidth. For purposes of this paper, only this type of duplexer will be considered from this point on.

Balanced Hybrid Duplexer Theory

Scattering Matrix of the Duplexer

Using nomenclature of Fig. 1, rearranging the scattering equations for identical switches, one can write

$$\begin{bmatrix} E_{0k} \\ E_{0l} \end{bmatrix} = S_{11} \begin{bmatrix} E_{ik} \\ E_{il} \end{bmatrix} + S_{12} \begin{bmatrix} E_{im} \\ E_{in} \end{bmatrix}. \tag{6}$$

The matrix equation for the duplexer then becomes

$$\begin{bmatrix} E_{0a} \\ E_{0b} \\ E_{0c} \\ E_{0d} \end{bmatrix} = \left[\begin{array}{cc|cc} S_{11} & \boldsymbol{H}^2 & S_{12} & \boldsymbol{H}^2 \\ S_{12} & \boldsymbol{H}^2 & S_{11} & \boldsymbol{H}^2 \end{array}\right] \begin{bmatrix} E_{ia} \\ E_{ib} \\ E_{ic} \\ E_{id} \end{bmatrix}. \tag{7}$$

$\boldsymbol{H}$ is the submatrix of (4) and may be written

$$\boldsymbol{H} = \begin{bmatrix} \sqrt{\dfrac{1+\alpha}{2}} & j\sqrt{\dfrac{1-\alpha}{2}} \\ j\sqrt{\dfrac{1-\alpha}{2}} & \sqrt{\dfrac{1+\alpha}{2}} \end{bmatrix}, \tag{8}$$

where α is a frequency-sensitive term governing the power split. Values of α by definition must lie in the range $-1 \leqq \alpha \leqq 1$.

There are two principal types of balanced duplexers. The first employs balanced tr switches which reflect the transmitted power into the antenna. The second type employs balanced arrays of atr tubes which reflect the received signal into the receiver. These will be designated type I and type II respectively. The principal pieces of information desired are the relationships between the transmitter and antenna during the transmitting period and between the receiver and antenna during the receiving period. To determine this, it is necessary to reduce (7) to one involving only two of the four terminals. This can be done by terminating each of the other two terminals with a load having a reflection coefficient Γ. The two cases of interest are where 1) two terminals at the same end of the duplexer such as a and b of Fig. 1 are to be related, and 2) diagonally opposite terminals such as a and d are to be related.

After rearranging (7) and introducing the reflection coefficients Γ_c and Γ_d at the corresponding terminals, one may write the matrix equation

$$\begin{bmatrix} E_{0a} \\ E_{0b} \end{bmatrix} = \left(S_{11}\boldsymbol{P} + S_{12}^2 \sum_{n=1}^{\infty} S_{11}^{n-1} (\boldsymbol{P}\boldsymbol{\Gamma}_1)^n \boldsymbol{P} \right) \begin{bmatrix} E_{ia} \\ E_{ib} \end{bmatrix}, \quad (9)$$

where

$$\boldsymbol{P} = \boldsymbol{H}^2 = \begin{bmatrix} \alpha & j\sqrt{1-\alpha^2} \\ j\sqrt{1-\alpha^2} & \alpha \end{bmatrix} \quad (10)$$

$$\boldsymbol{\Gamma}_1 = \begin{bmatrix} \Gamma_c & 0 \\ 0 & \Gamma_d \end{bmatrix}. \quad (11)$$

Relating a to d with b and c terminated gives

$$\begin{bmatrix} E_{0a} \\ E_{0d} \end{bmatrix} = \left(\boldsymbol{A} + \boldsymbol{B} \sum_{n=1}^{\infty} (\boldsymbol{\Gamma}_2 \boldsymbol{A})^{n-1} \boldsymbol{\Gamma}_2 \boldsymbol{B} \right) \begin{bmatrix} E_{ia} \\ E_{ib} \end{bmatrix} \quad (12)$$

where

$$\boldsymbol{A} = \begin{bmatrix} S_{11}P_{11} & S_{12}P_{12} \\ S_{12}P_{12} & S_{11}P_{11} \end{bmatrix} \quad (13)$$

$$\boldsymbol{B} = \begin{bmatrix} S_{11}P_{12} & S_{12}P_{11} \\ S_{12}P_{11} & S_{11}P_{12} \end{bmatrix} \quad (14)$$

$$\boldsymbol{\Gamma}_2 = \begin{bmatrix} \Gamma_b & 0 \\ 0 & \Gamma_c \end{bmatrix}. \quad (15)$$

Eqs. (9) and (12) describe the circuit characteristics of the two types of balanced duplexers being considered here. From them can be computed the vswr and insertion loss during both the transmitting and receiving phases. This is done by supplying the appropriate values of S_{11} and S_{12}, the switch tube parameters, which assume widely different values for the two operating conditions.

The Transmitting Condition

While the radar is transmitting, the tr and atr tubes will be ionized and may be represented by a short circuit. There is a finite voltage across these switches, but this is, in any practical case, several orders of magnitude below the line voltage and may be ignored.

In the case of the type I duplexer the tr tubes place a short circuit across the transmission line so that $S_{11} = -1$ and $S_{12} = 0$. Substituting this into (9) gives

$$\begin{bmatrix} E_{0a} \\ E_{0b} \end{bmatrix} = -1 \begin{bmatrix} \alpha & j\sqrt{1-\alpha^2} \\ j\sqrt{1-\alpha^2} & \alpha \end{bmatrix} \begin{bmatrix} E_{ia} \\ E_{ib} \end{bmatrix}. \quad (16)$$

The vswr seen by the transmitter is

$$R_{T1} = \frac{1+\alpha}{1-\alpha} \quad (17)$$

and the insertion loss (neglecting the loss in the gas discharge) expressed in db is

$$L_{T1} = 10 \log \frac{1}{1-\alpha^2}. \quad (18)$$

For the type II duplexer where the atr windows are in the plane of the waveguide walls, the application of high power produces a discharge which shorts out these windows and the switch section appears like a piece of unperturbed transmission line except for the negligible voltage across the window. For this case $S_{11} = 0$ and $S_{12} = 1$. Substituting into (12) and expanding to $n = 1$

$$\begin{bmatrix} E_{0a} \\ E_{0b} \end{bmatrix} = \begin{bmatrix} \Gamma_c\alpha^2 & j\sqrt{1-\alpha^2} \\ j\sqrt{1-\alpha^2} & \Gamma_b\alpha^2 \end{bmatrix} \begin{bmatrix} E_{ia} \\ E_{ib} \end{bmatrix}. \quad (19)$$

Terms of order higher than $n = 1$ will be multiplied by the factor $\Gamma_b\Gamma_c$. Γ_b is arbitrary and is usually made to equal zero by connecting a matched load to terminal b. Terminal c is connected to the receiver, which will normally be protected by an auxiliary tr tube. This will provide a short circuit at terminal c so we may set $\Gamma_c = 1$.

The vswr becomes

$$R_{T2} = \frac{1+\alpha^2}{1-\alpha^2}. \quad (20)$$

The insertion loss is the same as for the type I duplexer. In this case the reflected power is absorbed in the termination at terminal b rather than being reflected back into the transmitter.

The dissipation in the switch tubes is not considered in (18) and is obviously so small as to have negligible effect on the circuit performance as seen at the terminals. However in a high power radar the switch tube dissipation is very important, since it is one of the principal power limiting factors. While it is not possible to calculate accurately the switch tube dissipation, it is possible to make a comparison between the power-handling capabilities of the two duplexer systems if it is assumed that the switch tube windows are identical. This is not an unrealistic situation and affords a good starting point when considering power handling capabilities.

At the output of the first hybrid the currents will be $1/\sqrt{2}I_0$, assuming perfect hybrid balance, where I_0 is the line current at the input terminal corresponding to a power P_0. For the case of the type I duplexer, the tr tubes present a short circuit at which the current doubles. The window current is therefore $\sqrt{2}I_0$. If I_0 is the maximum current which the window can handle, then it is readily calculated that the line power must be reduced to $\frac{1}{2}P_0$. For the type II duplexer, the atr windows will be required to handle only $1/\sqrt{2}I_0$ and it is therefore possible to raise the transmitter power to $2P_0$ before the window capabilities are exceeded. All other things being equal, one would expect the atr type duplexer to handle four times the average power which can be switched by the tr type duplexer.

The transmitter load impedance is of importance in many applications. A comparison of (17) and (20), which are plotted in Fig. 3, shows that for the case of imperfect hybrids the atr duplexer has considerable advantage over the type I.

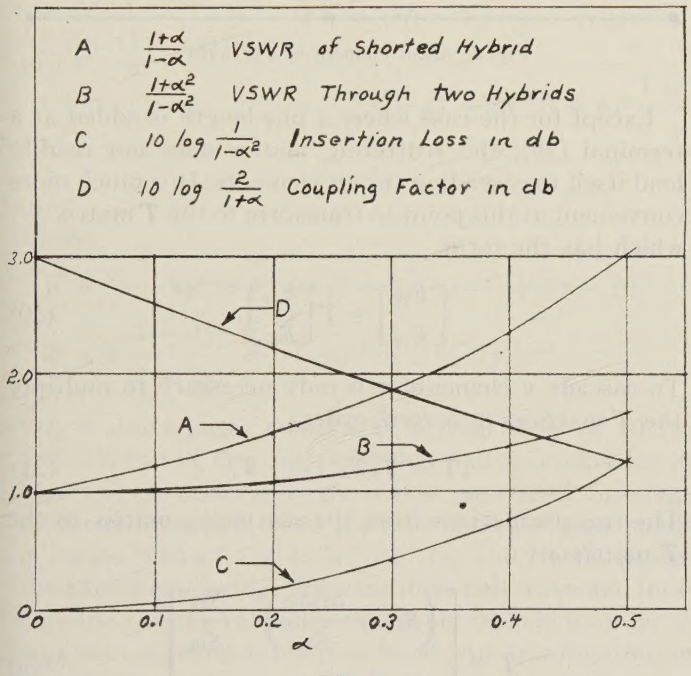

Fig. 3

The Receiving Condition

During the receiving interval, only very weak signals enter the duplexer, so the insertion loss between the antenna and receiver is the only feature of interest. The receiving situation with the type I duplexer is described by (12), where terminals a and d are the antenna and receiver respectively. Γ_b is the reflection coefficient of the transmitter, and Γ_c that of the arbitrary load. The insertion loss expanded to $n=1$ is

$$L_{R1} = 20 \log \left| \frac{1}{S_{12}\sqrt{1-\alpha^2} + S_{11}S_{12}\alpha\sqrt{1-\alpha^2}(\Gamma_b+\Gamma_c)} \right|. \quad (21)$$

Both S_{11} and α are normally small compared to unity within the useful pass band, so the second term in the denominator would ordinarily be neglected. S_{11} and S_{12} are the scattering coefficients for a particular tr switch.

The multiple-element broad-band tr tube is the switching element most used in the type I duplexer. This tube consists of several (usually two or three) quarter-wave-coupled resonant elements plus a low-Q window at each end which is also quarter-wave coupled to the other elements. There are a number of places in the literature where this type of band-pass filter is discussed.[5-7] Fig. 4 shows the band-pass characteristic for a 1B58, from which values of S_{11} and S_{12} can be estimated.

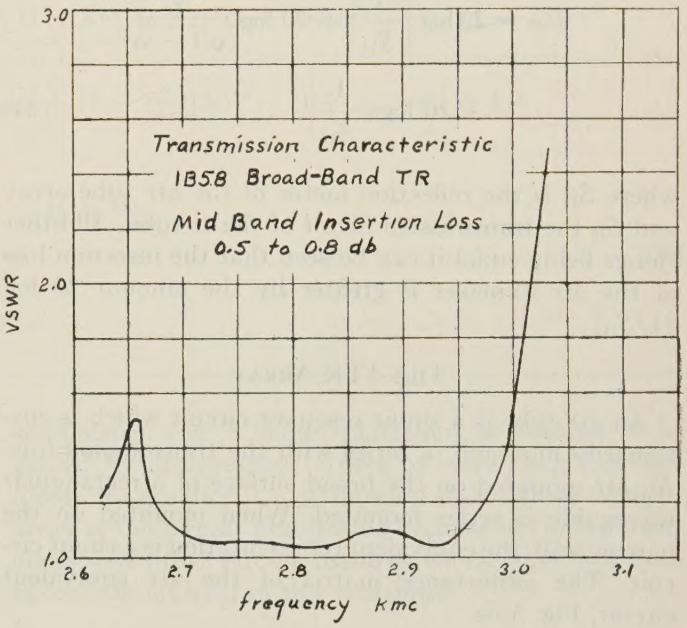

Fig. 4

During the receiving interval, the performance of the type II duplexer is described by (9). The switching circuit in this case is an array of one or more atr tubes. With the antenna at terminal a, the receiver at b, the transmitter having a reflection coefficient Γ_d at terminal d, and an arbitrary load of Γ_c at terminal c, the insertion loss expanded to $n=1$ is

$$L_{R2} = 20 \log \left| \frac{1}{S_{11}\sqrt{1-\alpha^2} + S_{12}^2\alpha\sqrt{1-\alpha^2}(\Gamma_c+\Gamma_d)} \right|. \quad (22)$$

In this case S_{11} and S_{12} are the scattering terms for an atr array.

With the exception of those instances where one is interested in the duplexer behavior outside of the pass

[5] W. L. Prichard, "Quarter wave coupled wave guide filters," *J. Appl. Phys.*, vol. 18, pp. 862–872; October, 1947.
[6] G. L. Ragan, "Microwave Transmission Circuits," M.I.T. Rad. Lab. Ser., McGraw-Hill Book Co., Inc., New York, N. Y., vol. 9, p. 683, 1948.
[7] Smullin and Montgomery, *op. cit.*, ch. 3.

band, the higher-order terms in the denominators of (21) and (22) can be ignored. In order to compare the performance of the two duplexers when receiving it is necessary to know the contributions to insertion loss made by the hybrids, the broad-band tr tubes, and the atr tube array. For type I

$$L_{R1} = 20 \log \left| \frac{1}{S_{12}} \right| + 20 \log \frac{1}{\sqrt{1 - \alpha^2}}, \tag{23}$$

where S_{12} is the transmission characteristic of the broad-band tr and α the balance factor of the hybrid. For type II, recalling that a broad-band tr is used in front of the receiver,

$$L_{R2} = 20 \log \left| \frac{1}{S_{11}} \right| + 20 \log \frac{1}{\sqrt{1 - \alpha^2}} + 20 \log \left| \frac{1}{S_{12}} \right|, \tag{24}$$

where S_{11} is the reflection factor of the atr tube array and S_{12} the transmission factor of the tr tube. All other things being equal it can be seen that the insertion loss of the atr duplexer is greater by the amount 20 log $|1/S_{11}|$.

The ATR Array

An atr tube is a shunt resonant circuit which is customarily mounted in series with the transmission line. An atr mounted on the broad surface of a rectangular waveguide is series mounted. When mounted on the narrow wall, the equivalent representation is a shunt circuit. The admittance matrix of the atr equivalent circuit, Fig. 5, is

$$Y = \begin{bmatrix} y & -y \\ -y & y \end{bmatrix} \tag{25}$$

where[8]

$$y = g + j2(1 + g)Q_L \frac{\Delta\omega}{\omega_0}. \tag{26}$$

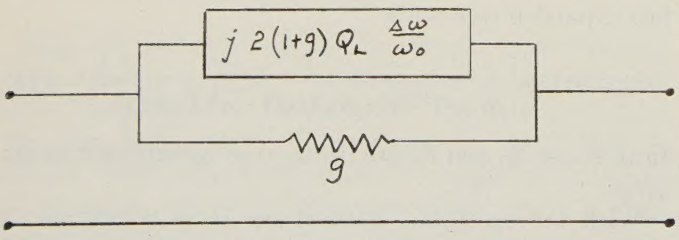

Fig. 5—Equivalent circuit of atr.

In order to compute the insertion loss of (22) it is necessary to obtain the scattering matrix for an array of tubes. This may be done by first obtaining the scattering matrix for a single tube using the relation[9]

$$S = (1 - Y)(1 + Y)^{-1} \tag{27}$$

with the result that

$$_1S = \frac{1}{1 + 2y} \begin{bmatrix} 1 & 2y \\ 2y & 1 \end{bmatrix}. \tag{28}$$

The second step is to cascade a line length θ with the atr circuit as shown in Fig. 6. This transformation[10] results in

$$S_\theta = \begin{bmatrix} S_{11} & S_{12}e^{-j\theta} \\ S_{12}e^{-j\theta} & S_{11}e^{-j2\theta} \end{bmatrix}. \tag{29}$$

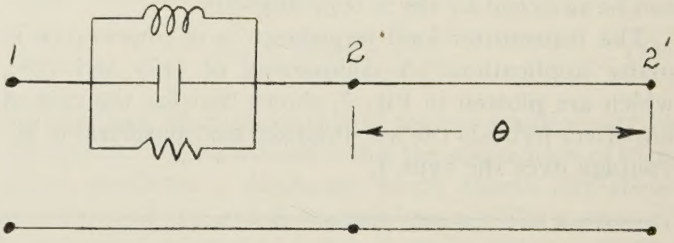

Fig. 6—Basic element of a tr array.

Except for the case where a line length is added at a terminal (29), the scattering matrix does not readily lend itself to cascading circuit elements. It is much more convenient at this point to transform to the T matrix[11,12] which has the form

$$\begin{bmatrix} E_{02} \\ E_{i2} \end{bmatrix} = T \begin{bmatrix} E_{i1} \\ E_{01} \end{bmatrix}. \tag{30}$$

To cascade n elements it is only necessary to multiply the T matrices in reverse order

$$_nT = T_nT_{n-1} \cdots T_1. \tag{31}$$

The transformations from the scattering matrix to the T matrix are

$$T = \begin{bmatrix} \left(S_{21} - \dfrac{S_{11}S_{22}}{S_{12}}\right) & \dfrac{S_{22}}{S_{12}} \\ -\dfrac{S_{11}}{S_{12}} & \dfrac{1}{S_{12}} \end{bmatrix} \tag{32a}$$

$$S = \begin{bmatrix} -\dfrac{T_{21}}{T_{22}} & \dfrac{1}{T_{22}} \\ \left(T_{11} - \dfrac{T_{12}T_{21}}{T_{22}}\right) & \dfrac{T_{12}}{T_{22}} \end{bmatrix}. \tag{32b}$$

The values of S_{11} for several arrays of identical atr tubes have been determined and are tabulated below.

[8] Smullin and Montgomery, *op. cit.*, p. 118.

[9] Montgomery, Dicke, and Purcell, *op. cit.*, p. 148.

[10] Montgomery, Dicke, and Purcell, *op. cit.*, p. 149.

[11] M. Tinkham and M. W. P. Strandberg, "The excitation of circular polarization in microwave cavities," Proc. IRE, vol. 43, pp. 734–738; June, 1955.

[12] Montgomery, Dicke, and Purcell, *op. cit.*, p. 150.

$$ {}_1S_{11} = \frac{1}{1+2y} \tag{33a} $$

$$ {}_2S_{11} = \frac{\frac{1-4y^2}{1+2y} - (1+2y)e^{j2\theta}}{1-(1+2y)^2e^{j2\theta}} \tag{33b} $$

$$ {}_3S_{11} = \frac{\frac{1-4y^2}{(1+2y)^2}\left[(1-4y^2)e^{-j2\theta} - (1+2y)^2\right] - \left[1-(1+2y)^2e^{j2\theta}\right]}{\frac{1}{1+2y}\left[(1-4y^2)e^{-j2\theta} - (1+2y)^2\right] - (1+2y)\left[1-(1+2y)^2e^{j2\theta}\right]} \tag{33c} $$

$$ {}_4S_{11} = \frac{\frac{1-4y^2}{(1+2y)^3}\left[(1-4y^2)^2e^{-j2\theta} - (3-4y^2)(1+2y)^2\right] + (1+2y)\left[3e^{j2\theta} - (1+2y)^2e^{j4\theta}\right] - 4y^2(1+2y)e^{j2\theta}}{\frac{1}{(1+2y)^2}\left[(1-4y^2)^2e^{-j2\theta} - (3-4y^2)(1+2y)^2\right] + (1+2y)^2\left[3e^{j2\theta} - (1+2y)^2e^{j4\theta}\right] + 4y^2} \tag{33d} $$

$$ {}_5S_{11} = \frac{\frac{1-4y^2}{(1+2y)^4}A - (1+2y)^2B - 4y^2\left[(3-4y^2)e^{j2\theta} - (1+2y)^2e^{j4\theta}\right]}{\frac{1}{(1+2y)^3}A - (1+2y)^3B + 4y^2\frac{1-4y^2}{1+2y}} \tag{33e} $$

where

$$ A = (1-4y^2)^3e^{-j2\theta} - 4(1+2y)^2(1-4y^2)(1-j^2) $$

$$ B = 6\frac{1-2y^2}{(1+2y)^2}e^{j2\theta} + 4e^{j4\theta} - (1+2y)^2e^{j6\theta}. $$

Fig. 7 (next page) consists of several plots of 20 log $1/S_{11}$. It can be demonstrated that half-wave spacing of identical atr tubes gives the widest pass band. Spacings different from half wave produce narrower pass bands or create "holes." Fig. 7(c), 7(d), 7(e), and 7(f) illustrates the effects of spacings different from half wave and indicate the spacing tolerance that must be held in order to maintain an acceptable pass band. An investigation of the effects of tuning errors in the atr circuits has not been attempted.

The curves of Fig. 7 have been plotted assuming an atr conductance of $g=0.02$. Several S-band tubes have been checked and it has been found that this is a realistic maximum figure. The resulting loss at band center is quite low, being less than 0.4 db for a single tube and less than 0.2 db for a three-tube array.

The 1-db insertion loss point has been arbitrarily chosen for bandwidth determination. The curve of Fig. 8 may be used for estimating bandwidth. This curve is a graphical determination from the data of Fig. 7 of the product BQ_L. It can be demonstrated that this product is very nearly constant for values of Q_L between three and ten. No attempt was made to obtain an explicit expression for $B=f(Q_L)$ because of the mathematical complexity. Fig. 8 shows that there is nothing to be gained by constructing arrays of more than four elements. In practice it may develop that a three-element array is the largest practicable because of tuning tolerances and other circuit features which have not been taken into account in this treatment.

Hybrid Characteristics

The short-slot hybrid[13] is extensively used in balanced duplexer applications. Where balanced tr tubes are used the hybrid is customarily the side wall type, in which case the coupling is accomplished by means of an aperture in the common narrow wall of the waveguide. The top wall coupler which has two slots in the common broad dimension of the waveguide can also be used, and is a convenient configuration of the atr duplexer. Of the two types of short-slot hybrids, the top wall configuration has the best pass-band characteristic, but the side wall coupler will handle the most power. An attempt has been made by H. J. Riblet, originator of these types of hybrids, to increase the power handling ability of the top wall coupler by increasing the radii on the common wall. This has met with some success, but sufficient data are not available to make a valid comparison of the two types. Fig. 9 is a photograph of these two hybrid junctions. Fig. 10 (p. 12), shows values of α measured for a single model each of the side wall coupler and low-power

[13] H. J. Riblet, "The short slot hybrid junction," Proc. IRE, vol. 40, pp. 180–184; February, 1952.

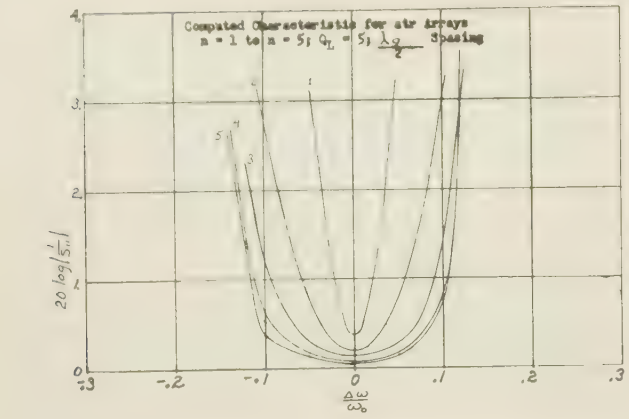

(a)

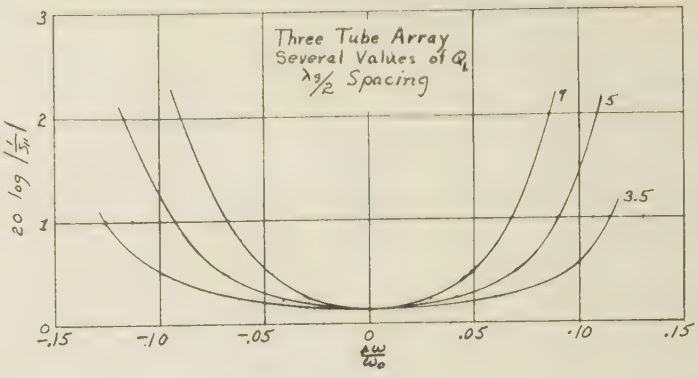

(b)

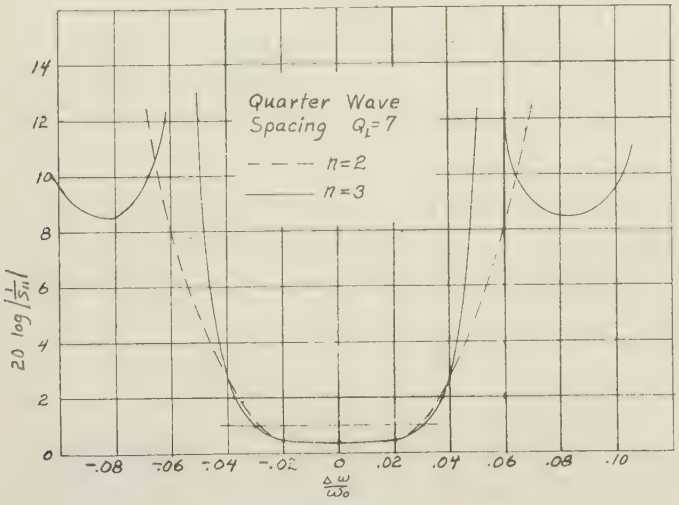

(c)

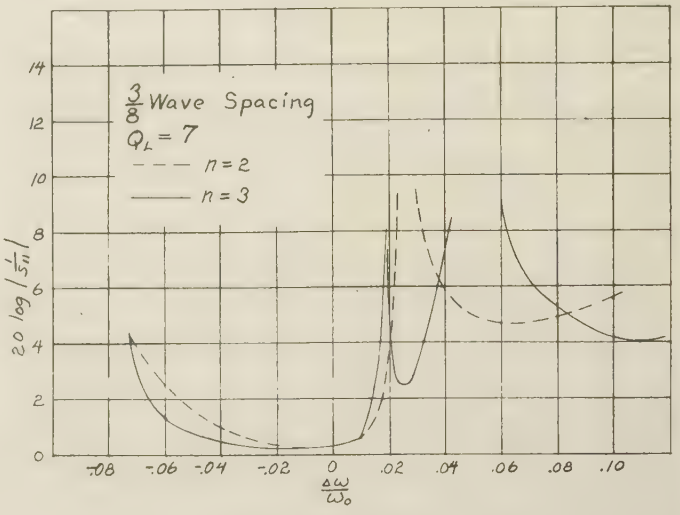

(d)

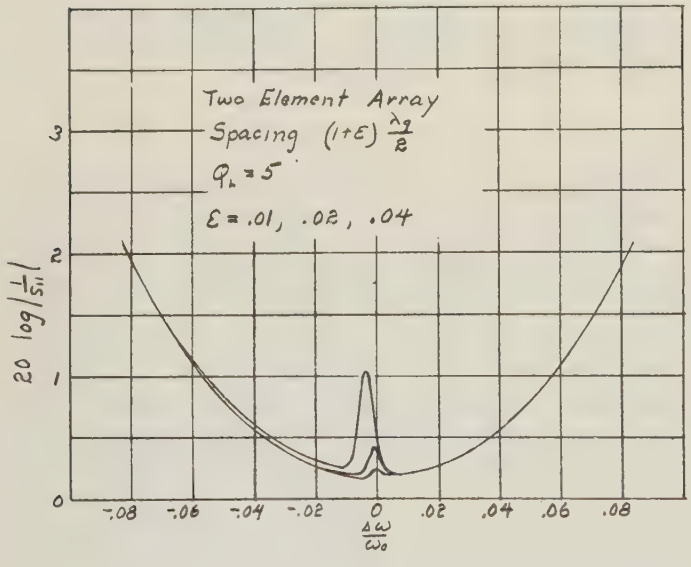

(e)

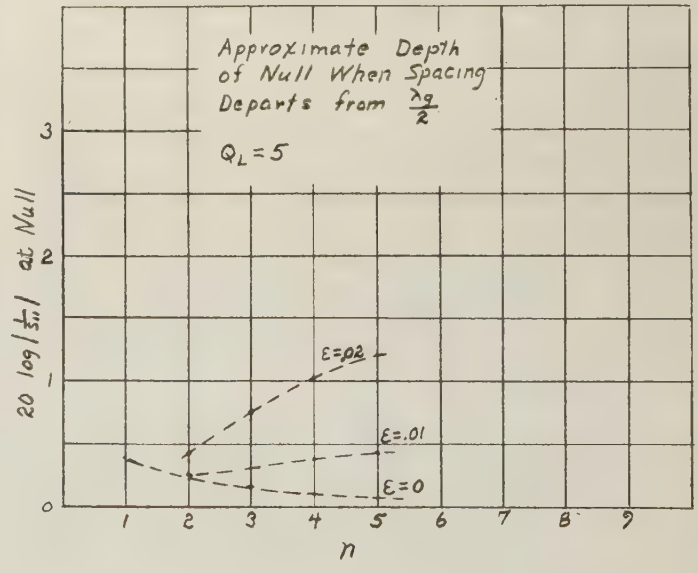

(f)

Fig. 7

top wall coupler, and the average of four models of the high power top wall coupler. In the latter case the units showed very little spread in characteristic over the band, 2600–3100 mc.

ATR Tubes

The choice of an atr tube array for the type II duplexer will be a compromise between bandwidth per

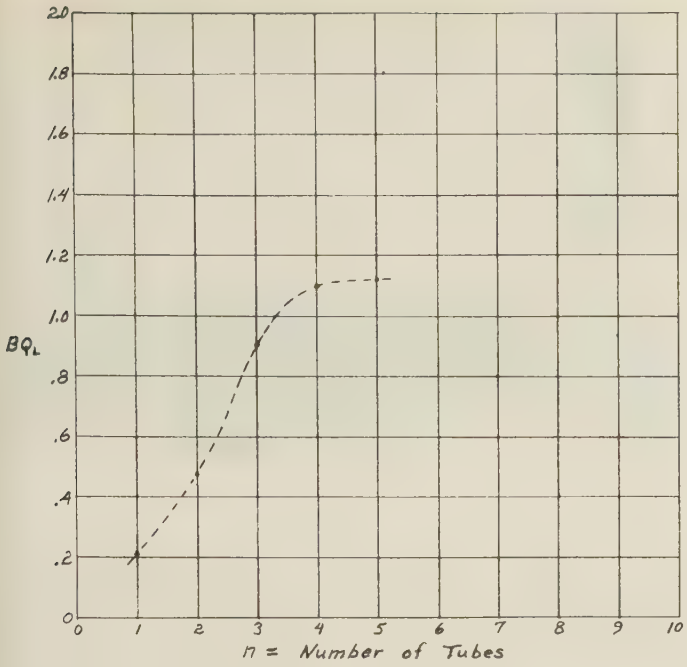

Fig. 8—Relationship between bandwidth ($B=\Delta\omega/\omega_0$ at 1 db) and number of half-wave spaced atr tubes.

Several *S*-band tubes have been procured from Bomac and Sylvania. Table I gives their low-level characteristics.

TABLE I*

Type	Q_L	mfr.
1B56	3.4	Bomac
1B56	3.3	Sylvania
BL623	5.5	Bomac
ATR788	5.5	Sylvania
BL632	9.4	Bomac

* $g \leqq 0.02$ for all tubes.

Experimental *S*-Band ATR Duplexer

Two atr duplexers were constructed, tested at low level, and then operated in radar systems in order to compare their performance with other existing duplexers. Unfortunately, the radars available did not have the transmitter power capabilities necessary for determining the useful upper limit of this type of duplexer. Some observations were made, however, which indicate that it is capable of handling high average power.

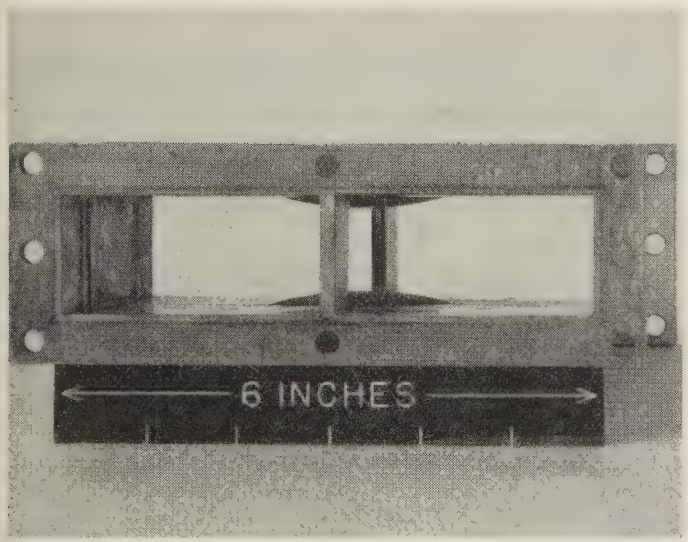

(a)

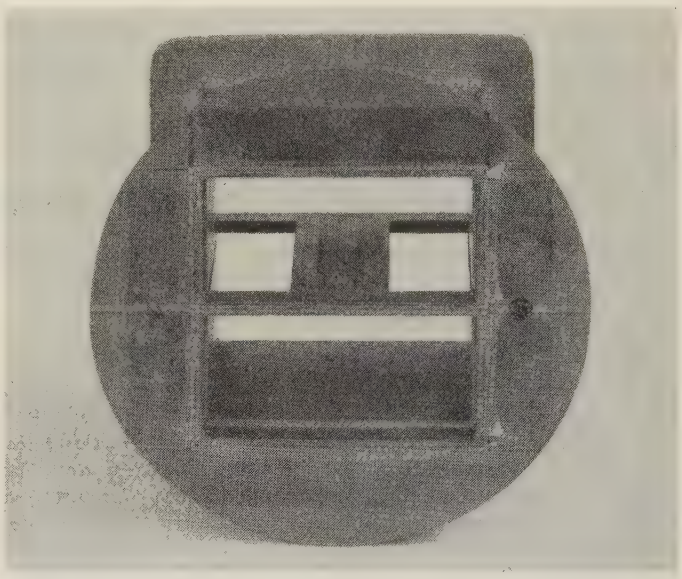

(b)

Fig. 9

tube and high level dissipation per tube. The higher the Q_L the greater the number of tubes required for a given bandwidth, but since the high-Q tubes have narrow windows, the arc voltage should be lower and one might expect the power lost per tube to be reduced. Sufficient data are not yet available regarding the relationship between dissipation and Q_L to form any conclusions at this point, but observations seem to confirm the suspicion that the dissipation goes at least as rapidly as $1/Q_L$ in the range $Q_L=3.4$ to $Q_L=9.4$.

The first of these duplexers employed two BL623 atr tubes (single-tube array) as the switching elements. The receiving bandwidth, which was that of the atr array, was 3.6 per cent. Bandwidth is arbitrarily defined as the per cent frequency between 1-db points of the atr array characteristic, *i.e.*, $L=20 \log \left|1/S_{11}\right| =1$. At 1.2 kw average power the switch tube temperature was about 140°F, as compared to a temperature in excess of 212°F for a 1B56 in a branching duplexer at the same power level. This is a crude comparison and should be

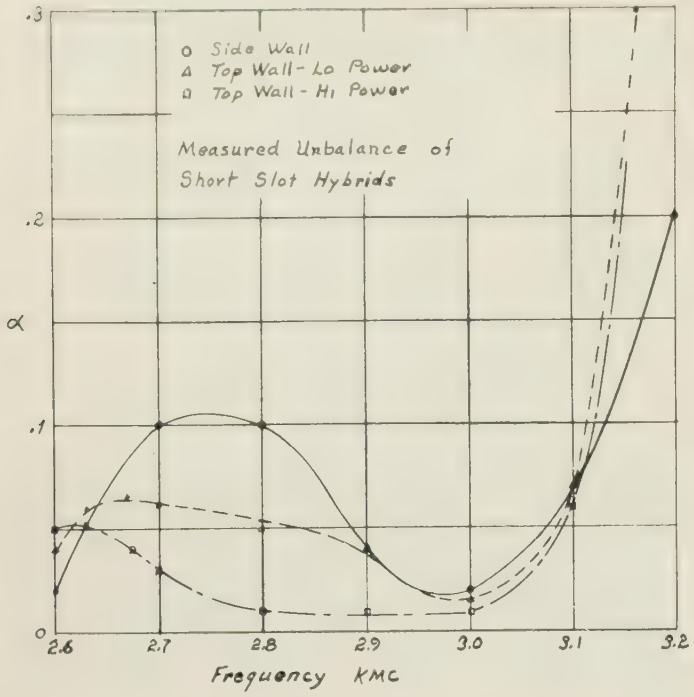

Fig. 10

Fig. 11

considered only as a qualitative indication of the power handling ability.

The second duplexer, employing two-tube arrays in the switching circuit, behaved in a similar fashion at high level and had the predicted receiving bandwidth. This duplexer is shown in Fig. 11 (above).

Calculation of the Parameters of Ridge Waveguides*

TSUNG-SHAN CHEN†

Summary—**In this paper an algebraic expression which constitutes an approximation to Cohn's transcendental equation is given for the determination of the dominant-mode cutoff wavelength of ridge waveguides. A modified derivation of Mihran's equation for calculating the characteristic impedance of ridge waveguides is discussed. Based upon these formulas, nomographs are constructed to permit the determination of these parameters with sufficient accuracy when the waveguide and the ridge dimensions vary. Experimental verification of the calculated cutoff wavelength is included.**

Introduction

RIDGE WAVEGUIDES have a longer cutoff wavelength and a lower characteristic impedance than conventional rectangular waveguides having the same internal dimensions. The ridge waveguides also have a wider bandwidth free from higher-mode interference. Because of these advantages, ridge waveguides have been used as transmission links in systems requiring a wide free range in the fundamental mode,[1] as matching or transition elements in waveguide-to-coaxial junctions,[2] as filter elements, and as components for other special purposes.[3] One type of slow-wave structure used with traveling-wave tubes consists of a ridge waveguide which is made periodic by means of equally spaced transverse slots. The transverse resonant frequency of this structure corresponds to the cutoff frequency of the ridge waveguide.[4]

In the development of tunable magnetrons, double-ridge waveguides have been used as external tuning cavities because their reduced cutoff frequency permits a compact cavity section. Because the electric field is concentrated between the ridges, satisfactory tuning characteristics are obtained by means of a plunger which short-circuits the narrow gap. In the electron-beam method of frequency modulation, the beam is introduced in this region of strong electric field between two parallel plates attached to the ridges.

* Manuscript received by PGMTT, March 14, 1956.
† Radio Corp. of America, Harrison, N. J.
[1] T. N. Anderson, "Double-ridge waveguide for commercial airlines weather radar installation," IRE Trans., vol. MTT-3, pp. 2–9; July, 1955.
[2] Radio Res. Lab. Staff, Harvard Univ., "Very High-Frequency Techniques," vol. II, pp. 678–684, 731–736, McGraw-Hill Book Co., Inc., New York, N. Y.; 1947.
[3] S. B. Cohn, "Properties of ridge waveguides," Proc. IRE, vol. 35, pp. 783–788; August, 1947.
[4] J. R. Pierce, "Traveling-Wave Tubes," D. Van Nostrand Co., New York, N. Y., ch. 4; 1950.

Ridge waveguides are also used as H-type output transformers in magnetrons for the purpose of transforming the high impedance of the waveguide used for power transmission to the low impedance level of the magnetron. If a rectangular waveguide transformer is employed, the dimensions required for impedance matching may be too large, especially for magnetrons having short block heights. When the H-type transformer is used, an effectively large width can be obtained with small physical sizes. In addition, good broadband characteristics may be provided by proper selection of the dimensions of the H section to yield a cutoff wavelength at least as long as that of the waveguide connected to the transformers.

In these applications of ridge waveguides, the cutoff wavelength and the characteristic impedance are important parameters to be known for design purposes, and approximate relations for their determination have been available.[5–7] Cohn[8] first developed the accurate transcendental expressions for cutoff wavelengths of odd and even TE_{mo} modes and also expressions for the attenuation and characteristic impedance of the TE_{10} mode. Recently Cohn's work has been extended to include unusual ridge dimensions and cross sections other than rectangular.[8–10] In this article, emphasis is laid upon the calculation of the dominant mode characteristics of rectangular ridge waveguides. Formulas for finding these characteristics are expressed explicitly in terms of the guide dimensions, and charts are constructed to facilitate computations for waveguides having various aspect ratios and having ridges of different widths and depths.

Cutoff Wavelengths for the Dominant Mode in Ridge Waveguides

Cross sections of single-ridge and double-ridge waveguides are shown in Fig. 1. In the derivations, mks units are used unless otherwise mentioned. In Fig. 2, a unit length of ridge waveguide is represented by a lumped-constant equivalent circuit consisting of capacitance and inductance in parallel. The capacitance, C, in the equivalent circuit consists of the electrostatic capacitance, C_s, and the discontinuity capacitance, C_d. When a single-ridge waveguide such as that shown in Fig. 1(a) is operating in the dominant mode, the capacitance, C_s, depends mainly on the region between the ridge and

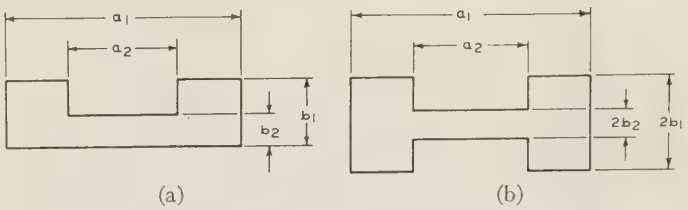

Fig. 1—Cross sectional view of (a) single-ridge and (b) double-ridge waveguides.

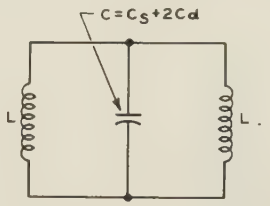

Fig. 2—Equivalent lumped-constant circuit for a unit length of ridge waveguide at cutoff wavelength.

the bottom plate, where a strong electric field exists This capacitance in farads per unit length of the guide is approximately given by

$$C_s = \frac{\epsilon a_2}{b_2} \tag{1}$$

where ϵ is the permittivity of the medium and in free-space equals 8.854×10^{-12} farad per meter.

The ridge in the waveguide presents discontinuities to the electromagnetic waves and causes local or higher-order waves. The effects of these local fields are included in the calculation by the addition at the proper location of the discontinuity susceptance which is here capacitive in nature. By the use of Hahn's method[11] of field matching, Whinnery and Jamieson[12] developed a series for the discontinuity capacitance, C_d, which depends on the step ratio, b_2/b_1, and, to a lesser extent, on the ratio a_2/b_2. The capacitance C_d along with the quantity $2C_d/\epsilon$ is plotted in Fig. 3 as a function of the step ratio b_2/b_1.

This discontinuity capacitance approaches closely the fringing capacitance in a constricted conductor, which is obtained by means of Schwarz-Christoffel transformation[12,13]

$$C_d = \frac{\epsilon}{\pi}\left[\frac{x^2+1}{x}\cosh^{-1}\left(\frac{1+x^2}{1-x^2}\right) - 2\ln\frac{4x}{1-x^2}\right] \tag{2}$$

where $x = b_2/b_1$. The value of C_d found from (2) can be shown to agree with that given by Fig. 3. The total capacitance C in farads per unit length of the waveguide is then

$$C = \frac{\epsilon a_2}{b_2} + 2C_d. \tag{3}$$

[5] G. B. Collins, ed., "Microwave Magnetrons," M.I.T. Rad. Lab. Ser., McGraw-Hill Book Co., Inc., New York, N. Y., vol. 6, pp. 198–203; 1948.

[6] G. L. Ragan, ed., "Microwave Transmission Circuits," M.I.T. Rad. Lab. Ser., McGraw-Hill Book Co., Inc., New York, N. Y., vol. 9, p. 57; 1948.

[7] S. Ramo and J. R. Whinnery, "Fields and Waves in Modern Radio," John Wiley and Sons, Inc., New York, N. Y.; 1944.

[8] Hans-Georg Unger, "Die Berechnung von Steghohlleitern," *Archiv Elekt. Uebertragung*, Band 9, Heft 4; April, 1955.

[9] J. M. Osepchuk, "Variational Calculations on Ridge Waveguides," Cruft Lab., Harvard Univ., Cambridge, Mass., Tech. Rep. No. 224; May 5, 1955.

[10] S. Hopfer, "The design of ridged waveguides," IRE Trans., vol. MTT-3, pp. 20–29; October, 1955.

[11] W. C. Hahn, "A new method for the calculation of cavity resonators," *J. Appl. Phys.*, vol. 12, pp. 62–68; January, 1941.

[12] J. R. Whinnery and H. W. Jamieson, "Equivalent circuits of discontinuities in transmission lines," Proc. IRE, vol. 32, pp. 98–116; February, 1944.

[13] Miles Walker, "Conjugate Functions for Engineers," Oxford University Press, Cambridge, Mass.; 1933.

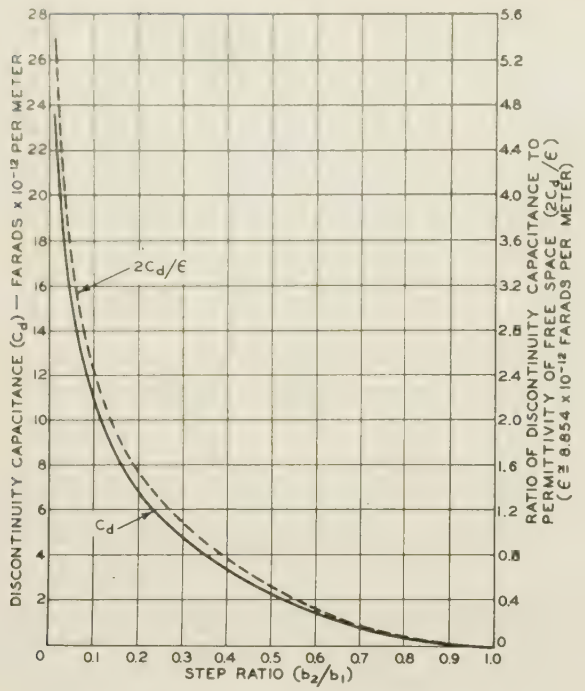

Fig. 3—Discontinuity capacitance, C_d, and the ratio, $2C_d/\epsilon$ as functions of the step ratio, b_2/b_1.

The inductances in the equivalent circuit show in Fig. 2 are determined by the sections of the waveguide on both sides of the ridge as shown in Fig. 1(a). The inductance, L, in henries due to either section per unit length of waveguide is given by

$$L = \frac{\mu(a_1 - a_2)}{2}(b_1), \tag{4}$$

where μ is the permittivity of the medium and equals $4\pi \times 10^{-7}$ henry per meter for free space. For the double-ridge waveguide depicted in Fig. 1(b), the capacitance C in (3) should be halved, and the inductance L in (4) doubled; the cutoff frequency remains unchanged.

At cutoff, the waves travel back and forth in the ridge waveguide in the transverse direction without longitudinal propagation; this condition corresponds to anti-resonance in the circuit shown in Fig. 2. The cutoff frequency, f_c', of the ridge waveguide in cycles per second is

$$f_c' = \frac{1}{2\pi\sqrt{(L/2)C}} \tag{5}$$

which, in conjunction with (3) and (4), becomes

$$f_c' = \frac{1}{\pi\sqrt{\mu\epsilon}\sqrt{\left(\frac{a_2}{b_2} + \frac{2C_d}{\epsilon}\right)(a_1 - a_2)(b_1)}}. \tag{6}$$

The cutoff wavelength, λ_c', of the ridge waveguide is given by $\lambda_c' = 1/(f_c'\sqrt{\mu\epsilon})$ and the cutoff wavelength λ_c of rectangular waveguide of width a_1 by $\lambda_c = 2a_1$. The ratio of these two cutoff wavelengths is

$$\frac{\lambda_c'}{\lambda_c} = \frac{\pi}{2}\sqrt{\left(\frac{a_2}{b_2} + \frac{2C_d}{\epsilon}\right)\left(\frac{b_1}{a_1}\right)\left(1 - \frac{a_2}{a_1}\right)}. \tag{7}$$

A nomograph for the determination of λ_c'/λ_c for ridge waveguides having known dimensions is shown in Fig. 4 (opposite). The value of $2C_d/\epsilon$ corresponding to a given step ratio, b_2/b_1, is found from Fig. 3. A line joining this value and the given point on the a_2/b_2 scales determines the sum $(a_2/b_2 + 2C_d/\epsilon)$. A second line is then drawn connecting the two given points a_1/b_1 and a_2/a_1 on the horizontal scales and cutting the diagonal at a definite point. A final line from the point $(a_2/b_2 + 2C_d/\epsilon)$ through this intersection determines the value of λ_c'/λ_c on the right-hand scale.

Cutoff Wavelengths for the Higher Modes in Ridge Waveguides

To find the cutoff wavelengths of higher modes, the single-ridge waveguide shown in Fig. 1(a) is considered as a composite transmission-line system having waves traveling in the transverse direction.[3] In Fig. 5(a), one half of a length, d, of the guide is represented by two sets of parallel plates separated by distances b_1 and b_2. The odd mode of the TE_{mo} wave requires a voltage loop and a current node at the center of the waveguide; the equivalent circuit shown in Fig. 5(b) should have an open circuit at the left end and a short circuit at the right end. In this circuit,

$\theta_1 = \left(1 - \frac{a_2}{a_1}\right)\frac{\lambda_c}{\lambda_c'}\frac{\pi}{2}$ = electrical length of section X_1 in radians.

$\theta_2 = \frac{a_2}{a_1}\frac{\lambda_c}{\lambda_c'}\frac{\pi}{2}$ = electrical length of section X_2 in radians.

$Y_{01} = \sqrt{\frac{\epsilon}{\mu}}\left(\frac{d}{b_1}\right)$ = characteristic admittance of section X_1 in mhos.

$Y_{02} = \sqrt{\frac{\epsilon}{\mu}}\left(\frac{d}{b_2}\right)$ = characteristic admittance of section X_2 in mhos.

$B_c' = 2\pi f_c' d C_d$ = discontinuity susceptance for a length d of the composite line in mhos.

The cutoff condition of the waveguide corresponds to resonance of the equivalent circuit,[3,10,14] which leads to an expression giving the cutoff wavelength, λ_c', implicitly in terms of the guide dimensions

$$\frac{b_1}{b_2} = \frac{\cot\left[\left(1 - \frac{a_2}{a_1}\right)\frac{\lambda_c}{\lambda_c'}\frac{\pi}{2}\right] - \frac{2C_d}{\epsilon}\frac{b_1}{a_1}\frac{\lambda_c}{\lambda_c'}\frac{\pi}{2}}{\tan\left(\frac{a_2}{a_1}\frac{\lambda_c}{\lambda_c'}\frac{\pi}{2}\right)}. \tag{8}$$

This equation is solved for the first order root to obtain the cutoff wavelength of the TE_{10} mode and for higher-

[14] N. Marcuvitz, "Waveguide Handbook," M.I.T. Rad. Lab. Ser., McGraw-Hill Book Co., Inc., New York, N. Y., vol. 10, pp. 399–402; 1951.

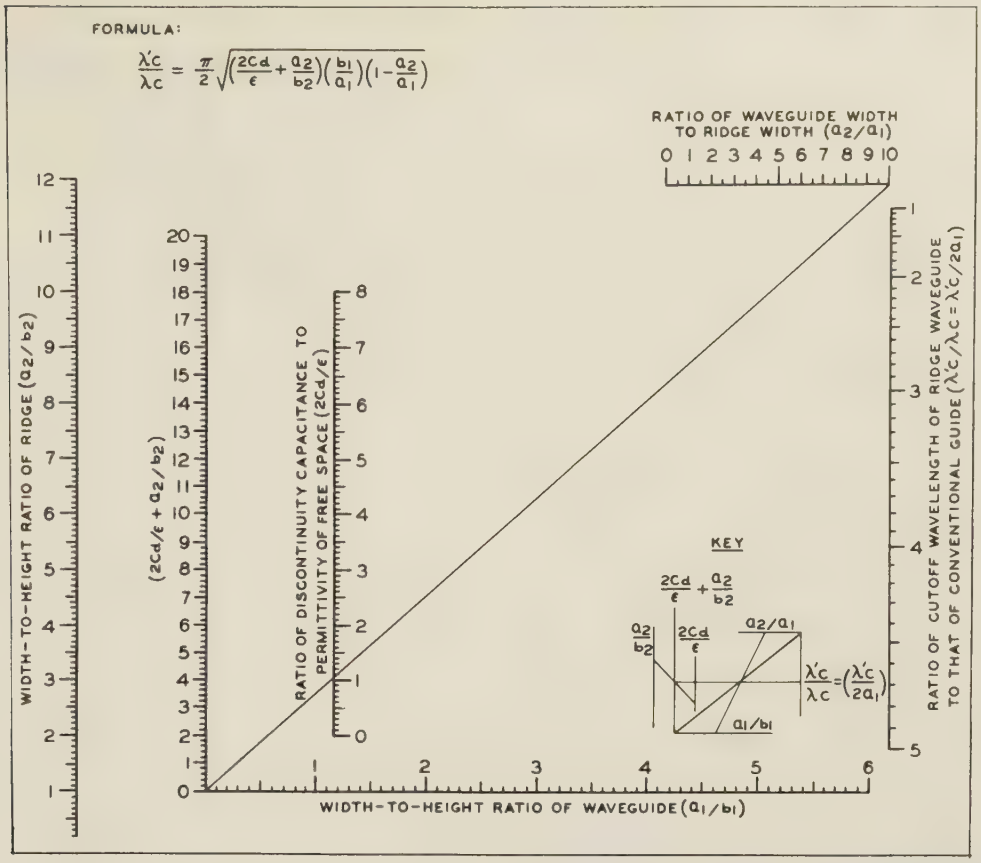

Fig. 4—Nomograph for the determination of the ratio, λ_c'/λ_c, of the cutoff wavelength, λ_c', of a ridge waveguide to the cutoff wavelength, λ_c, of a conventional rectangular waveguide having the same internal dimensions.

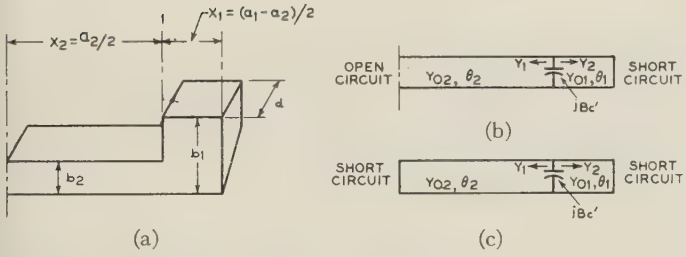

Fig. 5—Equivalent distributed parameter circuits for one half of a unit length of (a) ridge waveguide, (b) for odd modes of TE_{mo} waves, and (c) for even modes.

order roots to obtain the cutoff wavelengths of the higher-order odd TE_{mo} modes.

Because the ratios appearing in the arguments of the trigonometric functions are substantially less than unity, these functions can be replaced by the first two terms of their series expansions. Eq. (8) then becomes

$$\left[\frac{b_1}{b_2}\left(\theta_2+\frac{1}{3}\theta_2^3\right)+\frac{2C_d}{\epsilon}\frac{b_1}{a_2}\theta_2\right]\cdot\left[\left(\frac{a_1}{a_2}-1\right)\theta_2+\frac{1}{3}\left(\frac{a_1}{a_2}-1\right)^3\theta_2^3\right]=1. \quad (9)$$

When the cubic terms in (9) are discarded and remaining terms are solved for λ_c'/λ_c, (7) is obtained.

To improve the accuracy of λ_c'/λ_c determined from the chart, this approximate value is substituted only in the cubic terms of (9); the result is a quadratic equation θ_2 or in λ_c/λ_c'. This equation can be solved readily to obtain a more accurate value of λ_c'/λ_c.

The even modes of the TE_{mo} waves have voltage nodes at the center and at the end of the waveguide section in Fig. 5(a); the equivalent circuit for these modes becomes Fig. 5(c). The cutoff wavelengths of the TE_{20} and higher-order even modes as determined by the resonance of this circuit are given by

$$\frac{b_1}{b_2}=\frac{\frac{2C_d}{\epsilon}\frac{b_1}{a_1}\frac{\lambda_c}{\lambda_c'}\frac{\pi}{2}-\cot\left[\left(1-\frac{a_2}{a_1}\right)\frac{\lambda_c}{\lambda_c'}\frac{\pi}{2}\right]}{\cot\left(\frac{a_2}{a_1}\frac{\lambda_c}{\lambda_c'}\frac{\pi}{2}\right)}. \quad (10)$$

Characteristic Impedance of Ridge Waveguide

The characteristic impedance of ridge waveguide derived on the voltage-to-current basis is used in the calculation of tuning curves for a magnetron which is tuned by means of a ridge cavity attached to one of the magnetron resonators. This parameter is also used in impedance-matching problems. In the formulation of the voltage-to-current ratio, the current is separated into two components: 1) a longitudinal component on the top and bottom plates of the waveguide, which excites the principal fields, and 2) another longitudinal component at the point where the waveguide height changes, which produces the local fields.

The first component of current, I_{z1}, is determined by the field distribution along the waveguide cross section as shown in Fig. 6(a) and 6(b). Cohn[3] derived the expression for I_{z1} as

$$I_{Z1} = \frac{1}{Z_{TE}}\left(\frac{V_0}{b_2}\right)\left(\frac{\lambda_c'}{\pi}\right)\left(\sin\theta_2 + \frac{b_2}{b_1}\cos\theta_2\tan\frac{\theta_1}{2}\right) \quad (11)$$

where:

V_0 = the amplitude of voltage distribution at the center of the waveguide cross section

$$Z_{TE} = \frac{\sqrt{\frac{\mu}{\epsilon}}}{\sqrt{1-\left(\frac{\lambda}{\lambda_c'}\right)^2}} = \text{characteristic wave impedance.}$$

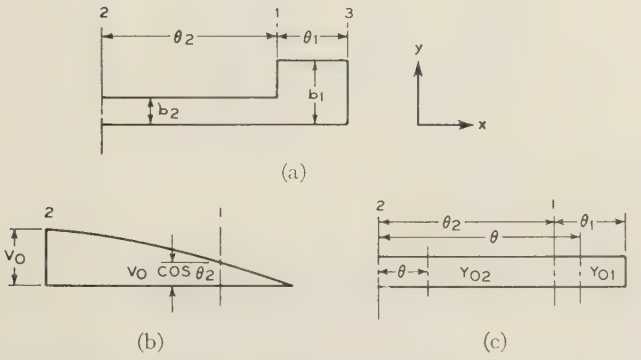

Fig. 6—(a) Cross section of ridge waveguide; (b) curve of voltage distribution across (a); (c) equivalent transmission line circuit.

Because the value of capacitance given by (2) agrees very closely with that found by the process of matching fields, the second current component, I_{z2}, can be determined from a consideration of the electrostatic field existing in the discontinuity region. Fig. 7 shows the field distribution at the ridge corner of a unit length of waveguide. In the derivation that follows, W represents the width of the region over which the local fields are predominant, Q the total charge over the same region, and E the electric field intensity at the discontinuity. The potential at plane 1 in Fig. 6(c) is given by

$$V_1 = V_0\cos\theta_2$$

and by the use of Gauss' law

$$\epsilon E(W)(1) = Q = C_d V_1 = C_d V_0\cos\theta_2,$$

from which

$$E = \frac{C_d V_0\cos\theta_2}{\epsilon W}.$$

The magnetic field strength, H, in ampere-turns per meter is given by $H = E/Z_{TE}$ and the longitudinal current for both sides of the ridge by

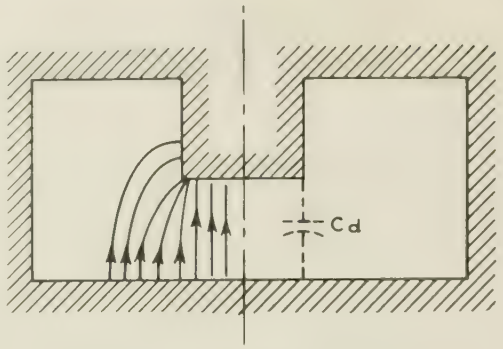

Fig. 7—Electrostatic-field distribution at corner of unit length of ridge waveguide.

$$I_{Z2} = 2HW = \frac{2C_d V_0\cos\theta_2}{\epsilon Z_{TE}}. \quad (12)$$

Eq. (12) agrees with Mihran's result.[15]

The characteristic impedance, Z_0, of the ridge waveguide is then

$$Z_0 = \frac{V_0}{(I_{Z1}+I_{Z2})} = \frac{Z_{0\infty}}{\sqrt{\left(1-\frac{f_c'}{f}\right)^2}}, \quad (13)$$

where

$$Z_{0\infty} = \frac{\sqrt{\frac{\mu}{\epsilon}}}{\frac{2C_d}{\epsilon}\cos\theta_2 + \frac{1}{\pi}\frac{\lambda_c'}{b_2}\left(\sin\theta_2 + \frac{b_2}{b_1}\cos\theta_2\tan\frac{\theta_1}{2}\right)}. \quad (14)$$

Because the ratios λ_c/λ_c' and a_2/a_1 are considerably less than unity for narrow ridges, $\cos\theta_2$ is approximately equal to 1, $\sin\theta_2$ to θ_2, and $\tan\theta_1/2$ to $\theta_1/2$. If the medium is free space and θ_2 and $\theta_1/2$ are less than 20°, (14) can be approximated by

$$Z_{0\infty} = \frac{120\pi}{\frac{2C_d}{\epsilon} + \frac{a_2}{b_2} + \frac{1}{2}\frac{a_1}{b_1}\left(1-\frac{a_2}{a_1}\right)^2}. \quad (15)$$

Based upon (15) and (13) the nomograph in Fig. 8 is constructed for the determination of $Z_{0\infty}$ and Z_0. For double-ridge waveguides, the value of Z_0 found from the left-hand side of the chart should be multiplied by 2.

Experimental Verification

In the development of a 10-kilowatt, 825-megacycle magnetron, a double-ridge waveguide was coupled to the magnetron to maintain a constant center frequency. The dimensions of the double-ridge cavity in centimeters were as follows: $a_1 = 16$, $a_2 = 2.56$, $2b_1 = 25.6$, and $2b_2 = 6$. Eqs. (7) and (9) are used to obtain $\lambda_c' = 2.095\,\lambda_c$ where $\lambda_c = 32$ centimeters. The guide wavelength, λ_g, is

[15] T. G. Mihran, "Closed- and open-ridge waveguides," Proc. IRE, vol. 37, pp. 640–644; June, 1949.

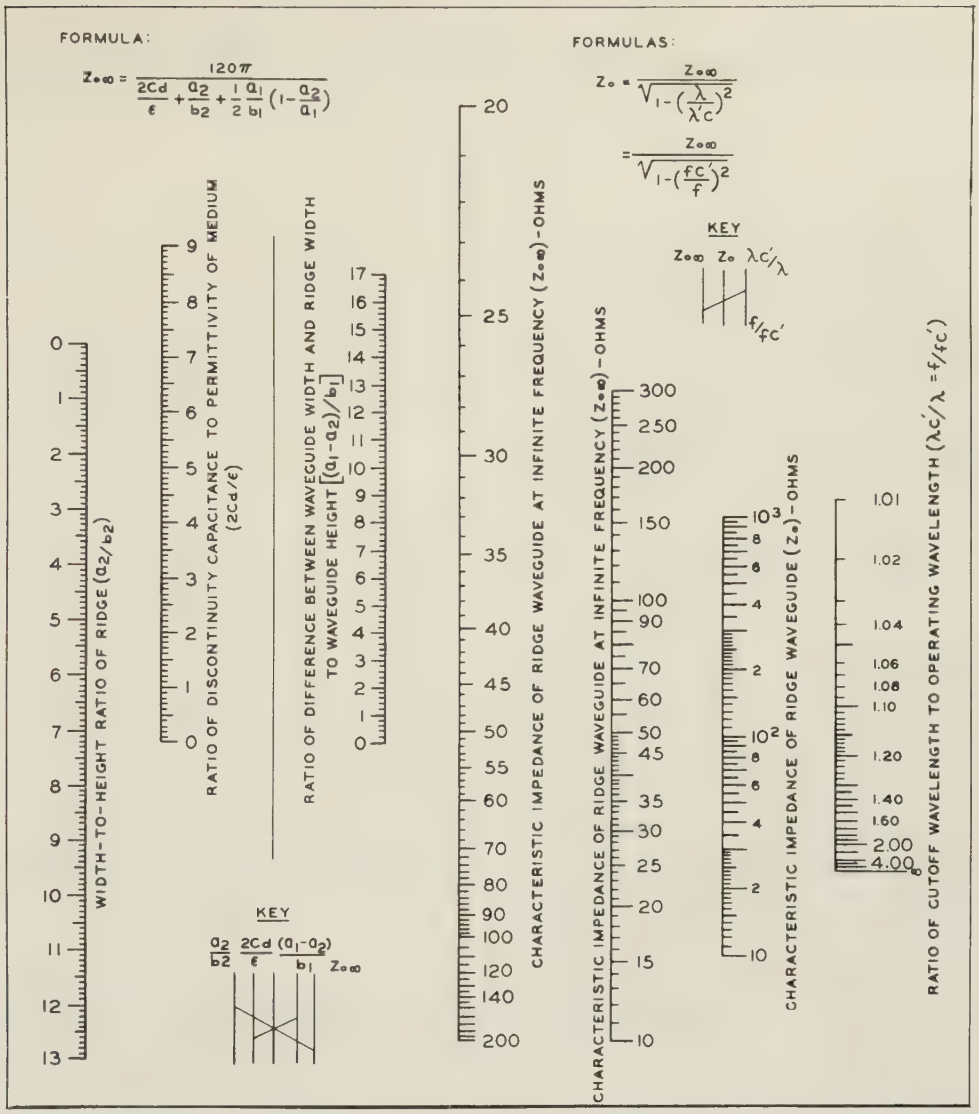

Fig. 8—Nomograph for determination of characteristic impedance of ridge waveguides having narrow ridges.

calculated from the relation

$$\lambda_g = \frac{\lambda}{\sqrt{1-\left(\frac{\lambda}{\lambda_c'}\right)}}$$

in which λ is the free-space wavelength corresponding to a particular frequency. At the resonant frequency, the cavity length should be half the guide wavelength of the ridge waveguide. For wavelengths of 40 and 30 centimeters, the calculated values of $\lambda_g/2$ as shown in Fig. 9 were 9.7 and 6.6 inches as compared with the measured values of 9.6 and 6.6 inches, respectively.

The characteristic impedance obtained from (15) and (13) was used to check the cold resonant frequency of the magnetron-cavity combination as a function of the cavity length. The measured and calculated results were in close agreement.

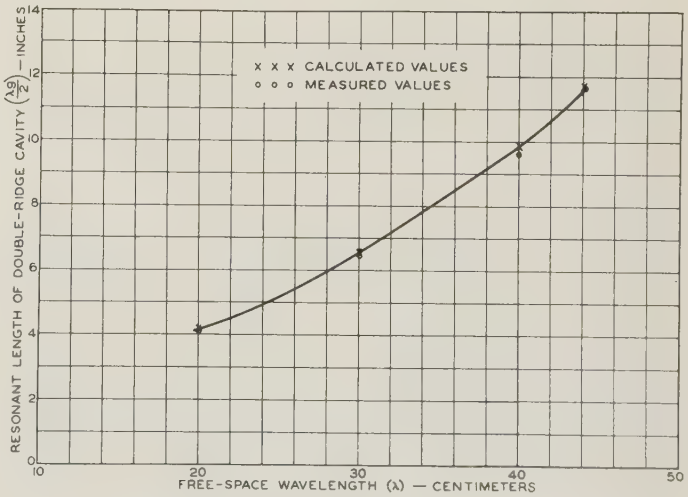

Fig. 9—Tuning curve for double-ridge cavity to be coupled to 10-kilowatt, 825-megacycle developmental tunable magnetron.

Excitation of Higher Order Modes in Spherical Cavities*

RABINDRA N. GHOSE†

Summary—An analysis for determining approximately the optimum position of the exciting source inside a spherical cavity for exciting any TE or TM mode is presented. For any TE or TM mode the orientation of the exciting probe or loop is determined by maximizing the surface integral of $\overline{H}$ or line integral of $\overline{A}$ which is proportional to the excitation coefficient for the corresponding mode. Specific examples of mode discrimination by proper orientation of the exciting source are also included in the paper. Besides, graphs of the surface integral of $\overline{H}$ and the line integral of $\overline{A}$ for various modes are presented to indicate the variation of mutual inductance for any mode, for different positions of the exciting source.

HIGHER ORDER modes, that is, modes having resonant frequencies higher than that of the dominant mode, can be excited in a resonant cavity either by a magnetic loop or by a short antenna or even by an aperture coupling. In general, in order to excite a cavity for any particular mode by a magnetic loop the plane of the loop is placed normal to the magnetic lines for the corresponding mode and preferably at a region where the magnetic lines are dense. Similarly, in order to excite a cavity for any desired mode with a short antenna, the axis of the antenna is placed parallel to the electric lines for the corresponding mode. The problem of excitation of a cavity by a circular or linear slit or aperture can be considered as a dual problem of exciting the cavity by a loop or as a short antenna, where the excited electric and magnetic fields are interchanged.

Theoretically, an infinite number of modes can be excited by a magnetic loop and a short antenna. However, for a practical purpose it is often desirable to energize a cavity for a particular mode and to optimize the excitation for that mode by suitably orienting the exciting source.

The problem of orientation of the source to obtain optimum excitation for a desired higher order mode in case of rectangular and cylindrical cavities is rather straightforward. Often determining the location of the source becomes obvious from the field configuration of the desired mode. In a spherical cavity, however, the field configurations are a little more complex, and further insight into the field distribution becomes desirable. In the present paper, attempts have been made to present an analytical treatment of the excitation problem to indicate how the exciting source should be oriented in order to obtain an optimum excitation for any desired higher order mode in spherical cavities. Specific examples are shown to indicate the nature of discrimination between the desired and undesired modes when the desired mode is optimized.

* Manuscript received by the PGMTT, April 6, 1956.
† Ramo-Wooldridge Corp., Los Angeles, Calif., formerly with RCA Victor Division, Camden, N. J.

Excitation by a Magnetic Loop

Let a small wire loop carrying a uniform current be enclosed in a cavity to energize it. Following the method introduced by Condon[1] it is often convenient to assume that the total magnetic potential $\overline{A}$ can be expanded in terms of arbitrary orthogonal modes such that

$$\overline{A}(\overline{S}, t) = \sum_{k=0}^{\infty} \overline{A}_k(\overline{S}) T_k(t) \tag{1}$$

and

$$\iiint_V \overline{A}_n(\overline{S})\overline{A}_m(\overline{S})dV = 0 \quad \text{for} \quad n \neq m$$
$$= V \quad \text{for} \quad n = m \tag{2}$$

where $\overline{A}_K(\overline{S})$ is the resonant wave pattern of the magnetic potential for the kth mode and is a function of space alone, $T_k(t)$ is the corresponding time function, V is the volume of the enclosure, and k, n, m are integers. Similarly, one can also assume that the time and the space distribution of the exciting current can be expanded in terms of $I_k(t)$ and $\overline{A}_k(\overline{S})$, that is,

$$i(\overline{S}, t) = \sum_{k=0}^{\infty} I_k(t)\overline{A}_k(\overline{S}). \tag{3}$$

The coefficients $I_k(t)$ can now be evaluated by using the orthogonality property assumed in (2).

$$I_k(t) = \frac{1}{V}\iiint_V \overline{A}_k(\overline{S})\, i(\bar{s}, t)dV. \tag{4}$$

It can be shown[1] that for a short magnetic loop in which the current is confined to a wire of small cross-sectional area

$$I_k(t) = \frac{I}{V} M_k \tag{5}$$

where M_k is the flux through the current carrying loop caused by unit amplitude of excitation of the kth mode. Therefore M_k is the mutual inductance between the exciting loop and the cavity for the kth mode.

The excitation coefficients for any mode can now be determined in terms of this mutual inductance, from the following differential equation derived from Maxwell's equation and (2) and (3).

$$\ddot{T}_k + \frac{\omega_k}{Q_k}\dot{T}_k + \frac{1}{\mu\epsilon}\left[\beta_k{}^2 T_k - I_k(t)\right] = 0 \tag{6}$$

where μ and ϵ are permeability and dielectric constants of free space respectively,

[1] E. U. Condon, "Forced oscillations in cavity resonators," *J. Appl. Phys.*, vol. 12, pp. 129–132; February, 1941.

$\omega_k = 2\pi \times$ resonant frequency for the kth mode
$\beta_k = 2\pi/\lambda_k$
$\lambda_k =$ resonant wavelength for the kth mode
$Q_k =$ resonant Q of the cavity for the kth mode.

If a time variation of $e^{i\omega t}$ is assumed such that $T_k = T_k e^{i\omega t}$

$$-\omega^2 T_k + \frac{i\omega\omega_k}{Q_k} T_k + \omega_k^2 T_k = c^2 \frac{I}{V} M_k. \tag{7}$$

At resonance

$$|T_k|_{\omega\to\omega_k} = c^2 \frac{I}{V} \frac{M_k Q_k}{\omega_k^2}. \tag{8}$$

From (5)

$$M_k = -\frac{1}{T_k} \int\int_S \overline{H}_{kn} dS \tag{9}$$

where $\overline{H}_{kn}$ is the magnetic field intensity for the kth mode normal to differential area ds on the plane of the current loop.

For any particular cavity, Q_k, ω_k, etc. corresponding to the kth mode are usually fixed and hence

$$T_k = N \sqrt{\left| \int\int \overline{H}_{kn} dS \right|} \tag{10}$$

N being a constant. Thus, the excitation for the kth mode can be optimized by making the surface integral in (10) maximum.

Excitation by a Probe

With the probe or electric coupling one can no longer assume that the resonator is charge free, and hence the introduction of both scalar and vector potential will be necessary to describe the entire electromagnetic field. Thus,

$$\overline{E} = -\mu \dot{\overline{A}} - \text{grad } \Phi \tag{11}$$

where Φ is the scalar potential function.

Substitution in Maxwell's equation gives

$$-\mu \frac{\partial}{\partial t} \text{div } \overline{A} - \nabla^2 \Phi = \rho/\epsilon$$

$$\nabla \times \nabla \times \overline{A} + \mu\epsilon \ddot{\overline{A}} = i(s, t) - \epsilon \text{ grad } \dot{\Phi}. \tag{12}$$

If $[i(\bar{s}, t) - \epsilon \text{ grad } \dot{\Phi}]$ is expanded such that

$$[i(\bar{s}, t) - \epsilon \text{ grad } \dot{\Phi}] = \sum_{k=0}^{\infty} I_k(t) \overline{A}_k(\bar{S})$$

the expression for $I_k(t)$ corresponding to (4) becomes

$$I_k = \frac{1}{V} \int\int\int_V [i(\bar{s}, t) - \epsilon \text{ grad } \dot{\Phi}] \overline{A}_k dV. \tag{13}$$

The contribution[1] due to the integral involving the displacement current vanishes, and so $I_k(t)$ remains same as that in (4).

$$I_k(t) = \frac{I}{V} \int \overline{A}_k \cdot dS \tag{14}$$

$$T_k = c^2 \frac{I}{V} \frac{\int \overline{A}_k \cdot dS}{\left[\omega_k^2 - \omega^2 - \frac{i\omega_k\omega}{Q_k}\right]}.$$

At resonance

$$|T_k| = c^2 \frac{I}{V} \frac{\left| \int \overline{A}_k \cdot dS \right|}{\omega_k^2} Q_k \tag{15}$$

which implies that T_k can be optimized by maximizing the integral.

Loop Coupling in Spherical Cavity

Let it be assumed that a spherical cavity is to be excited for a given TE mode by a loop. One may ask whether there is any optimum position at which the loop can be placed in order to obtain maximum excitation for the mode under consideration and if so how to determine this position.

For TE spherical modes $E_r = 0$, and the amplitude of the radial magnetic field is maximum near the axis $\phi = 0$. Hence, it will be desirable to place the plane of the loop perpendicular to this axis for the corresponding mode. Let the coordinates of the center of the loop as shown in Fig. 1 be $(\alpha, 0, 0,)$, and let a and δ be the radii of the sphere and the loop respectively.

The magnetic field equations[2] corresponding to any TE n, m, o mode are

$$H_r = i(n+1)nk_n \frac{\beta}{\omega\mu} \left[\frac{j_n(\beta r)}{\beta r}\right] P_n(\cos\theta) e^{i\omega t}$$

$$H_\theta = \frac{i\beta k_n}{\omega\mu} P_n'(\cos\theta) \frac{1}{\beta r} \frac{\partial}{\partial(\beta r)} [\beta r j_n(\beta r)] e^{i\omega t} \tag{16}$$

$$H_\phi = 0.$$

where k_n is proportional to the nth-mode amplitude.

From (14), it appears that the excitation for nth mode can be optimized by maximizing

$$\int\int_S \overline{H}_{nn} dS.$$

But as symmetry in the ϕ direction is assumed

$$\int\int_S \overline{H}_{nn} dS = 2\pi \int_0^\delta \overline{H}_{nn} \rho d\rho$$

where $\overline{H}_{nn}$ is the magnetic intensity for the nth mode normal to the loop. From Fig. 1, $\rho = \alpha \tan\theta$; $\gamma' = \alpha/\cos\theta$

[2] J. A. Stratton, "Electromagnetic Theory," McGraw-Hill Book Co., Inc., New York, N. Y.; 1941. The units are in unrationalized mks system which should not make any difference for the purpose of this analysis.

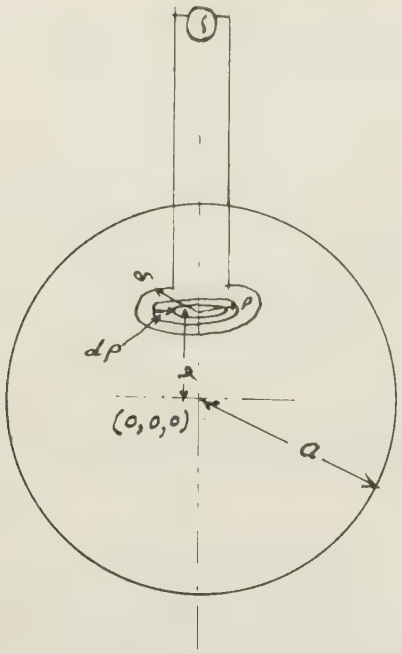

Fig. 1—Excitation of a spherical cavity by a loop.

$$\iint_S \overline{H}_{nn} dS = i(n^2+n) k_n \frac{\beta}{\omega\mu} \frac{2\pi\alpha}{\beta} \cdot \int_0^{\theta_0} j_n\left(\frac{\beta\alpha}{\cos\theta}\right) P_n(\cos\theta) \frac{\sin\theta}{\cos^2\theta} d\theta \quad (17)$$

where

$$\theta_0 = \tan^{-1}\delta/\alpha.$$

Expanding $P_n(\cos\theta)$ and interchanging the order of integration and summation one obtains

$$\iint \overline{H}_{nn} dS = i2k_n \frac{\pi\alpha}{\omega\mu} \sum_{p=0}^{t} \frac{1}{\Gamma(1/2)} \frac{(-1)^p \Gamma(n-p+\frac{1}{2}) 2^{n-2p}}{\Gamma(n-2p+1)p!} (n^2+n) \cdot \int_0^{\theta_0} j_n\left(\frac{\beta\alpha}{\cos\theta}\right) (\cos\theta)^{n-2p-2} \sin\theta d\theta \quad (18)$$

where

$$t = \frac{n}{2} \quad \text{for } n \text{ even}$$

$$= \frac{n-1}{2} \quad \text{for } n \text{ odd.}$$

But

$$j_n\left(\frac{\beta\alpha}{\cos\theta}\right) = \sqrt{\frac{\pi\cos\theta}{2\beta\alpha}} J_{n+1/2}\left(\frac{\beta\alpha}{\cos\theta}\right) = \sum_{q=0}^{\infty} \frac{\sqrt{\pi}(-1)^q \left(\frac{\beta\alpha}{2}\right)^{n+2q}}{2 \cdot q!\Gamma(q+n+3/2)} (\cos\theta)^{-n-2q}.$$

Substituting this expression for $j_n(\beta\alpha/\cos\theta)$ in (18) and evaluating the integral one obtains

$$\left|\iint_S \overline{H}_{nn} dS\right| = k_n(n^2+n) \frac{\pi\alpha}{\omega\mu} \sum_{p=0}^{t} \frac{1}{\Gamma(1/2)} \frac{(-1)^p \Gamma(n-p+1/2) 2^{n-2p}}{p!\Gamma(n-2p+1)} \cdot \sum_{q=0}^{\infty} \frac{\sqrt{\pi}}{2q!} \frac{(-1)^q \left(\frac{\beta\alpha}{2}\right)^{n+2q}}{\Gamma(q+n+3/2)} \cdot \left[\frac{1}{q+p+1/2} \left\{\left(1+\frac{\delta^2}{\alpha^2}\right)^{q+p+1/2} - 1\right\}\right]. \quad (19)$$

If

$$\delta \ll \alpha, \quad \left|\iint_S \overline{H}_{nn} dS\right| = k_n \frac{A\beta}{\omega\mu}(n^2+n) \frac{j_n(\beta\alpha)}{\beta\alpha} \quad (20)$$

where A is the area of the loop.

The condition for maximum excitation[3] is obtained by solving the following equation for α

$$\frac{\delta}{\delta(\beta\alpha)}\left[\iint_S \overline{H}_{nn} dS\right] = 0 \quad (21)$$

which yields the transcendental equation

$$\alpha\beta = n \frac{j_n(\beta\alpha)}{j_{n+1}(\beta\alpha)} \quad (22)$$

It should be noted that (22) shows the optimum position for the loop to obtain maximum excitation for the nth mode, for $m=1$, provided $j_n(\beta\alpha) \neq 0$ when α is non zero. This exception is seen to be obvious from (20) since the excitation approaches zero at the "zeros" of $j_n(\beta\alpha)$. Because of symmetry it will be desirable to place similar loop or loops at the corresponding positions where $m>1$.

Let the case of exciting the dominant mode be considered as an example. From (16) one finds that the first resonance occurs at

$$\tan\beta a = \beta a$$

$$\beta a = 4.493.$$

The condition for the maximum excitation of the dominant mode is obtained from (22), which, for $TE_{1,1,0}$ mode,[4] yields $\alpha\beta = 0$.

In order to observe the nature of discrimination against undesired modes when the desired mode is optimized, the relative variation of $\left|\iint \overline{H}_{nn} dS\right|$ for various positions of the exciting source and for different modes are shown in Fig. 2. It appears that if it is desired to excite the dominant mode in a spherical cavity,

[3] If δ is not too small in comparison with α the condition of maximum excitation is obtained by differentiating (19) directly with respect to α and setting the result equal to zero.

[4] From (20) it may appear that this solution is not permissible as $\delta \ll \alpha$ and $\alpha = 0$, also $\delta > 0$. But from the original equation for the magnetic field intensity as shown in (16) it can be shown that this solution is valid.

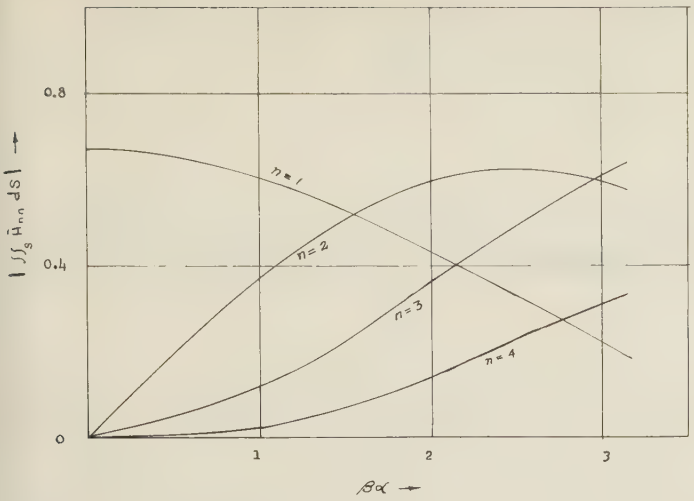

Fig. 2—Relative variation of $\iint H_{nn} dS$ for various positions of the loop and for different TE modes.

the best position at which the exciting loop can be placed is at the center of the sphere. An analysis for the excitation of the dominant mode in a spherical cavity by a loop placed at the center of the sphere has been made by Schelkunoff.[5]

Similarly when it is desired to optimize $TE_{2,1,0}$ mode, the transcendental (22) yields a numerical solution

$$\beta a = 2.5.$$

It can be seen that considerable discriminations can be made against the undesired modes when $\beta\alpha$ is chosen equal to 2.5 for $TE_{2,1,0}$ mode. The optimum positions of the loop for other modes can be determined similarly. The surface integral $\iint \overline{H}_{nn} dS$ when divided by T_n, as shown in (9) yields the mutual inductance for the nth mode. Thus Fig. 2 may be helpful to evaluate the mutual inductance of any mode for different positions of the loop at any frequency.

It may be remarked here that in the preceding analysis, the effect of distortion of the field due to the loop has been neglected. Furthermore, the loop has to be supported in the desired position inside the cavity by some means which may cause distortion. However, if δ is made reasonably small as is assumed in the analysis and the loop is supported by means of two parallel wires spaced very close to each other, the wave patterns will not change appreciably. If the total distortionless field components say H_r due to all the modes is represented as

$$H_r = \sum a_n \frac{(n^2 + n)}{\beta^2 r^2} [(\beta r) j_n(\beta r)] P_n(\cos\theta)$$

the distorted field under the above said conditions may be represented as

$$\overline{H}_r = \sum \bar{a}_n \frac{(n^2 + n)}{\beta^2 r^2} [(\beta r) j_n(\beta r)] P_n(\cos\theta)$$

[5] S. A. Schelkunoff, "Electromagnetic Waves," D. Van Nostrand Co., Inc., New York, N. Y., p. 298; January, 1956.

where

$$a_n \neq \bar{a}_n.$$

This inequality, however, will not affect the analysis for the optimization of the coupling for any mode considered independently.

Excitation of Higher Order Transverse Magnetic Modes

For transverse magnetic modes $H_r = 0$, and the loop excitation as described in the preceding section can no longer be used to excite higher order TM modes in the spherical cavity. A short antenna or probe (Fig. 3), introduced through the periphery of the sphere radially at $\phi = 0$, can be used, however, to excite spherical TM modes.

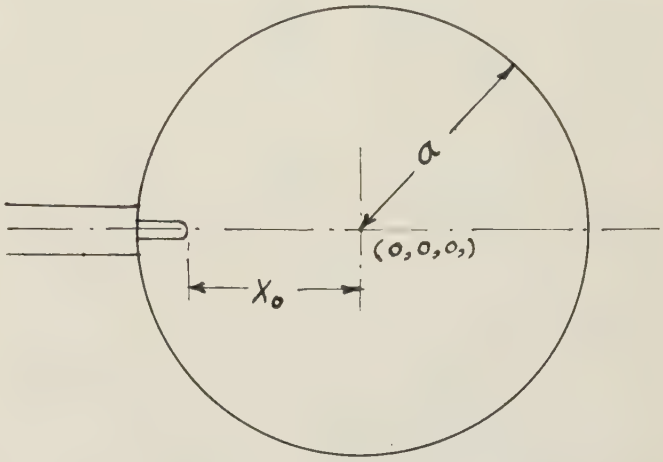

Fig. 3—Excitation of a spherical cavity by a probe.

For probe excitation as discussed in the previous section one finds

$$\overline{E} = -\mu \dot{\overline{A}} - \text{grad } \Phi.$$

When a time variation of $e^{i\omega t}$ is assumed

$$\overline{A} = \frac{i}{\omega\mu} [\overline{E} + \text{grad } \Phi]. \tag{23}$$

If the depth of penetration is the only variable to cause any change in the excitation T_k, $\int \overline{A}_k \cdot dS$ becomes maximum when

$$\int_{\beta X_0}^{\beta a} \frac{j_n(\beta r)}{\beta r} d(\beta r) = k \int \overline{A}_n \cdot dr \tag{24}$$

is maximum, K being a constant.

As the integral exists everywhere in the interval $[\beta a, \beta X_0]$, the integral can be expressed as

$$I = F(\beta a) - F(\beta X_0) \tag{25}$$

where

$$F(x) = \left[\int \frac{j_n(\xi)}{\xi} d\xi \right]_{\xi = x}.$$

In order to determine optimum depth of penetration which will optimize the line integral of $\overline{A}_n$, one can set

$$\frac{dI}{dX_0} = 0 \tag{26}$$

and obtain a solution for X_0 which will yield a maximum value of the integral I. From (25) and (26) it will appear that $\int \overline{A} n \cdot dS$ is maximum when

$$j_n(\beta X_0) = 0. \tag{27}$$

Fig. 4 shows the relative variation of $\int A_k \cdot dS$ for $k = 1, 2$, which correspond to $TM_{1,1,0}$, and $TM_{2,1,0}$ modes, when the cavity is designed for TM_{110} resonance which occurs at

$$\beta a = 2 \cdot 74.$$

It may be remarked that Fig. 4 not only indicates the nature of discrimination against undesired $TM_{2,1,0}$ mode, but also shows the variation of the mutual inductance for $TM_{1,1,0}$ and $TM_{2,1,0}$ modes for different probe lengths.

It is obvious that for any mode, $X_0 = 0$, which corresponds to a probe length equal to the radius of the sphere, is a solution of (26). In fact, for any mode such as the dominant mode where no zero of $j_n(\beta X_0)$ exists between βa and 0, the probe has to be extended up to the center of the sphere in order to obtain the maximum excitation. However, the probe length can be reduced for any higher order mode ($n > 1$) if the root of (27) be such that $\beta a > \beta X_0 > 0$. Under these circumstances it will not only be desirable but also necessary to extend the probe up to $X_0 \neq 0$, in order to avoid simultaneous excitation of the undesired modes.

It should be noted that the distortion of the wave pattern of the field components has not been considered in the present analysis. Thus the solution of the problem so obtained is an approximate one, and it approaches the true solution when the probe is made infinitely thin. The field distortion due to relative change in amplitude of the different mode components, however, will not affect the analysis for the optimization of the excitation coefficient as stated before.

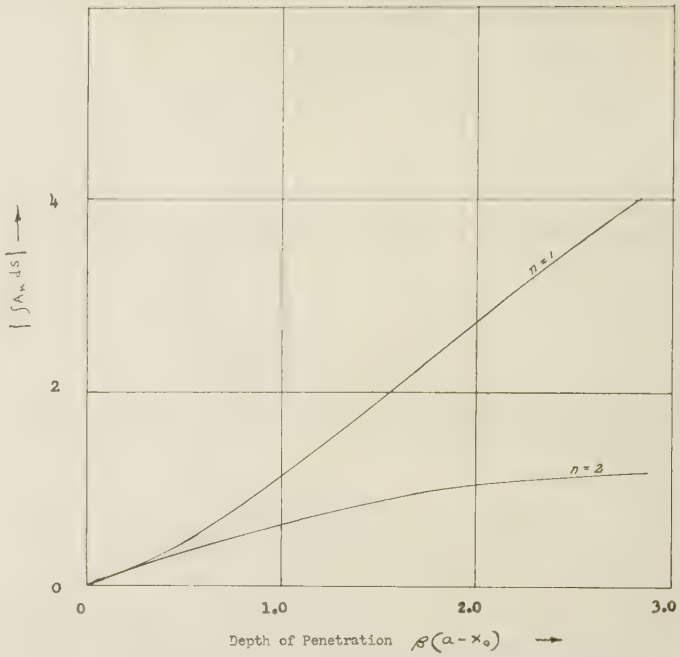

Fig. 4—Relative variation of $\int A_K dS$ for different probe length when the cavity is designed for TM_{110} mode.

Conclusion

A theoretical analysis for the excitation of higher order TE and TM modes in a spherical cavity is presented to indicate the optimum orientation of the loop or probe so as to obtain maximum excitation for any desired mode. A general expression for the position of a magnetic loop which can be used to excite any particular radial TE mode in a spherical cavity is found so that the excitation of the cavity for this particular mode becomes maximum at the corresponding position. Similarly, an expression for the probe length, in case of an antenna coupling, which will yield optimum excitation for any desired TM mode, is obtained. Although the problem of excitation of higher order modes in the spherical cavity alone has been discussed in the present paper, the basic principles can easily be extended to the problems of optimum excitation in rectangular, cylindrical, and elliptical cavities.

Strip Line Hybrid Junction*

HERBERT G. PASCALAR†

Summary—**The equivalent circuit of a strip line network is shown to display the properties of a hybrid junction. An application is illustrated by design of a balanced mixer and the presentation of the resultant measured data.**

Introduction

IN APPLICATIONS where two signal sources supply a common load, a high degree of isolation is required between the two sources if impedance matching between the load and one of the sources is not to be affected by the output impedance of the second source. This requirement is readily met through the use of a hybrid circuit. Hybrid circuits are of two general types.[1]

1) Hybrid rings or "rat races," where the isolation is accomplished by having two equal coupling paths between the two sources. At the desired operating frequency these path lengths differ by one half wavelength.
2) Hybrid junctions or magic tees, wherein isolation results from the symmetry relations between the electric and magnetic fields excited by the first input and those excited by the second input.

In the hybrid ring the isolation is frequency dependent; however, in the hybrid junction the isolation is independent of frequency. An additional feature of such a junction is that it incorporates independent tuning adjustments for matching the two sources to the load. Consequently a hybrid junction is preferable for wideband operation. For this reason a strip line hybrid junction was developed.

This report describes the action of one particular type of strip line hybrid junction, together with the design aspects and experimental results obtained in a typical application.

General Hybrid Junction

An equivalent circuit for the hybrid junction is given in Fig. 1(a), which is readily converted to the representation in Fig. 1(b). It is apparent that with respect to source 3 the loads R_1 and R_2 appear in parallel, while for source 4 the loads appear in series. At the load junction the voltage developed by source 3 is unbalanced, but the voltage there resulting from source 4 must be balanced with respect to ground.

In strip line where the dominant mode is TEM, the primary problem in constructing a magic tee is the design of a frequency insensitive balun for transforming the normally unbalanced transmission line to a line balanced with respect to ground.

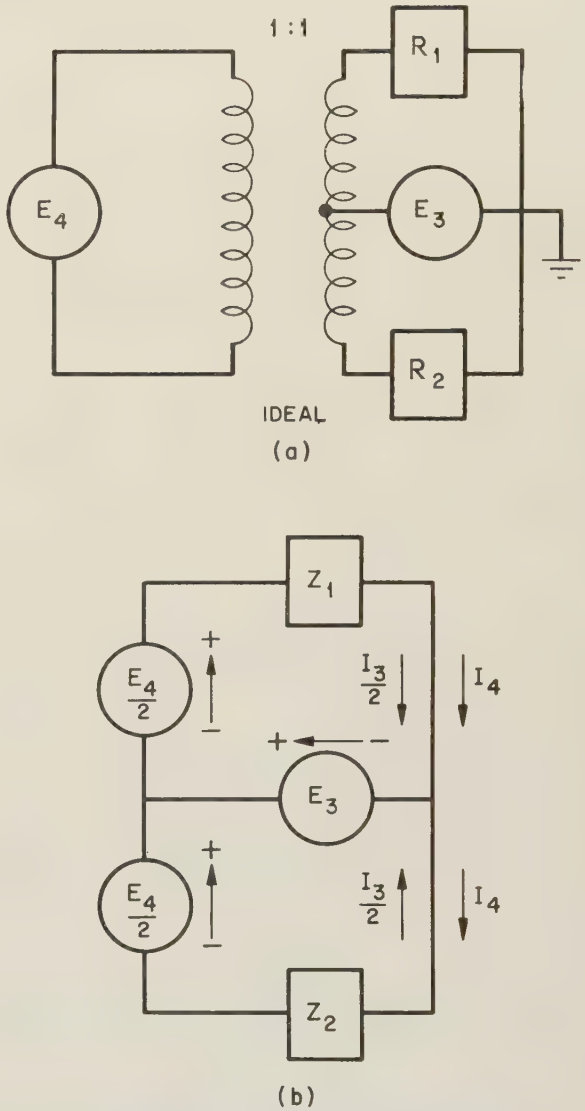

Fig. 1—Equivalent circuit of magic tee junction.

Wideband Balun

The balun to be considered[2] here may be represented as in Fig. 2(a). The individual conductors a, b, c are planes parallel to w, the ground plane. The equivalent

* Manuscript received by the PGMTT, May 3, 1956. The research in this paper was supported jointly by the Army, Navy, and Air Force under contract with the Mass. Inst. of Tech.

† Lincoln Lab., M.I.T., Cambridge, Mass.

[1] C. G. Montgomery, R. H. Dicke, and E. M. Purcell, "Principles of Microwave Circuits," M.I.T. Rad. Lab. Ser., McGraw-Hill Book Co., Inc., New York, N. Y., vol. 8, ch. 9; 1948.

[2] E. G. Fubini and P. J. Sutro, "A wide-band transformer from an unbalanced to a balanced line," Proc. IRE, vol. 35, pp. 1153–1155; October, 1947.

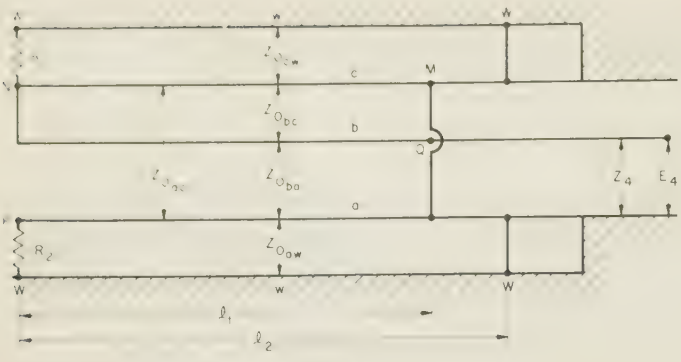

(a)

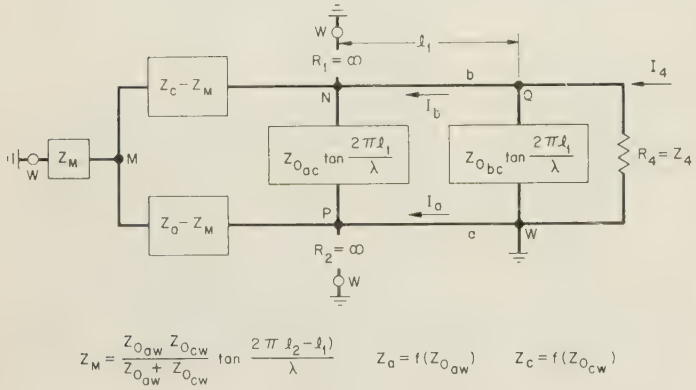

(b)

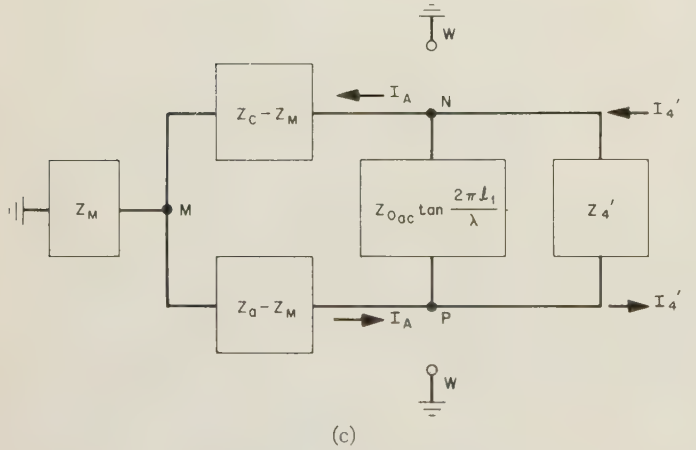

(c)

Fig. 2—(a) Wideband balun. (b) Equivalent circuit of balun. (c) Modified equivalent circuit.

circuit of this balun, for the unloaded condition at the output, is given in Fig. 2(b). Where the transmission line conductors b and a are planes, the transmission line currents I_a and I_b are restricted to the inside surfaces of a and b. The unbalanced input line of characteristic impedance Z_4 and open circuit voltage E_4 is replaced with the equivalent current source.

It is convenient to designate the unbalanced currents and voltages as symmetrical mode components I_s and V_s respectively. Likewise the balanced currents and voltages are designated as antisymmetrical current and voltage I_A and V_A respectively. In terms of the conductor currents and voltages at the output the definitions are:

$$V_s = \frac{V_{NW} + V_{PW}}{2} \tag{1}$$

$$I_s = \frac{I_b + I_a}{2} \tag{2}$$

$$V_A = \frac{V_{NW} - V_{PW}}{2} = \frac{V_{NP}}{2} \tag{3}$$

$$I_A = \frac{I_b - I_a}{4} \tag{4}$$

where V_{NW} and V_{PW} are the voltages of the nodes N and P with respect to the ground node W, and I_b and I_a are the conductor currents of the transmission line $b-a$ entering the nodes N and P.

The unbalance of the output voltage and current may be expressed by the ratios of the symmetrical to the antisymmetrical components. The criteria for perfect balun function is that these ratios both be equal to zero.

$$\frac{V_s}{V_a} = 0 \qquad \frac{I_s}{I_A} = 0. \tag{5}$$

If the output is short circuited at the node pair NP then the values of the various components are:

$$V_s = 0 \qquad I_s = 0$$
$$V_A = 0 \qquad I_A = I_b = -I_a. \tag{6}$$

For the short-circuited output both components of voltage are zero and the output current is completely antisymmetrical. Thus the transmission line to the right of the node pair NP may be replaced with a generator whose short-circuit current is completely antisymmetrical. In the modified equivalent circuit of Fig. 2(c) Z_4 and I_4 are the generator impedance and short circuit current referred to the plane of node pair NP. In the open-circuit condition the balun output is seen to be a reactive network excited by an antisymmetrical current generator. From (1) and (5) the open-circuit condition to be satisfied is:

$$V_s = \frac{V_{NW} + V_{PW}}{2} = 0. \tag{7}$$

If one considers the terminal pair mw open-circuited this becomes

$$V_s = I_A(Z_c - Z_a) = 0. \tag{8}$$

This requirement is fulfilled by setting:

$$Z_{0cw} = Z_{0aw} \tag{9}$$

then for any arbitrary value of Z_M

$$V_{PW} = -V_{NW}. \tag{10}$$

Thus, although the magnitudes of the antisymmetrical or balanced short-circuit current and open-circuit voltage are functions of frequency, the corresponding values of symmetrical or unbalanced components are zero at all frequencies.

The unloaded network has been shown to have perfect balun function independently of frequency; for this to remain true in the loaded condition requires the equality of the loads, *i.e.*,

$$R_1 = R_2. \tag{11}$$

Strip Line Hybrid Junction

A strip line hybrid junction is shown in Fig. 3. It consists of the above described balun to which is joined a symmetrical mode input network formed by the conducting planes *d* and *e* together with the ground plane *w*.

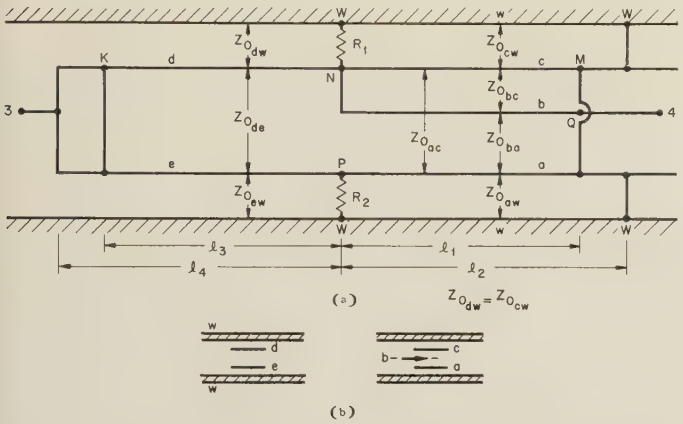

Fig. 3—Strip line magic tee junction. (a) Transmission line diagram. (b) Cross sections at plane *n-p-w*.

The equivalent circuit of the symmetrical mode input network is given in Fig. 4. In this circuit the reactance of the shorted line $Z_{0_{de}}$ connected between the nodes N and P can be excited by the antisymmetrical mode. Antisymmetrical currents on conductors *d* and *e* cancel at node K when

$$Z_{0_{dw}} = Z_{0_{ew}}. \tag{12}$$

Observing this condition together with the equality of the loads R_1 and R_2 insures that symmetrical input at terminal pair 3 produces equal voltages across the node pairs NW and PW.

The equivalent circuit of the hybrid junction is given in Fig. 5.

The midband wavelengths for inputs 3 and 4 are designated as λ_3 and λ_4 respectively. The conditions for unity power transfer (*i.e.*, zero reflection) at the center frequencies are:

Symmetrical network 3

$$l_2 = l_4 = \lambda_{3/4}$$

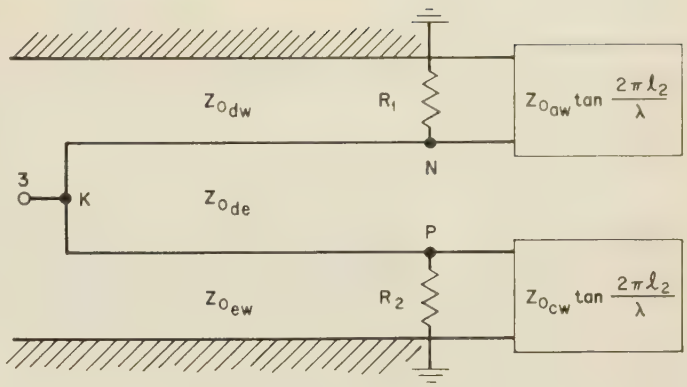

Fig. 4—Equivalent circuit of input 3.

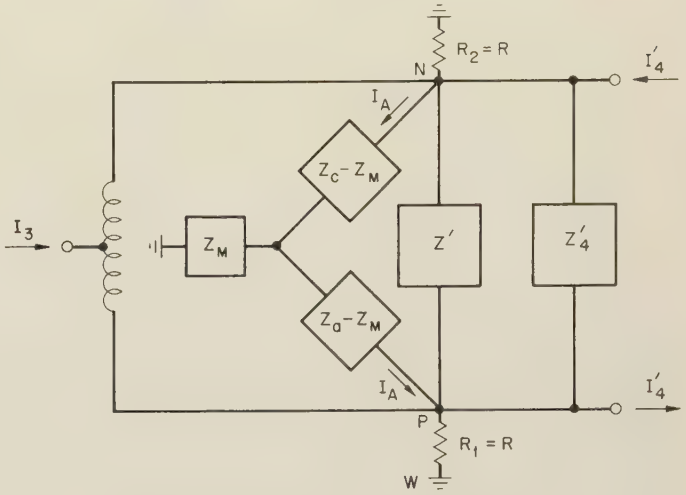

Fig. 5—Equivalent circuit for hybrid junction.

therefore

$$(Y_{0_{aw}} = Y_{0_{cw}}) \cot \frac{2\pi l_2}{\lambda_3} = 0$$

$$Z_{0_{dw}} = Z_{0_{ew}} = \sqrt{2R \cdot Z_3}.$$

Antisymmetrical network 4

$$l_1 = l_3 = \frac{\lambda_4}{4}$$

therefore

$$(Y_{0_{ac}} + Y_{0_{de}}) \cot \frac{2\pi l_1}{\lambda_4} = 0$$

$$Z_{0_{ba}} = \sqrt{2RZ_4}.$$

Assume the two center frequencies approximately equal and circuit Q's low.

Then at a frequency between the two center frequencies the inputs 3 and 4 are each closely matched to the loads R_1 and R_2. Input 3 excites the loads symmetrically, input 4 excites them antisymmetrically. The elements of the scattering matrix are thus:

$S_{33} = 0 \qquad S_{44} = 0 \qquad S_{34} = 0 \quad S_{43} = 0.$

$$S_{31} = S_{13} = \frac{1}{\sqrt{2}} \qquad S_{41} = S_{14} = \frac{1}{\sqrt{2}}$$

$$S_{32} = S_{23} = \frac{1}{\sqrt{2}} \qquad S_{42} = S_{24} = -\frac{1}{\sqrt{2}}$$

Hence:

$$S_{11} = 0$$
$$S_{22} = 0$$
$$S_{12} = S_{21} = 0.$$

The scattering matrix thus has the form

$$[S] = \begin{bmatrix} 0 & 0 & \frac{1}{\sqrt{2}} & \frac{1}{\sqrt{2}} \\ 0 & 0 & \frac{1}{\sqrt{2}} & \frac{-1}{\sqrt{2}} \\ \frac{1}{\sqrt{2}} & \frac{1}{\sqrt{2}} & 0 & 0 \\ \frac{1}{\sqrt{2}} & \frac{-1}{\sqrt{2}} & 0 & 0 \end{bmatrix}.$$

Because of the symmetrical nature of the junction the power division between R_1 and R_2, when fed from either 3 or 4 input, remains equal for all frequencies. The relative magnitude of symmetrical and antisymmetrical mode energy developed in the loads at a given frequency depends upon the relative value of the two transfer functions at the frequency in question.

In addition to the properties of the junction discussed above, which correspond to those commonly associated with hybrid junctions, there is the property of independent impedance matching of the loads to the individual inputs 3 and 4. This feature is particularly useful when the loads are not purely resistive or when two generators of widely different frequencies are to be employed. The length l_2 can be adjusted for matching the loads to the 3 input while l_1 and l_3 may likewise be adjusted for optimizing the match of the loads to the generator at input 4. There is no interaction between these two sets of adjustments. The only restrictions are that $l_2 \geqq l_1$ and $l_3 \leqq l_4$. Therefore it is apparent that 3 should be the low frequency input.

Design of a Balanced Mixer Employing a Strip Line Magic Tee

Initially a strip line magic tee junction was constructed following exactly the geometry as shown in Fig. 3(a) and 3(b). Since a balanced mixer was one of the more immediate applications contemplated, the line impedances were selected so as to provide impedance matching between fifty ohm input loads and two approximately equal crystal diode impedances. In the first model constructed, a pair of equal resistances equivalent to the crystal resistance was used to simulate the crystal diode loads. With this model, designed to operate in the uhf region, it was found possible to tune the inputs independently over a two-to-one frequency range, and throughout this region to maintain an isolation

$$\left(\frac{\text{power in 4 or 3}}{\text{power out 3 or 4}}\right)$$

between inputs in excess of 30 db.

On the basis of these results a new model was designed with the intention of achieving a reasonably compact and convenient construction. The only additional transmission circuitry required for the mixer is a band reject filter at the output of the IF terminals of the crystals, to provide a very low impedance of the rf return path to ground over a large frequency range. The location and construction of the filter are indicated in Fig. 6. The principal change in geometry was that instead of the transmission lines from 3 and 4 to the *NPW* plane lying on the same axis they were brought parallel to each other for reasons of space reduction and convenience of construction. They were, however, arranged so that symmetry with respect to the ground planes was preserved. To avoid mutual coupling the spacing between the axes of the lines was made much greater than the spacing between the conductors of either line. In Fig. 3(a) and 3(b) all the spaces between the conductors are assumed to have a relative dielectric constant of $\epsilon_r = 1$. However in the actual construction, the space between the planes containing conductors *a* and *c* as well as between conductors *d* and *e* contains teflon-fiberglass with $\epsilon_r = 2.5$. Aside from these differences in construction the arrangement and connection of conductors in the second model was the same as shown in Fig. 3(a).

Impedance measurements indicate that, in the uhf region, silicon and germanium microwave crystal diodes can be approximated as a parallel *RC* circuit with $R = 220$ ohms, $C = 3.75\ \mu\mu fd$. With the load impedances thus determined the values of $Z_{0_{ba}}$, $Z_{0_{dw}}$, and $Z_{0_{ew}}$ are fixed for the proper impedance transformation to the 50 ohm inputs. Thus, with crystal diode loads,

$$Z_{0dw} = Z_{0ew} = 2\sqrt{110 \cdot 50} = 148.6\Omega$$

for a length $(\lambda_3)/4$ starting at the *NPW* plane in the direction of input 3. For these lines $\epsilon_r = 1$. Since $f_3 = 390$ mc, $\lambda_3/4 = 7.58$ inches. The balun output is terminated in a resistance of 440 Ω at the frequency f_4. To obtain the required 8.8:1 transformation ratio within reasonable limits over a sufficiently wide frequency band a cascade of three one-quarter-wave length transformers was employed.[3] Starting at the *NPW* plane the characteristic

[3] J. C. Slater, "Microwave Transmission," McGraw-Hill Book Co., Inc., New York; N. Y.; 1942.

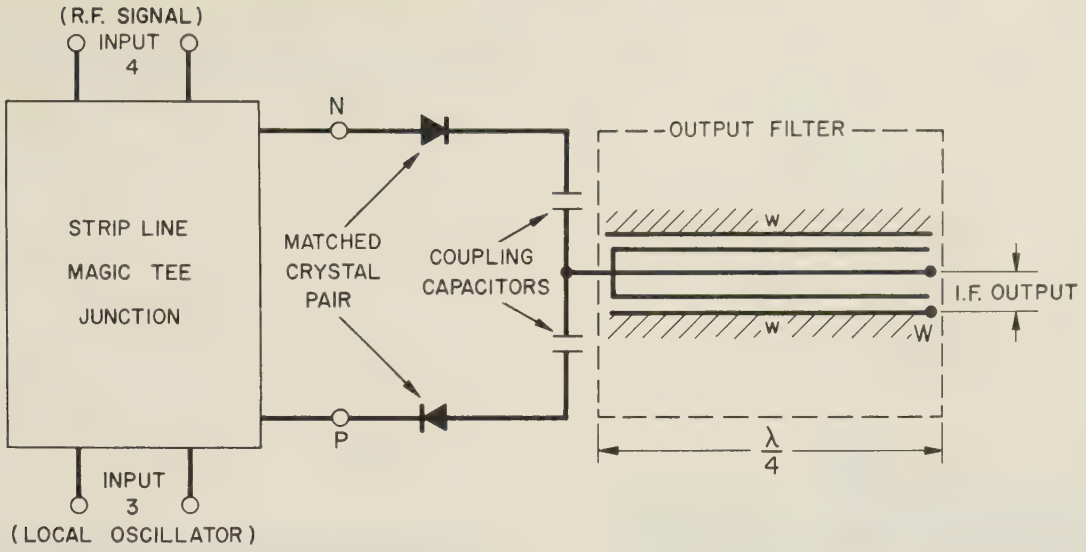

Fig. 6—Transmission line diagram of balanced mixer.

impedances are 225 ohms, 150 ohms, and 100 ohms respectively. With $f_4 = 450$ mc and $\epsilon_r = 2.5$ (Teflon fiberglass),

$$\lambda_4/4\sqrt{\epsilon_r} = 4.125 \text{ inches.}$$

Thus far in the design process no specification had been made for the characteristic impedances $Z_{0_{ca}}$, $Z_{0_{de}}$, $Z_{0_{bc}}$, $Z_{0_{aw}}$, and $Z_{0_{cw}}$. Wideband impedance matching, however, dictates that these values be as high as possible. Other factors restrict this choice, since in each of these transmission lines one or both conductors enter into the determination of other characteristic impedances. Because the final values of $Z_{0_{cw}}$, $Z_{0_{de}}$, $Z_{0_{aw}}$, and $Z_{0_{cw}}$ result from compromises between various design aspects including the physical configuration of the several conductors, it is well to discuss here the physical construction.

The dielectric sheets employed were of a standard thickness; consequently the width of conductor b is established by the required value of $Z_{0_{ba}}$. Since $Z_{0_{bc}} = Z_{0_{ba}}$ (225 ohms in the present case), the shunt reactance across nodes $M-Q$ due to the shorted length l_1 of transmission line $b-c$, is high at the frequency, f_4. Thus this shunting reactance will have a small effect.

To avoid coupling between inputs 3 and 4, the leakage field from conductor b must be kept to a minimum. Zero leakage would require conductors c and a to be infinitely wide; however, for widths greater than twice that of b the leakage is negligibly small.[4] The width of b is approximately 1/64 inch; thus making a and c 1/16 inch wide insures adequate shielding of b. Widths a and c are fixed in this way, and the spacing to the ground planes is selected to give a high value of $Z_{0_{cw}}$ and $Z_{0_{aw}}$. With a 1 inch spacing between the ground planes this value becomes 210 ohms.

The quarter wavelength short-circuited sections of lines cw and aw appear directly in parallel with the crystal diodes for an input at 3. These lines have a high characteristic impedance. This fact, together with the fact that no other shunt reactances occur and the required impedance transformation is only 2.2:1, yields a very broad-band impedance match for input 3.

Returning to considerations for input 4: $Z_{0_{ac}}$ and $Z_{0_{de}}$ remain to be determined. $Z_{0_{ac}}$ actually has already been fixed at 80 ohms by the standard dielectric thickness and the previously selected widths of a and c. The widths of conductors d and e were chosen as small as practically possible to yield a value of $Z_{0_{de}} \approx 220$ ohms. Assuming

$$l_3 = l_1 = \frac{\lambda_4}{4\sqrt{\epsilon_r}},$$

then at the NPW plane, for input 4, the total load resistance of 440 ohms is shunted by a reactance

$$57 \tan \frac{\pi}{2} \frac{\lambda_4}{\lambda}.$$

From this it appears that the maximum bandwidth for a vswr of 2:1 is 25 per cent. Clearly the useful operating bandwidth of input 4 will be considerably more limited than that of input 3. The ground plane spacings to conductors d and e was reduced to maintain $Z_{0_{dw}}$ and $Z_{0_{ew}}$ at the values required for the proper impedance transformation from input 3.

The values of the various transmission line impedances employed in the balanced mixer are listed in Fig. 7. At the crystal output, the transmission line band reject filter is equivalent to the choke type conventionally employed in coaxial lines.

[4] F. Assadourian and E. Rimai, "Simplified theory of microstrip transmission systems," Proc. IRE, vol. 40, pp. 1651–1657; December, 1952.

$Z_{0_3} = Z_{0_4} = 50$ ohms

$Z_{0_{aw}} = Z_{0_{cw}} = 210$ ohms

$Z_{0_{ba}} = Z_{0_{bc}} = 225$ ohms

$Z_{0_{dw}} = Z_{0_{ew}} = 149$ ohms

$Z_{0_{ac}} = 80$ ohms

$Z_{0_{de}} = 220$ ohms

Three stage quarter-wave section transformer
50 ohms–440 ohms.

Characteristic impedance of quarter-wave sections
100 ohms, 150 ohms and 225 ohms.

Fig. 7—Characteristic impedances in hybrid junction mixer.

folded conductor differs very little from the equivalent straight conductor in the uhf region. Conductors *a* and *c* were correspondingly enlarged to form the necessary outer conductor.

Type IN263 crystal diodes were employed because of their convenient construction and uniformity of electrical characteristics.

Measured Data on Strip Line Hybrid Junction Mixer

In Fig. 9 (opposite) is plotted the input vswr of the two inputs when l_2 was adjusted to tune input 3 to a center frequency of 560 mc, l_1 was equal to l_2, but l_3 was set to tune input 4 at a center frequency of 350 mc. Since the quarter-wave transformers for input 3 and 4 were designed for 390 mc and 450 mc respectively, there was, in this case, a considerable displacement from the optimum operating frequencies. As a consequence the bandwidths and match at the center frequencies were some-

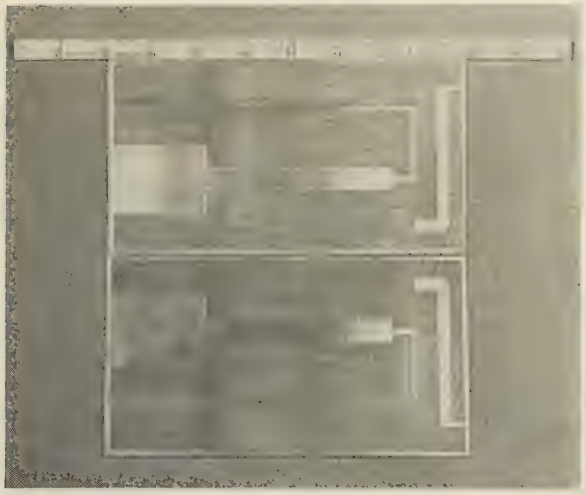

(a)

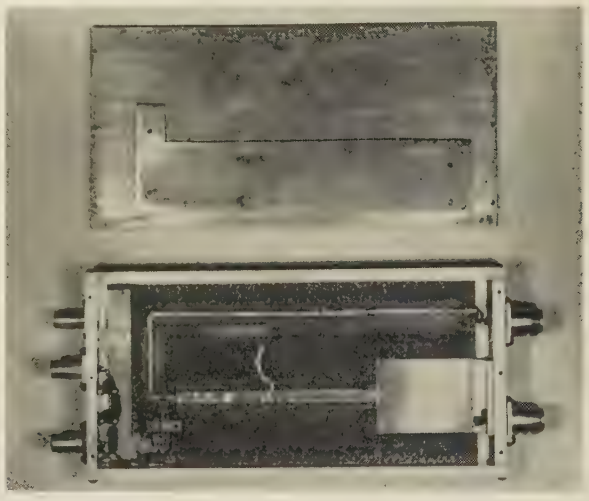

(c)

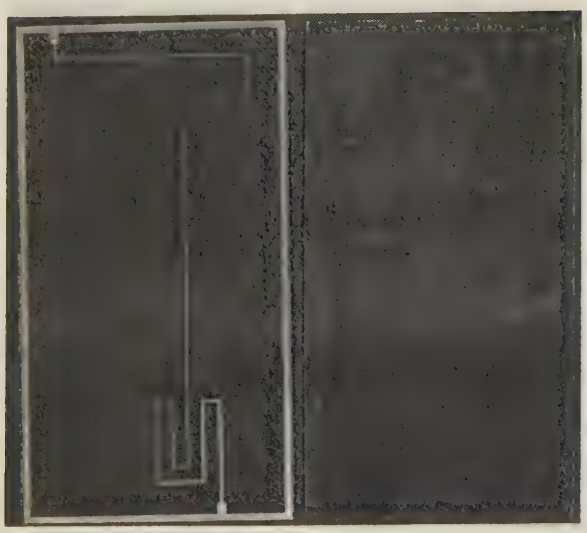

(b)

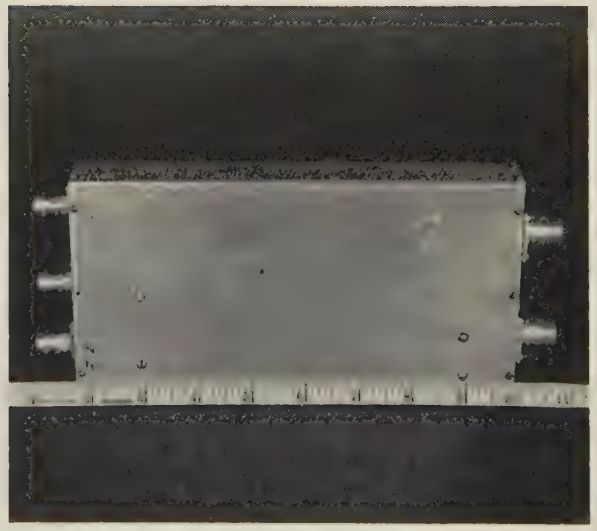

(d)

Fig. 8—(a) Printed board components on the sides facing the ground planes. (b) Sides facing each other. (c) Mixer with one of the ground planes removed. (d) Mixer completely assembled.

The construction details are shown in Fig. 8(a) to 8(d). The folded conductor seen in Fig. 8(b) is conductor *b*. Folded construction is employed to conserve space. For the particular dimensions and spacing chosen, the

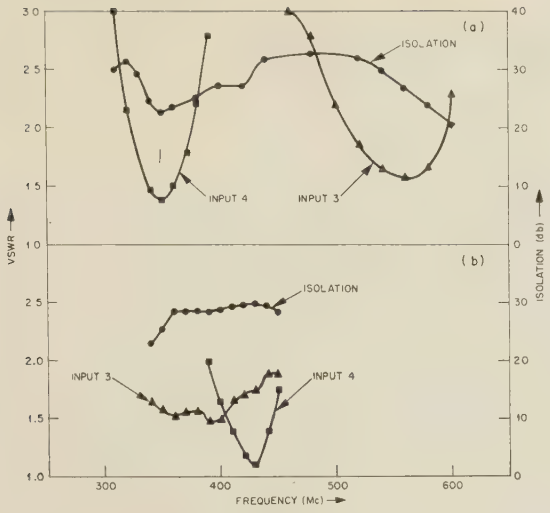

Fig. 9—Strip line magic tee mixer 1N263 crystals $I_x = 0.6$ ma. Input vswr and isolation vs frequency two sets [(a) and (b)] of l_1, l_2, l_3.

what impaired, but are still adequate for many applications. For a vswr $\leqq 2.0:1.0$ input 3 had a 15.2 per cent bandwidth and input 4 a 14.8 per cent bandwidth. Over the entire range from 300 mc to 600 mc the isolation between the two inputs exceeds 20 db. Fig. 9(b) gives the same data for the case where the inputs were tuned to frequencies corresponding to those of their quarter-wave impedance transformers. In this case for vswr 2.0:1.0, bandwidths were 3–36 per cent, 4–16.3 per cent. These results were very closely repeated by other crystals as shown in Fig. 10 where the input 3 impedance is given as a function of frequency for five different crystal pairs. For the data shown in Figs. 9(b) through 12, l_1, l_2, and l_3 were kept constant. Fig. 11 (next page) gives the impedance spread for five crystal pairs as seen from input 4. Fig. 12 shows the measured range of isolation for five crystal pairs for frequencies 340 mc through 460 mc.

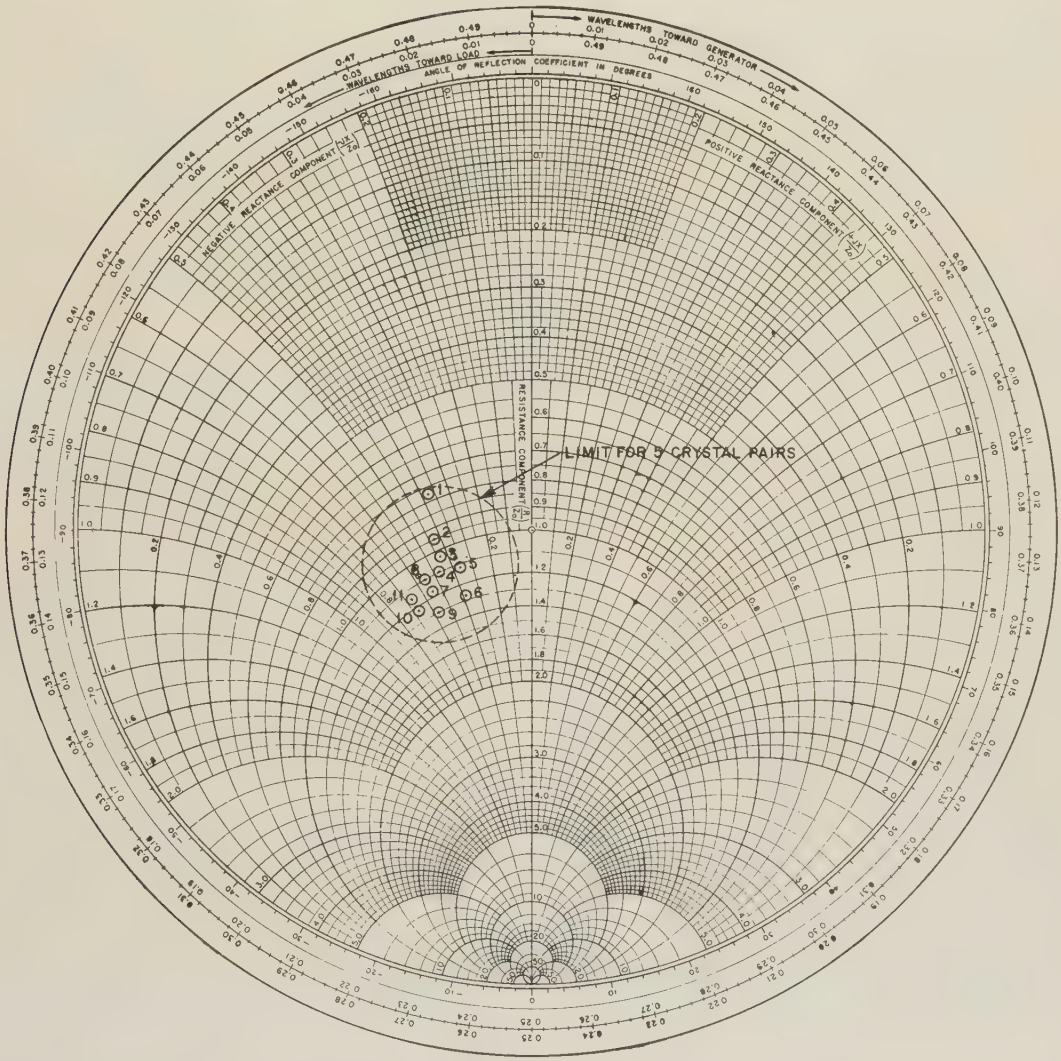

Point Frequency (mc)

1—340	5—390	8—420
2—350	6—400	9—430
3—360	7—410	10—440
4—370		11—450

Fig. 10—Impedance vs frequency, input 3 typical pair of 1N263 crystals $I_x = 0.6$ ma.

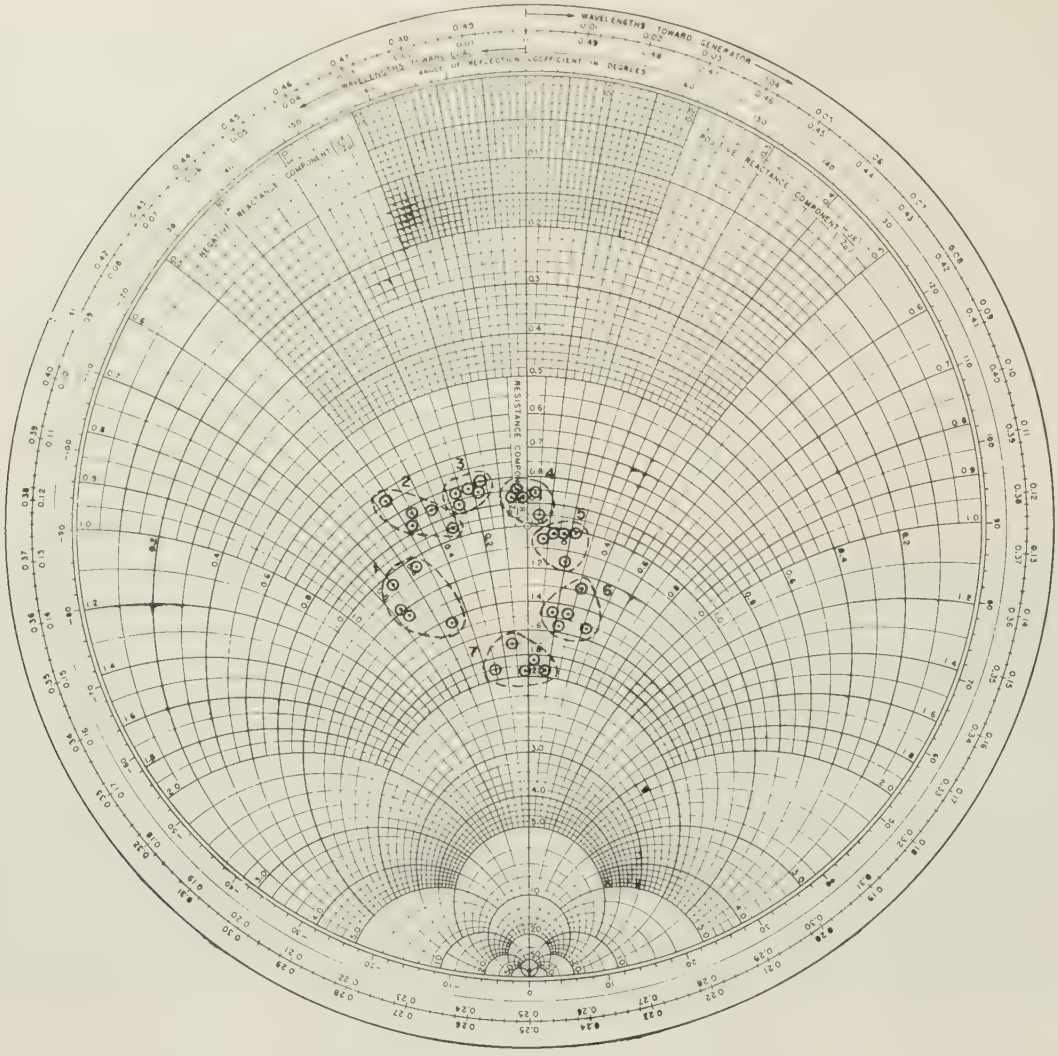

Group Frequency (mc)

1—390	3—410	6—440
2—400	4—420	7—450
	5—430	

Fig. 11—Impedance vs frequency, input 4 five pairs of 1N263 crystals $I_x = 0.6$ ma.

Conclusion

A strip line hybrid junction has been devised which maintains a relatively high degree of isolation between two inputs over a two to one frequency range. The inputs are capable of being independently tunable anywhere in these frequency ranges. Since the configuration is easily reproducible by printed circuit techniques, economy and space reduction are also available for the magic tee as well as hybrid rings now commonly used in strip line work. It would appear that this form of hybrid junction would be particularly well suited for applications in the uhf and vhf regions.

Acknowledgment

The author is indebted to E. Maxwell and C. E. Chase for helpful comments, and to P. S. Ambeau and D. F. Wiggin for assistance with the experimental work.

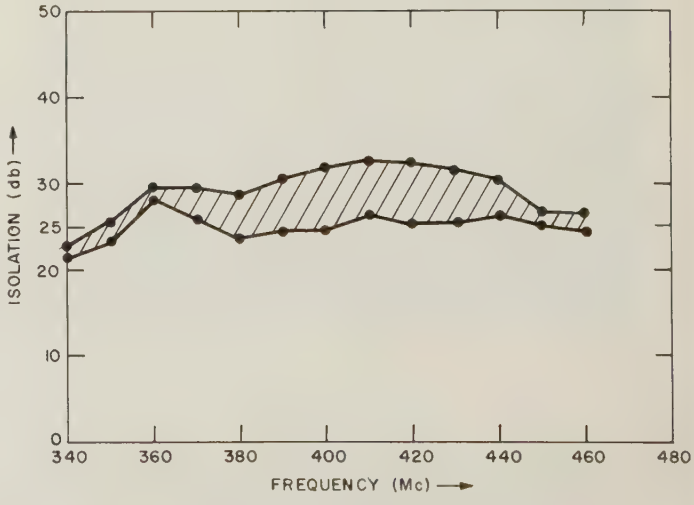

Fig. 12—Strip line magic tee mixer max and min isolation of five (1N263) crystal pairs.

Losses in Dielectric Image Lines*

D. D. KING† AND S. P. SCHLESINGER‡

Summary—The dipole mode in a dielectric rod permits an image system in which half the dielectric and its surrounding field are replaced by a metal sheet. If the field is allowed to extend many wavelengths outside the rod, the resulting line has very low losses. The contribution of the image surface to line loss is calculated, and shown to be generally less than the dielectric loss. Radiation from obstacles along the line is also discussed. Such obstacles in closed single-mode waveguides are useful for matching purposes. Although matching elements are easily constructed for the image line, radiation loss proves difficult to control.

Introduction

LOW ATTENUATION and freedom from higher modes are the principal advantages of the thin dielectric waveguide operated in the HE_{11} or dipole mode. However, supports and bends are difficult to achieve in the open waveguide. An image system which takes advantage of the plane of symmetry in the HE_{11} mode removes the support problem and facilitates the design of bends. The properties of bends and various circuit elements in dielectric image line have been discussed in earlier papers.[1,2] In the work to be described, losses in the image line are investigated.

In general, three types of dissipation contribute to the over-all loss in the dielectric image line. They are dielectric loss, conduction loss on the image surface, and radiation. The first of these, dielectric loss, has been calculated for circular rods by Elsasser.[3] We shall extend his formulation of the problem to include the calculation of ohmic loss on the image surface. Experimental results on the various kinds of loss are given, including radiation caused by obstacles along the line.

Calculation of Losses

The field components of the HE_{11} mode in a circular rod of radius a can be derived from the longitudinal components by differentiation. These are, inside the rod,

$$\begin{aligned} E_z &= AJ_1(p\rho/a)\cos\phi \\ H_z &= BJ_1(p\rho/a)\sin\phi \end{aligned} \tag{1}$$

and outside the rod,

$$\begin{aligned} E_z &= CK_1(q\rho/a)\cos\phi \\ H_z &= DK_1(q\rho/a)\sin\phi. \end{aligned} \tag{2}$$

Here the common factor $e^{-i\delta z+i\omega s}$ has been omitted. The parameters p and q are related to the propagation constant δ by the following relations

$$\begin{aligned} \delta^2 + (p/a)^2 &= \omega^2\mu_1\epsilon_1 \\ \delta^2 - (q/a)^2 &= \omega^2\mu_2\epsilon_2. \end{aligned} \tag{3}$$

The subscript 1 refers to the constants of the rod, 2 to the space outside the rod. Since only changes in dielectric constants are involved, it is convenient to write

$$\mu_1 = \mu_2$$

$$\epsilon = \epsilon_1/\epsilon_2 = \text{relative dielectric constant of the rod.}$$

Application of the boundary conditions yields a secular equation giving allowed values of p and q associated with a particular diameter-to-wavelength ratio for the dielectric rod, $2a/\lambda_0$. This parameter is given by

$$\frac{2a}{\lambda_0} = \frac{1}{\pi}\left(\frac{p^2+q^2}{\epsilon-1}\right)^{1/2}.$$

The secular equation is

$$(\epsilon f + g)(f+g) - (\epsilon/p^2 + 1/q^2)(1/p^2 + 1/q^2) = 0 \tag{4}$$

where the relative permeability μ is taken as unity and

$$f = \frac{J_1'(p)}{pJ_1(p)} \qquad g = \frac{K_1'(q)}{qK_1(q)}.$$

To calculate the attenuation α, we must find the quantity

$$\left|\frac{1}{\Phi}\frac{d\Phi}{dz}\right| = 2\alpha \tag{5}$$

where Φ is the total power flow along the line.

$$\Phi = \int S_z dA$$

$$S_z = E_\rho H_\phi^* - E_\phi H_\rho^*.$$

For dielectric loss in a dielectric rod of conductivity σ we have

$$\frac{d\Phi}{dz} = -\sigma\int_V E^2 dV.$$

We therefore obtain the following final form

$$\left|\frac{1}{\Phi}\frac{d\Phi}{dz}\right| = \frac{2\pi\sigma\int_0^a (E_\rho E_\rho^* + E_\phi E_\phi^* + E_z E_z^*)\rho d\rho}{2\pi\left|\int_0^a S_z\rho d\rho + \int_a^\infty S_z\rho d\rho\right|}. \tag{6}$$

The expression for attenuation obtained by Elsasser is

* Manuscript received by the PGMTT, May 5, 1956. Supported by AF Cambridge Res. Ctr., Air Res. and Dev. Command.

† Electronic Communications Inc.; formerly with Johns Hopkins Univ., Baltimore, Md.

‡ Columbia Univ., New York, N. Y.; formerly with Johns Hopkins Univ., Baltimore, Md.

[1] D. D. King, "Properties of dielectric image lines," IRE TRANS., vol. MTT-3, pp. 75–81; March, 1955.

[2] D. D. King, "Circuit components in dielectric image lines," IRE TRANS., pp. 35–39; December, 1955.

[3] W. M. Elsasser, "Attenuation in a dielectric circular rod," *J. Appl. Phys.*, vol. 20, pp. 1192; December, 1949.

$$\alpha_d = \tfrac{1}{2}\sigma\eta \text{ nepers/m} \qquad (\eta = \sqrt{\mu_0/\epsilon_0})$$
$$= 25.3(\epsilon\phi_0/\lambda_0)R \text{ db/m} \qquad (\phi_0 = \sigma/\omega\epsilon_1). \tag{7}$$

The ratio factor R is a complicated function which we display in the appendix together with a similar factor for the image surface loss.

The loss on the conducting surface of resistance $R_s = \sqrt{\omega\mu/2\sigma}$ is given by

$$\frac{d\Phi}{dz} = 2R_s\left|\int_0^a (H_\rho H_\rho^* + H_z H_z^*)d\rho + \int_a^\infty (H_\rho H_\rho^* + H_z H_z^*)d\rho\right|_{\phi=\pi/2}. \tag{8}$$

This gives for the attenuation

$$\frac{1}{\Phi}\frac{d\Phi}{dz} = \frac{2R_s\left|\int_0^a (H_\rho H_\rho^* + H_z H_z^*)d\rho + \int_a^\infty (H_\rho H_\rho^* + H_z H_z^*)d\rho\right|_{\phi=\pi/2}}{\pi\left|\int_0^a S_z\rho d\rho + \int_a^\infty S_z\rho d\rho\right|}. \tag{9}$$

The evaluation of this expression is only slightly more difficult than that of (6), which was done by Elsasser.

The resulting expression for α_c is

$$\alpha_c = (8R_s/\eta\lambda_0)R' \text{ nepers/m}$$
$$\alpha_c = (69.5R_s/\eta\lambda_0)R' \text{ db/m}. \tag{10}$$

The two ratio factors R and R' are displayed in the Appendix, together with the definitions of the quantities involved.

Comparison of Dielectric and Image Losses

Curves of the attenuation constants α_d and α_c are shown in Fig. 1 (opposite). These curves show that the image attenuation α_c is generally less than the dielectric attenuation in polystyrene. This is true except when the wave is very loosely bound and the dielectric loss becomes extremely small. Even a nichrome image surface fails to raise α_c to the level of dielectric attenuation α_d over an appreciable range of $2\alpha/\lambda_0$.

Measured points are shown on the curves for both dural and nichrome surfaces. The total attenuation $\alpha = \alpha_c + \alpha_d$ was measured, and a calculated value of α_d inserted to obtain α_c. The loss tangent for polystyrene is usually taken as 0.001; this value was used by Chandler[4] and yielded excellent agreement for α_d. Since the rod used in the present work was milled flat under oil, and glued to the surface with vinylite cement, some slight increase in the loss tangent might occur. The value 0.002 gives exact agreement between measured and predicted values as shown on the curve. The curve of α_d shown is based on a compromise value of 0.0015 for the loss tangent.

[4] C. H. Chandler, "An investigation of dielectric rod as wave guide," *J. Appl. Phys.*, vol. 20, pp. 1188–1192; December, 1949.

The resonator with nichrome image surface in place is shown in Fig. 2. A transmission measurement was made to obtain the resonance curve, and hence the loaded Q. The end losses were separated out by varying the resonator length through a number of resonances. The resulting data are shown in Fig. 3.

The slope of the L/Q vs length curves yields the line $Q = \beta/2\alpha$, and thence the total attenuation α. Even with the nichrome image surface, $\beta/2\alpha = 4000$. The over-all Q measured for the full length resonator was about 3000 for nichrome and 5400 for dural image surfaces. A rod with a smaller diameter than 5/16 inch yields a higher Q, but the 24-inch image surface is too narrow to prevent significant leakage at the edges; this results in unstable operation due to stray coupling.

Radiation Loss

In the absence of artificial boundaries to the field, there is no radiation loss, *i.e.*, the radial component of the Poynting flux is purely imaginary. On the other hand, the launching elements, bends or obstacles as well as a finite image surface, provide boundaries at which radiation occurs. The case of obstacles suitable for matching purposes is of particular interest, and we shall confine our discussion to such matching elements.

In hollow waveguides, an obstacle which sets up a reflected wave in the dominant mode also produces higher modes which provide reactive energy storage. This process is accompanied only by conduction loss, since the system is enclosed. In the open dielectric line, discontinuities in the line provide reflection in the dominant mode, but the higher modes excited at the obstacle radiate.

To investigate this effect, a number of obstacles have been measured on the interferometer bridge.[2] For unit incident power, the reflected power ρ^2 and the transmitted power τ^2 were measured simultaneously by the bridge circuit shown in Fig. 4. The results for an iris of 0.035-inch aluminum are plotted in Figs. 5 and 6 (p. 34). Here we note that the radiated power

$$\gamma^2 = 1 - \rho^2 - \tau^2$$

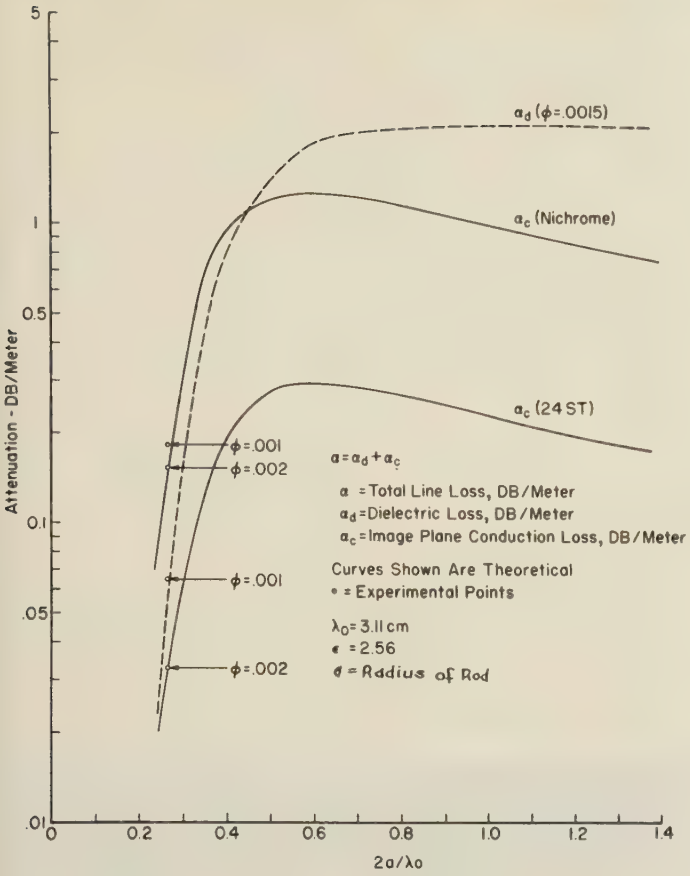

Fig. 1—Calculated attenuation curves for α_d, polystyrene dielectric, and α_c, a dural or nichrome image surface. Experimental points for the two image surfaces are shown for two assumed values of dielectric loss tangent ϕ.

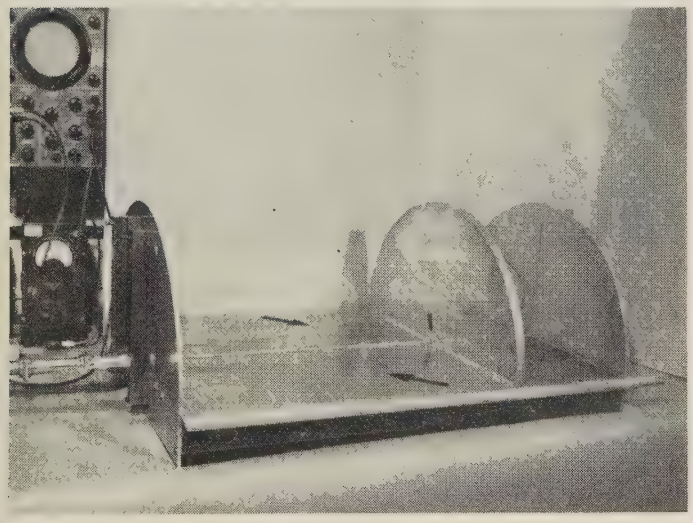

Fig. 2—Resonator for loss measurements at 9636 mc. Large arrows show the nichrome sheet glued to the aluminum surface. Small arrow shows field probe.

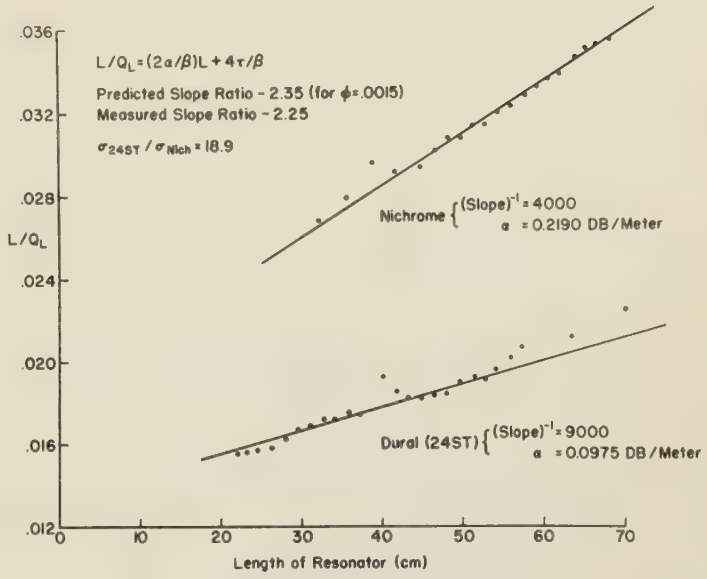

Fig. 3—Plot for separating line loss $(2\alpha/\beta)$ from end-face loss $(\beta/4\tau)$.

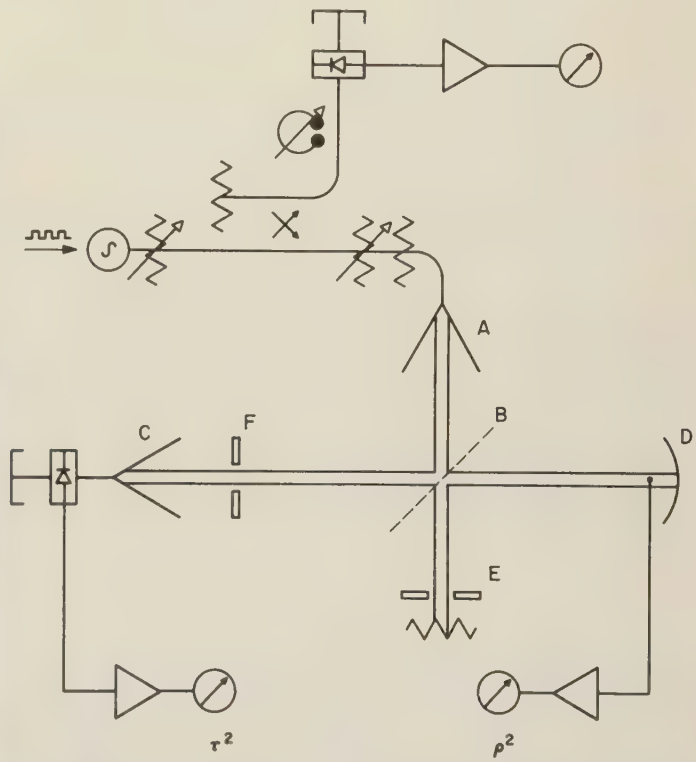

Fig. 4—Interferometer bridge—A) launching horn, B) half-reflecting mirror, C) receiving horn, D) parabolic reflector and coaxial detector, E) matched load, F) obstacle under test.

is small for both small and large reflections, but becomes large at intermediate ranges. For small apertures the reflecting surface is very sensitive to alignment, as might be expected. A slight backward tilt immediately reduces the reflections along the line and proportionately increases the radiation loss.

A plot of radiation loss γ^2 as a function of reflection coefficient ρ^2 for several obstacles is shown in Fig. 7. These include the iris, $\frac{1}{4}\times\frac{1}{8}$-inch strips, thin pins, and a dielectric sheet. A photograph of some of these obstacles placed along the line appears in Fig. 8. In general, the radiation loss is least for obstacles acting

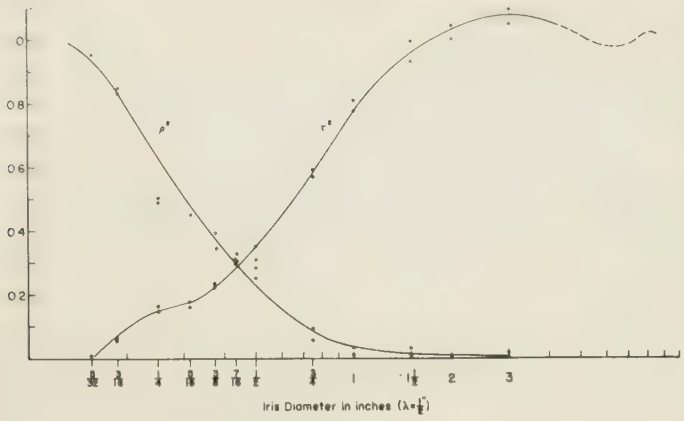

Fig. 5—Reflected power ρ^2 and transmitted power τ^2 for unit incident power on an iris.

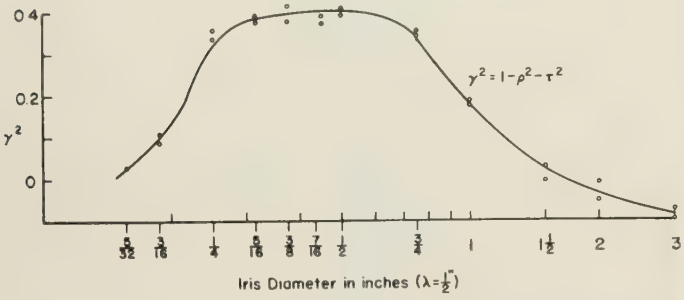

Fig. 6—Radiated power γ^2 for unit incident power on an iris.

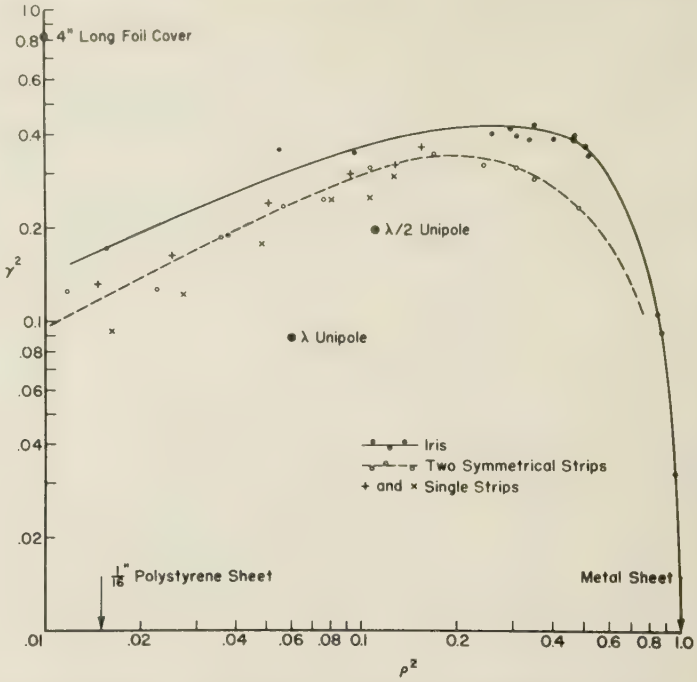

Fig. 7—Radiated power γ^2 as a function of reflected power τ^2.

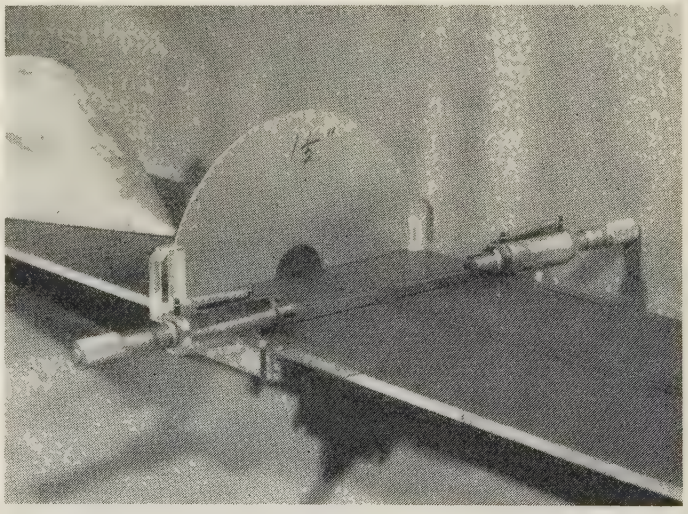

Fig. 8—Obstacles on the image line: (from right to left) adjustable matching pins; 0.20-inch unipole; 1½-inch iris; and tapered matched load.

in regions of high field close to the dielectric. An obstacle presenting only a flat surface across the entire guide produces no radiation, as might be expected by symmetry. Failing this, action on the field near or in the dielectric is most efficient in minimizing radiation loss. Detaching the field from the dielectric altogether is easy to do without reflections. A thin foil cover a few inches long performs this function admirably (see top of Fig. 7).

Conclusion

Both theory and experiment confirm the fact that an adequate image surface does not significantly alter the attenuation of the HE_{11} mode. The image loss is generally smaller than the dielectric loss, and decreases in the same rapid manner with the ratio $2a/\lambda_0$. This permits extremely low over-all attenuation on image lines with a large cross section in terms of wavelength. Since even a nichrome surface can be operated without objectionable losses, the type of image surface is not critical, even at very short wavelengths. A fine polish, such as is desirable in hollow guide for millimeter operation, is not required on the large image surface which carries low current densities.

The reflection data presented indicate that conventional matching elements produce appreciable radiation loss on an image line. A flat dielectric sheet having the desired reflection coefficient seems to be the most efficient matching element available. However, where loss is not important, very convenient adjustable pins can be mounted on the image surface to produce any desired reflections.

Appendix

The integration of (6) yields a final expression for dielectric rod attenuation given by (7) and repeated below

$$\alpha_d = 27.3(\epsilon\phi_0/\lambda_0)R \text{ db/m.} \tag{7}$$

The ratio factor R is given as

$$R = \frac{\dfrac{\epsilon - 1}{q^2}\,\dfrac{f^2 + \left(\dfrac{1}{p^2}\right) - \left(\dfrac{1}{p^4}\right)}{\left(\dfrac{1}{p^2} + \dfrac{1}{q^2}\right)} + (U^2 + V^2)X + \dfrac{4UV}{p^4}}{D} \tag{11}$$

where

$$D = UX(\epsilon + V^2) + UY(1 + V^2) + \frac{2V}{p^4}(\epsilon + U^2) - \frac{2V}{q^4}(1 + U^2)$$

$$U = \left[\frac{\left(\dfrac{\epsilon}{p^2} + \dfrac{1}{q^2}\right)}{\left(\dfrac{1}{p^2} + \dfrac{1}{q^2}\right)}\right]^{1/2}$$

$$V = \left[\frac{(\epsilon f + g)}{(f + g)}\right]^{1/2}$$

$$X = f^2 + \frac{(2f + 1)}{p^2} - \frac{1}{p^4}$$

$$Y = -g^2 - \frac{(2g - 1)}{q^2} + \frac{1}{q^4}.$$

Carrying out the operations indicated by (9) yields a final value of image surface loss

$$\alpha_c = 69.5(R_s/\eta\lambda_0)R' \text{ db/m.} \tag{10}$$

The ratio factor R' turns out to be

$$R' = \frac{\dfrac{f(I)}{J_1^2(p)} + \dfrac{f(H)}{K_1^2(q)}}{\pi\left(\dfrac{2a}{\lambda_0}\right) \cdot D}. \tag{12}$$

Here

$$f(I) = \frac{2}{3}\epsilon^2 \frac{S(2S + 3)}{p^3}\{I_1 + J_0(p)J_1(p)\} + I_1 \frac{V^2(\epsilon - 1)}{p(p^2 + q^2)} - \frac{1}{3} I_0 \epsilon^2 \frac{(S^2 - 3)}{p^3} - \frac{1}{3}\epsilon^2 \frac{S^2}{p^4} J_1^2(p)$$

$$f(H) = -\frac{2}{3}\frac{T(2T + 3)}{q^3}\{H_1 + K_0(q)K_1(q)\} + H_1 \frac{V^2(\epsilon - 1)}{q(p^2 + q^2)} - \frac{1}{3} H_0 \frac{(T^2 - 3)}{q^3} - \frac{1}{3}\frac{T^2}{q^4} K_1^2(q).$$

For the above

$$I_0 = \int_0^p J_0^2(z)dz \qquad I_1 = \int_0^p J_1^2(z)dz$$

$$H_0 = \int_q^\infty K_0^2(z)dz \qquad H_1 = \int_q^\infty K_1^2(z)dz$$

$$S = \left(\frac{UV}{\epsilon} - 1\right) \qquad T = (UV - 1).$$

General Synthesis of Quarter-Wave Impedance Transformers*

HENRY J. RIBLET†

Summary—This paper presents the general synthesis of a radio frequency impedance transformer of n quarter-wave[1] steps, given an "insertion loss function" of permissible form. This procedure parallels that of Darlington for lumped constant filters by providing the connection between Collin's canonical form for the insertion loss function and Richards' demonstration that a reactance function may always be realized as a cascade of equal length impedance transformers terminated in either a short or open circuit. In particular, it is shown that insertion loss functions of the form selected by Collin are always realizable with positive characteristic impedances, and that the synthesis procedure, for maximally flat and Tchebycheff performance, involves the solution, at most, of quadratic equations. In addition, this procedure permits the proof of Collin's conjecture that, for his insertion loss function, the resulting reflection coefficients are symmetrical. Finally, closed expressions are given for the coefficients of the input impedance of a given n section transformer in terms of the n characteristic impedances and vice versa.

Introduction

POSSIBLY the most frequent problem encountered in the design of distributed constant high frequency transmission line circuits, is that depicted in Fig. 1, where the several unknown characteristic

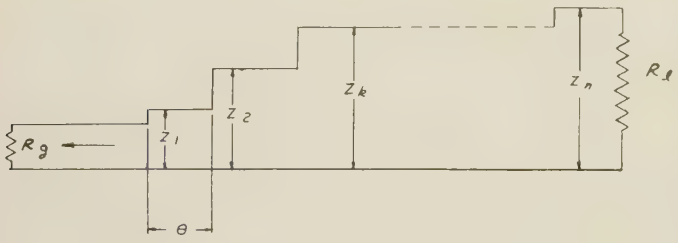

Fig. 1—Schematic of n section transformer.

impedances are to be chosen so as to minimize the input vswr over a given band of frequencies. The exact solution for a single step transformer is given by the well-known relationship $Z_1 = \sqrt{R}$. This result has found wide practical application. Nevertheless, in the range of microwave frequencies there are many problems which require more elaborate transformer designs. It is only recently that Collin[2] has given exact solutions for the cases of two, three, and four transformer sections. Previously the designer had available only approximate solutions depending on the assumption that the individual reflections are so small that multiple reflections can be neglected.

It is on this basis that the well known solution, that the logarithms of the ratios of the characteristic impedances vary according to the binomial coefficients, may be derived. Recently Cohn[3] has used the same approximation to obtain Tchebycheff performance in the band of low vswr. The same idea was applied by Riblet[4] to the equivalent directional coupler problem.

Although approximate solutions are easier to use and may be adequate for most applications, they cannot, in general, provide limits on optimum performance and do not provide a satisfactory foundation for a deeper understanding of the problem. For example, this exact synthesis procedure will prove certain general results which were only conjectured by Collin and not even suggested by those concerned with approximate solutions.

Now Collin's exact solution for cases $n = 2, 3, 4$ is not a true synthesis, but rather a solution by the method of undetermined coefficients. He determines the insertion loss function of a general transformer containing n unknown characteristic impedances by equating the unknown general insertion loss function to a special insertion loss function having the desired performance. The procedure leads, in general, to the simultaneous solution of higher degree algebraic equations each containing some or all of the unknowns. Disregarding the numerical difficulties involved, the process leaves a number of questions unanswered. Of these, the most important is the question of physical realizability, since Collin's procedure gives no assurance that the characteristic impedances obtained from the simultaneous algebraic equations will be positive real numbers. Without this assurance, no claim for optimum performance is justified.

* Manuscript received by the PGMTT May 18, 1956. Presented before the IRE West Coast Convention, August 1955, San Francisco, Calif. Since this paper was first submitted to the Proc. IRE for possible publication, the writer has learned of three other papers on the filter aspects of this theory. Why the treatment of physical realizability in each of these is incomplete, is discussed at the end of this paper.

† Microwave Development Labs., Wellesley, Mass.

[1] This discussion is in no way limited to quarter-wave transformers, since the only assumption required is that the steps be of the same length. This special case has been chosen, however, because the use of quarter-wave transformers rules out the possibility of super match, and because it is very likely that the optimum general monotonic transformer has quarter-wave steps, since this has already been demonstrated by the writer in the limiting case of narrow bandwidth and small impedance transformation, with the assistance of a key theorem proved for the purpose by J. E. Eaton.

[2] R. E. Collin, "Theory and design of wide-band multisection quarter-wave transformers," Proc. IRE, vol. 43, pp. 179–185; February, 1955.

[3] Seymour B. Cohn, "Optimum design of stepped transmission-line transformers," IRE Trans., vol. MTT-3, pp. 16–21; April, 1955.

[4] H. J. Riblet, "Super directivity with directional coupler arrays," Proc. IRE, vol. 40, pp. 994–995; August, 1952.

Now the key to physical realizability is provided by a theorem due to Richards,[5] which he has applied to the realization of reactance functions as a cascade of impedance transformers terminated in an open or short circuit.[6] In order to extend this synthesis procedure to a cascade of impedance transformers terminated in a resistance, it will be necessary and sufficient to impose an additional condition on the class of allowable impedance functions, and it will be shown that this condition is consistent with Collins' canonical insertion loss function so that one may proceed from the given insertion loss function to a step by step reconstruction of the network as a cascade of impedance transformers terminated in a resistance.

The Problem

Consider a section of uniform lossless transmission line of characteristic impedance Z_c, phase constant $2\pi/\lambda_g$, and length l. Then it is readily shown that the voltage and current at the input to the line section are linearly related to the voltage and current at the output by the equations

$$v_i = \cos\theta v_0 + jZ_c \sin\theta i_0$$

$$i_i = j \sin v_0 + \cos\theta i_0$$

with $\theta = 2\pi l/\lambda g$. In vector notation this is written

$$\begin{pmatrix} v_i \\ i_i \end{pmatrix} = \begin{pmatrix} \cos\theta & j\sin\theta Z_c \\ \dfrac{j\sin\theta}{Z_c} & \cos\theta \end{pmatrix} \cdot \begin{pmatrix} v_0 \\ i_0 \end{pmatrix}. \tag{1}$$

The matrix appearing above will be called the impedance matrix. The elements appearing in it are the general circuit parameters; and its determinant, as a consequence of reciprocity, is equal to unity. If the line section is terminated in an impedance Z_L so that $v_0 = Z_L i_0$, the input impedance, Z_i is readily found from (1). The impedance matrix of a cascade of line sections, as is shown in Fig. 1, is obtained by multiplication of the impedance matrices of the individual line sections. It is readily shown by induction that the impedance matrix of a cascade of n sections will have the form,

$$\begin{pmatrix} a_0 \cos^n\theta + a_2 \cos^{n-2}\theta + \cdots & \\ \qquad j \sin\theta(a_1 \cos^{n-1}\theta + a_3 \cos^{n-3}\theta + \cdots) & \\ j \sin\theta(c_1 \cos^{n-1}\theta + c_3 \cos^{n-3}\theta + \cdots) & \\ \qquad c_0 \cos^n\theta + c_2 \cos^{n-2}\theta + \cdots & \end{pmatrix} \tag{2}$$

with leading coefficients a_0, a_1, c_0, c_1 all real and greater than zero. By a well-known theorem in the theory of determinants, it is known that the determinant of (2) is again unity. The input impedance of such a cascade, for an arbitrary termination R is obtained as above by multiplying elements of the first column by R and dividing the sum of the resulting terms in the first row by the sum of those in the second.

It will be convenient, numerically, to reverse the procedure by constructing the impedance matrix from a known input impedance. This requires the identification of R, and the restoration of any constant multiplicative factor which may have been cancelled out. Both of these questions are resolved by making use of the fact that the impedance matrix (2) must reduce to the unit matrix for $\cos\theta = 1$.

The general theorems of analytic function theory are made available to us by the introduction of the frequency variable $p = -j \cos\theta/\sin\theta$.[7] Now as the guide wavelength λ_g varies from zero to infinity, *i.e.*, over all positive real frequencies, p ranges over all negative and positive values infinitely often. By theorems on analytic continuation, any formal result which is proved for a single determination of p will be valid for all the others. Thus we may treat p as a frequency variable in the familiar sense without any limitation on bandwidth. With this in mind, we may write

$$\begin{pmatrix} \cos\theta & j\sin\theta Z_c \\ \dfrac{j\sin\theta}{Z_c} & \cos\theta \end{pmatrix} = j\sin\theta \begin{pmatrix} p & Z_c \\ \dfrac{1}{Z_c} & p \end{pmatrix}. \tag{3}$$

Thus the impedance transformation for a single section of line may be written,

$$Z_i = Z_c \frac{pZ_L + Z_c}{Z_L + pZ_c} \tag{4}$$

where Z_L is the impedance terminating the transformer section. It is clear that the term $j \sin\theta$ appearing in (3) cancels out in (4). The same is true for the input impedance of a cascade of such transformers. The general input impedance of a cascade of such transformer sections, terminated in R can readily be shown to be

$$Z_i = \frac{(p^n + \sigma_2{}^e p^{n-2} + \cdots)R + (\sigma_1{}^e p^{n-1} + \sigma_3{}^e p^{n-3} + \cdots)}{\sigma_1{}^0 p^{n-1} + \sigma_3{}^0 p^{n-3} + \cdots)R + (p^n + \sigma_2{}^0 p^{n-2} + \cdots)} \tag{5}$$

with the σ's all real and positive.

If we consider complex as well as imaginary values of p and write $p = \sigma + iw$ and consider values of Z_i corresponding to values of p for which $\sigma \geqq 0$, we find by simple calculation that, whenever the real part of Z_L is positive, so is the real part of Z_i. In the terminology of Brune,[8] Z_i is a positive real function of p, whenever Z_L is positive real. We thus find, as a necessary condi-

[5] P. I. Richards, "A special class of functions with positive real part in a half-plane," *Duke Math. J.*, vol. 14, pp. 777–786, th. 6; September, 1947. See p. 779.

[6] P. I. Richards, "Resistor-transmission-line circuits," Proc. IRE, vol. 34, pp. 217–220; September, 1946. See p. 219.

[7] This differs from the frequency variable chosen by Richards and was selected so that $p = 0$ for transformer sections one-quarter wavelength long.

[8] O. Brune, "Synthesis of a finite two-terminal network whose driving point impedance is a prescribed function of frequency," *J. of Math. and Phys.*, vol. 10, pp. 191–236; October, 1931.

tion, that all impedance functions of p, of the form in (5), realizable as a cascade of transformer sections terminated in a resistance, must be positive real functions of p. Furthermore, we observe that the determinant of (3), neglecting $j \sin\theta$, is equal to p^2-1. Consequently, the product of the two polynomials in (5) beginning with p^n minus the product of the remaining polynomials is necessarily equal to $R(p^2-1)^n$. This theorem forms the basis for the synthesis procedure and may be summarized as described below.

Synthesis Theorem

The necessary and sufficient conditions that a rational function of p with real coefficients, written in the form

$$Z = \frac{m_1(p) + n_1(p)}{m_2(p) + n_2(p)}$$

with m_1 and m_2 odd or even and n_1 and n_2 even or odd, be the input impedance of a cascade of n, equal-length transmission line sections terminated in a resistance are: 1) Z must be a positive real function of p, and 2) $m_1(p)m_2(p) - n_1(p)n_2(p) = C(p^2-1)^n$. That these conditions are necessary has already been proven; that they are also sufficient is shown in an appendix.

Now it is well known that the insertion loss function P_L giving the ratio of the power available from a generator of internal impedance R_g to that dissipated in a termination of impedance R_L, through a network having the general circuit parameters A, B, C, D is

$$P_L = \frac{|AR_L + DR_g + B + CR_gR_L|^2}{4R_gR_L}. \tag{6}$$

We thus immediately infer from (2) that the insertion loss function can always be expressed as an even real polynomial in $\cos\theta$. This is Collin's theorem.

If we write the power loss ratio as

$$P_L = 1 + P_n(\cos^2\theta) \tag{7}$$

where P_n is a real polynomial of nth degree, we may attempt to select P_n so that all of its zeros fall in the frequency band of low vswr. This will give the maximum number of frequencies of zero loss. To avoid values of P_L less than 1, these roots must be double and we are led to the form,

$$P_L = 1 + Q_n^2(\cos\theta) \tag{8}$$

where Q_n is even or odd in $\cos\theta$. Collin has chosen $Q_n(\cos\theta) = kTn(\cos\theta/s)$ for Tchebycheff performance and $k\cos^n\theta$ for maximally flat performance, but the conclusions to follow will be true for any power loss ratio of the form (8).

Our problem then is to reverse the procedure above. We will start with a given power loss ratio of the form (8) and show how one may proceed step by step to determine the characteristic impedances Z_i which will result in the required power loss ratio. The numerical work is carried through most conveniently with the impedance matrices of the form of (2). Proof of physical realizability in terms of positive characteristic impedances will require the use of the synthesis theorem.

Along the way, we shall prove Collin's conjecture that $Z_iZ_{n+1-i} = R$ and derive closed expressions for the σ's of (5) in terms of the Z_i's, and, conversely, express the Z_i's explicitly in terms of the a's and c's of (2).

Solution of Problem

Now

$$P_L = \frac{1}{1 - |\Gamma|^2}$$

where $|\Gamma|^2$ is the square of the magnitude of the input reflection coefficient. Thus

$$|\Gamma|^2 = \frac{Q_n^2(\cos\theta)}{1 + Q_n^2(\cos\theta)}. \tag{9}$$

When $\cos^2\theta$ is replaced in (9) by p^2/p^2-1, condition 1[9] of the basic theorem, plus the requirement that Γ have the proper value at infinite frequency, yields a unique determination for Γ. Consider $\Gamma = Z-1/Z+1$. Since Z is to be pr, $|\Gamma| \leqq 1$ for all values of p in the right half plane. In particular, Γ can have no poles in the right half plane. Consider the zeros of $1+Q_n^2(\cos\theta)$. We need be concerned only with the n zeros of the expression as a function of $\cos^2\theta$. Now $p^2 = \cos^2\theta/(\cos^2\theta-1)$. Thus to each $\cos^2\theta$ root there exist two p roots differing in argument by 180°. Of these, one must fall in the left half plane except for the possibility that the two roots are imaginary. This is contrary to our choice of the power loss ratio, because it implies actual frequencies at which the power loss ratio is zero. Thus we select the n p-roots which fall in the left half plane, and use them to construct the denominator of Γ. When p is replaced by $-j\cos\theta/\sin\theta$, it will be found that

$$\Gamma = \frac{\alpha Q_n(\cos\theta)}{\cos^n\theta + \cdots + j\sin\theta(\cos^{n-1}\theta + \cdots)}. \tag{10}$$

The value of the complex constant α is uniquely determined from the requirement that

$$\Gamma = \frac{R-1}{R+1} \text{ for } \cos\theta = 1.$$

If Γ is written in p form the same determination can be made by putting $p = \infty$. Having constructed Γ, the input impedance Z is immediately determined from the

[9] For a discussion of the consequences of this assumption, the reader is referred to E. A. Guillemin, "The Mathematics of Circuit Analysis," John Wiley and Sons, Inc., New York, N. Y., 1949. See ch. 6, arts. 26–27.

equation

$$Z = \frac{1+\Gamma}{1-\Gamma}. \tag{11}$$

We must show that our construction of Γ, to avoid poles in the right half plane, yields a function which satisfies the *pr* condition of the theorem. Now, since Γ is analytic in the right half plane, according to the maximum modulus theorem, the maximum absolute value which it can achieve in the right half plane is attained on the imaginary axis. By construction, however, its value here is given by (9) and thus $|\Gamma| \leqq 1$ for all values of p in the right half plane. From (1) the real part of Z is readily found to be $(1-|\Gamma|^2)|1-\Gamma|^2$ and thus Z is *pr*.

It remains to show that the Z so constructed must satisfy condition 2 of the synthesis theorem. If the $\cos^2\theta$ in (9) is replaced by p^2/p^2-1, $|\Gamma|^2$ can be written

$$|\Gamma|^2 = \frac{R_n(p^2)}{(p^2-1)^n + R_n(p^2)}. \tag{12}$$

Now the Z obtained from (10) may be written in the form

$$Z = \frac{m_1(p) + n_1(p)}{m_2(p) + n_2(p)} \tag{13}$$

where m_1 and m_2 are even or odd and n_1 and n_2 are odd or even. Since Z is positive real, it is well known[10] that all the coefficients appearing in Z are of the same sign, and the degree of the numerator and denominator differ at most by unity. From (13), Γ becomes

$$\Gamma = \frac{m_1 - m_2 + (n_1 - n_2)}{m_1 + m_2 + (n_1 + n_2)}. \tag{14}$$

Now since $p = -j\cos\theta/\sin\theta$, $|\Gamma|^2$ is

$$|\Gamma|^2 = \frac{(m_1-m_2)^2 - (n_1-n_2)^2}{(m_1+m_2)^2 - (n_1+n_2)^2}.$$

The difference between the denominator and numerator of this fraction is $4m_1(p)m_2(p) - 4n_1(p)n_2(p)$. Comparing this with (12) we see that

$$m_1(p)m_2(p) - n_1(p)n_2(p) = Cp^2-1)^n.$$

Thus condition 2 is satisfied by our construction. It is also readily argued that the numerator and denominator of (13) must be of the same degree.

Once Z is known, the first unknown characteristic impedance is readily determined by subjecting Z to the transformation inverse to (4) with Z_c selected to have the value of Z for $p=1$, so that the degree of the resulting impedance function is one less than the degree of Z. This procedure can then be repeated, and the synthesis theorem assures us that all of the characteristic impedances so found are real, positive numbers.

[10] *Ibid.*, pp. 396–411.

For the purpose of numerical computation, it appears to be a little more convenient to use the impedance matrix in the form of (2) which is obtained by substituting (10) in (11). The load resistance R and proper multiplicative constant for the numerator and denominator are obtained from the condition that (2) must reduce to the unit matrix for $\cos\theta = 1$. If we multiply (2), either on the left or the right, by the inverse of (1)

$$\begin{pmatrix} \cos\theta & -j\sin\theta Z_c \\ \dfrac{-j\sin\theta}{Z_c} & \cos\theta \end{pmatrix}$$

the characteristic impedance, of either the first or last sections of the transformer may be determined from the condition that the resulting matrix must have elements whose degrees in $\cos\theta$ are reduced by one.

Special Results

We are now in a position to prove Collin's conjecture that, for power loss ratios of the form

$$P_L = 1 + Q_n^2(\cos\theta)$$

the impedances Z_i will satisfy the relationship $Z_iZ_{n+1-i} = R$. Since the numerator of $|\Gamma|^2$ is a perfect square, involving only $\cos\theta$, [see (9)], Γ has the form of (10). Since Γ is real for $\cos\theta = 1$, α must be real. Consequently the input impedance has the form

$$Z = \frac{A + j\sin\theta B}{D + j\sin\theta C}$$

with $C = B$. Thus the impedance matrix has the form

$$\begin{pmatrix} A/R & j\sin\theta B \\ j\sin\theta B/R & D \end{pmatrix}. \tag{15}$$

The important point is that the matrix is symmetric, except for the factor R, and this is the necessary and sufficient condition for the result. Consider

$$\begin{pmatrix} \cos\theta & -j\sin\theta Z_1 \\ \dfrac{-j\sin\theta}{Z_1} & \cos\theta \end{pmatrix} \cdot \begin{pmatrix} A/R & j\sin\theta B \\ j\sin\theta B/R & D \end{pmatrix} \cdot \begin{pmatrix} \cos\theta & -j\sin\theta Z_n \\ \dfrac{-j\sin\theta}{Z_n} & \cos\theta \end{pmatrix}. \tag{16}$$

If one considers the term in the first row and column of the left hand product, Z_1 must be chosen so that the coefficient of the highest power of $\cos\theta$ vanishes. Thus Z_1 is equal to the ratio of the highest coefficient of A divided by the leading coefficient in B. Thus $Z_1 = R/Z_n$, if one applies the same argument to the right hand product. If one evaluates the diagonal elements in the triple product, it is found that they have the same type of symmetry as is shown in (15). Thus the same arguments

may be repeated with the general consequence that $Z_iZ_{n+1-i}=R$.

It should be observed that, if one assumes symmetry about the other diagonal so that $A=D$, one is led to insertion loss functions of the form

$$P_L = 1 + \sin^2\theta Q_{n-1}^2(\cos\theta)$$

and one has end-for-end symmetry of the characteristic impedances, and the other properties of a band-pass filter.

We conclude the general discussion of the problem by exhibiting the bi-rational relationships between the coefficients in the impedance function, and the characteristic impedances. Consider the elementary symmetric functions σ_i of the n characteristic impedances $Z_1, \cdots, Z_n$, defined by the sums

$$\sigma_i = \sum Z_j \cdots Z_k$$

where summation is taken over all combinations of the n characteristic impedances taken i at a time. It is further assumed that the Z_i's in each term are ordered so that the index of any Z_i in a term is less than the indices of all the Z_i's which follow it, in same term. This is so-called lexicographical ordering. Then it may be shown by induction that the σ's of (5) may be constructed from the σ_i's as follows:

σ_i^e is constructed from σ_i by replacing alternate Z_i's, starting with the second, in each term by the reciprocal $1/Z_i$.

σ_i^0 is constructed as above except one starts with the first Z_i in each term.

For example for $n=3$, $\sigma_2^0=Z_3/Z_1+Z_3/Z_2+Z_2/Z_1$ and $\sigma_3^e=Z_1Z_3/Z_2$.

For the reverse of this procedure, it is convenient to assume that the input impedance is known in the form of the impedance matrix (2). One will find, in general, that

$$Z_{k+1} = \alpha_{k+1}/\beta_{k+1} \tag{17}$$

where

$$\alpha_{k+1} = \frac{\begin{vmatrix} 1 & 0 & 1 & 0 & \cdots & 1 \\ a_0 & -c_1 & 0 & 0 & \cdots & 0 \\ a_2 & c_1-c_3 & a_0 & -c_1 & \cdots & 0 \\ \cdot & \cdot & a_2 & c_1-c_3 & \cdots & 0 \\ \cdot & \cdot & \cdot & \cdot & \cdots & \cdot \\ a_{2k} & c_{2k+1}-c_{2k-1} & \cdot & \cdot & \cdots & 0 \end{vmatrix}}{\begin{vmatrix} 1 & 0 & 1 & 0 & \cdots & 0 \\ a_0 & -c_1 & 0 & 0 & \cdots & 0 \\ a_2 & c_1-c_3 & a_0 & -c_1 & \cdots & \cdot \\ \cdot & \cdot & \cdot & \cdot & \cdots & \cdot \\ \cdot & \cdot & \cdot & \cdot & \cdots & \cdot \\ a_{2k} & c_{2k+1}-c_{2k-1} & \cdot & \cdot & \cdots & -1 \end{vmatrix}}$$

and

$$\beta_{k-1} = \frac{\begin{vmatrix} 1 & 0 & 1 & 0 & \cdots & 1 \\ c_1 & -a_0 & 0 & 0 & \cdots & 0 \\ c_3 & -a_2 & c_1 & -a_0 & \cdots & 0 \\ \cdot & \cdot & \cdot & \cdot & & \\ \cdot & \cdot & \cdot & \cdot & & \\ \cdot & \cdot & \cdot & \cdot & & \\ c_{2k+1} & -a_{2k} & \cdot & \cdot & \cdots & 0 \end{vmatrix}}{\begin{vmatrix} 1 & 0 & 1 & 0 & \cdots & 0 \\ c_1 & -a_0 & 0 & 0 & \cdots & \cdot \\ c_3 & -a_2 & c_1 & -a_0 & \cdots & \cdot \\ \cdot & \cdot & \cdot & \cdot & \cdots & \cdot \\ \cdot & \cdot & \cdot & \cdot & \cdots & \cdot \\ c_{2k+1} & -a_{2k} & \cdot & \cdot & \cdots & -1 \end{vmatrix}}.$$

These determinations are obtained by extending the idea shown in the left hand product of (16). The first impedances $Z_1, \cdots, Z_k$ are assumed known, and the product of the corresponding inverse impedance transformations is written in general form with the coefficients of the elements in the first row given the general designations, $X_1, \cdots, X_k$. When this inverse matrix of degree k in $\cos\theta$ is multiplied by the given impedance matrix, a matrix of degree $k+n$ in $\cos\theta$ results. All the coefficients of $\cos\theta$ in the first row and column of this matrix must be zero, except the coefficient, α_{k+1}, of $\cos^{n-k}\theta$, and the coefficients of lower degree terms. If we treat α_{k+1} as an unknown, we find that we have exactly $k+1$ linear equations for the determination of $k+1$ unknowns, $X_1, \cdots, X_k$ and α_{k+1}. The use of Cramer's rule yields α_{k+1} in determinant form. If the same procedure is applied to $Y_1, \cdots, Y_k$, the coefficients in the 2nd row of the inverse determinant, then β_{k+1}, the highest nonzero coefficient of the lower left hand corner element of the product matrix, can also be determined. The value of Z_{k+1} follows immediately.

Numerical Example

As an illustrative example, consider the problem of designing a transformer from characteristic impedance unity to characteristic impedance 0.440 in waveguide having a cutoff wavelength of 5.680 inches, subject to the requirement that vswr $\leqq 1.05$ from 2600–3600 mc.

It is readily determined that this requires that P_L shall have 3 roots in the pass band, and we select an insertion loss function of the form

$$P_L = 1 + k^2T_3^2\left[\frac{\cos\theta}{s}\right]$$

with $\theta=2\pi l/\lambda_g$. If l is to be chosen so that $\cos\theta=0$ at the center of the band and of equal magnitude at the ends of the band

$$l = \frac{\lambda_{g1}\,\lambda_{g2}}{2(\lambda_{g1}+\lambda_{g2})}$$

where λ_{g1} and λ_{g2} are the extreme guide wavelengths. s is chosen by the requirement that the argument of $T_3(\cos\theta/s)$ shall be unity at the ends of the band, and is found to be numerically equal to 0.464. k is determined by the requirement that, at infinite frequency, the transformer shrinks to zero length and P_L is that resulting from the terminating impedance R. In general

$$\frac{(R+1)^2}{4R} = 1 + k^2 T_3^2(1/s)$$

and in our example $k^2 = 1.5777 \times 10^{-4}$. Now

$$|\Gamma|^2 = \frac{P_L - 1}{P_L} = \frac{k^2 T_3^2\left(\frac{\cos\theta}{s}\right)}{0.253\cos^6\theta - 0.0817\cos^4\theta + 0.00659\cos^2\theta + 1}.$$

If, in the denominator, we make the substitution $p = -j\cos\theta/\sin\theta$, its p roots are found to be

$$p_1 = \pm(1.034 + j0.351)$$
$$p_2 = \pm 0.772$$
$$p_3 = \pm(1.034 - j0.351).$$

If we select those roots lying in the left half plane, the denominator of Γ, except for a multiplicative constant, is $p^3+2.841p^2+2.790p+0.921$. We may then write

$$\Gamma = \frac{\alpha k T_3(\cos\theta/s)(p^2-1)^{3/2}}{p^3 + 2.841p^2 + 2.790p + 0.921}.$$

The multiplicative constant α is chosen by the requirement that $\Gamma = R-1/R-1$ when $\cos\theta = 1$ and $p = \infty$. Then Γ may be written

$$\Gamma = \frac{0.921\cos\theta(0.503\cos^2\theta - 0.0812)}{\cos\theta(-3.790\cos^2\theta + 2.790) - j\sin\theta(3.762\cos^2\theta + 0.921)}$$

and the input impedance is

$$Z = \frac{\cos\theta(-3.327\cos^2\theta + 2.716) + j\sin\theta(-3.762\cos^2\theta + 0.921)}{\cos\theta(-4.254\cos^2\theta + 2.865) + j\sin\theta(-3.762\cos^2\theta + 0.921)}.$$

The fact that the imaginary parts of the numerator and denominator of Z are equal assures us of a transformer having symmetrical reflection coefficients as previously proven. The impedance matrix giving rise to this input impedance can be written

$$\begin{bmatrix} \frac{\cos\theta}{R_L}(-3.327\cos^2\theta + 2.716) & j\sin\theta(-3.762\cos^2\theta + 0.921) \\ \frac{j\sin\theta}{R_L}(-3.762\cos^2\theta + 0.921) & \cos\theta(-4.254\cos^2\theta + 2.865) \end{bmatrix}$$

except for a multiplicative factor in each term. Now R_L and the multiplicative factor are uniquely determined by the condition that the impedance matrix must reduce to the unit matrix for $\cos\theta = 1$. Thus the impedance matrix becomes

$$\begin{bmatrix} \cos\theta(5.442\cos^2\theta - 4.442) & j\sin\theta(2.710\cos^2\theta - 0.664) \\ j\sin\theta(6.154\cos^2\theta - 1.507) & \cos\theta(3.064\cos^2\theta - 2.064) \end{bmatrix}.$$

If this is multiplied on the left by the inverse of (1)

$$\begin{bmatrix} \cos\theta & -j\sin\theta Z_1 \\ \frac{-j\sin\theta}{Z_1} & \cos\theta \end{bmatrix}$$

4 equivalent conditions result that the powers of $\cos\theta$ occurring in the result will be at most of second degree. For the coefficient of $\cos^4\theta$ appearing in the upper left hand element, one obtains the coefficient $5.442 - 6.154Z_1$, so that $Z_1 = 0.884$. When this transformer element is removed, the impedance matrix for the balance of the transformer is

$$\begin{pmatrix} 2.34\cos^2\theta - 1.335 & j\sin\theta(1.17\cos\theta) \\ j\sin\theta(3.52\cos\theta) & 1.74\cos^2\theta - 0.749 \end{pmatrix}.$$

The next step yields $Z_2 = 0.668$ and a remaining transformer having an impedance matrix

$$\begin{pmatrix} 0.998\cos\theta & -0.498j\sin\theta \\ 2.01j\sin\theta & 1.02\cos\theta \end{pmatrix}$$

corresponding to an impedance of 0.495. The last step will result in the unit matrix and provides a check on the accuracy of the numerical calculations.

Conclusion

A general solution of the synthesis of equal length impedance transformers with given insertion loss function has been obtained. It shows that optimum Tchebycheff characteristics can be physically realized and are true optimums for quarter wavelength transformers. Collin's conjecture regarding the symmetry of the optimum transformer is proved and closed expressions are given for the bi-rational transformations relating the characteristic impedances to the coefficients occurring in the impedance functions. Finally it is shown

that the determination of the characteristic impedances for Tchebycheff or maximally flat performance involves at most the solution of quadratic equations.

Appendix

We wish to prove that a rational function of p with real coefficients, of degree n, in numerator and denominator written

$$Z = \frac{m_1(p) + n_1(p)}{m_2(p) + n_2(p)} \tag{20}$$

with m_1 and m_2 either even or odd and then n_1 and n_2 odd or even is the impedance function of a cascade of equal-length impedance transformers terminated in a resistance if 1) Z is positive real; and 2)

$$m_1(p)m_2(p) - n_1(p)n_2(p) = C(p^2 - 1)^n.$$

This will have been shown, if we can demonstrate the existence of a positive real number Z_c such that the transformation, inverse to (4),

$$Z = Z_c \frac{pZ - Z_c}{-Z + pZ_c} \tag{21}$$

when applied to (20), results in a rational function of one lower degree, with real coefficients for which conditions (1) and (2) are again satisfied. Repetition of this procedure must result in an impedance function which is a positive constant; and, at this point, the synthesis is complete.

Now the general possibility of this reduction is the result of the theorem of Richards previously referred to, with the addition of condition (2). What is required by Richards is that $Z(-1) = -Z(1)$. For the reactance functions considered by Richards, this is almost trivially true at each stage of the synthesis, and is readily derived from condition (2) for the case of resistive terminations as follows

$$Z(1) = \frac{m_1(1) + n_1(1)}{m_2(1) + n_2(1)}$$

but from 2, $m_1(1)m_2(1) = n_1(1)n_2(1)$. Therefore

$$-\frac{m_1(-1)}{n_2(-1)} = \frac{m_1(1)}{n_2(1)} = \frac{n_1(1)}{m_2(1)} = -\frac{n_1(-1)}{m_2(-1)} = r$$

since $n_i(p)/m_i(p)$ is certainly odd. Thus

$$Z(1) = r = -Z(-1).$$

We may now prove, after Richards, that, if we select Z_c to have the value of Z at $p=1$, Z' will be of one less degree in p and be positive real. In the first place, the numerator of Z' vanishes for $p=1$ and hence contains $p=1$ as a factor. It also vanishes for $p=-1$, since $Z(1) = -Z(-1)$, and so contains a factor p^2-1. The same statements are true for the denominator of Z', and thus it too contains a factor p^2-1 which may be cancelled out with the same factor in the numerator. Thus Z' is a rational function of p whose numerator and denominator are of exactly one less degree than the numerator and denominator of Z.

It is pr. Consider the function $(Z'-1)/(Z'+1)$. Clearly a necessary and sufficient condition that Z' be pr is that $\left|(Z-'1)/(Z'+1)\right| \leqq 1$ for the Re $(p) \geqq 0$. This is apparent on consideration of the magnitude of the vectors $Z'-1$ and $Z'+1$. Now

$$\frac{Z'/Z(1) - 1}{Z'/Z(1) + 1} = \frac{Z - Z(1)}{Z + Z(1)} \frac{p+1}{p-1}. \tag{22}$$

In the first place, the function on the left is analytic in the right half plane, since Z is known to be pr so that the only zero of the denominator of (22) must occur at $p=1$ where it is cancelled out by a corresponding zero in $Z-Z(1)$. Now it is well known (maximum modulus theorem again) that an analytic function assumes the maximum value for its absolute values on the boundary of its region of analyticity. Thus the absolute value of (22) in the right half plane is less than or equal to the minimum absolute value assumed by it on the imaginary axis. Here $\left|(p+1)/(p-1)\right| = 1$. Moreover since Z is assumed pr, $\left|[Z-Z(1)]/[Z+Z(1)]\right| \leqq 1$. Thus

$$\left|\frac{Z'/Z(1) - 1}{Z'/Z(1) + 1}\right| \leqq \left|\frac{Z - Z(1)}{Z + Z(1)}\right| \cdot \left|\frac{p+1}{p-1}\right| \leqq 1$$

on the imaginary and hence everywhere in the right half plane. Accordingly $Z'/Z(1)$ is pr, and then so is Z' since $Z(1)$ is positive.

The proof of the synthesis theorem will be completed when we argue that for Z' written in the form

$$(m_1'(p) + n_1'(p))/(m_2'(p) + n_2'(p)),$$

$$m_1'(p)m_2'(p) - n_1'(p)n_2'(p) = C(p^2 - 1)^{n-1}.$$

Consideration of the inverse transformation (22) shows that the corresponding impedance matrix has the determinant, p^2-1, just as the transformation (4). Before any cancellation then

$$m_1'(p)m_2'(p) - n_1'(p)n_2'(p) = C(p^2 - 1)^{n+1}.$$

When $Z_c \to Z(1)$, Richards' theorem shows that a term p^2-1 factors from both numerator and denominator. Actually p^2-1 must factor from both even and odd parts of numerator and denominator, and when this is done the result follows.

Discussion

H. Seidel in a doctoral dissertation dated May, 1954 has shown that an exact synthesis can be carried

through, starting from an insertion loss function of allowed form. His procedure parallels that used in our numerical example. He does not introduce a complex variable equivalent to p, however, and thus does not have Richards' theorem available for proving physical realizability. In particular, he makes no point of the second condition for the physical realizability of an impedance function. Ozaki and Ishii,[11] clearly state this second condition, but they do not parallel Darlington by starting from a given insertion loss function. E.M.T. Jones in the 1956 IRE Convention Record uses a complex variable, but he makes no mention of the second condition for physical realizability, and appears, in his proof of physical realizability, to have appealed to Richards for a theorem which Richards did not prove.

[11] H. Ozaki and J. Ishii, "Synthesis of transmission-line networks and the design of uhf filters," IRE Trans., vol. CT-2, p. 325–336; December, 1955.

Acknowledgment

The author wishes to acknowledge the assistance of Walter Whelan who worked through the details of the numerical example.

An Analysis of the Diode Mixer Consisting of Nonlinear Capacitance and Conductance and Ohmic Spreading Resistance*

ALAN C. MACPHERSON†

Summary—A method is presented for calculating the mixer admittance matrix Y' which results when an ohmic impedance is connected in series with a diode mixer described by an admittance matrix Y. There are no restrictions on the frequency dependence of the ohmic impedance nor on the number of harmonic sidebands considered. The equations are worked out in detail for the "low Q" case in which signal, image, and intermediate frequencies are considered, and it is shown that Y' in this case is "nearly low Q." As a result of this analysis the usual criterion for good high-frequency mixing, *i.e.*, that the product of the spreading resistance and the barrier capacitance be small compared with unity, is criticized and a new figure of merit is proposed.

Explicit formulas have been derived for calculating the elements of Y' when Y represents the parallel combination of a nonlinear conductance and capacitance. In general, these formulas are cumbersome, but three special cases have been considered in detail.

Case 1: Zero spreading resistance and equal admittances connected to image and signal terminals. Results: a) The conversion gain is independent of the contact area. b) Regions of negative IF conductance are always associated with arbitrarily high gain.

Case 2: High-frequency, small spreading resistance, image shorted across nonlinear conductance and capacitance. Results: a) The conversion loss and the IF admittance can be given by closed equations. b) The IF conductance can be negative. c) Regions of negative IF conductance are bounded by regions of arbitrarily small IF conductance. d) The conversion loss can *decrease* with increasing frequency. e) Low conversion loss is accompanied by narrow bandwidth.

Case 3: The spreading resistance is zero and the image is shorted. Results: a) Above a certain frequency negative IF conductance is obtained and arbitrarily low conversion loss is possible. b) The situation is quite similar to that of Case 1.

Measurements of mixer performance at the "available terminals" are discussed and the failure of the "phenomenological theory of mixing" as a basis for making such measurements is emphasized.

* Manuscript received by the PGMTT, May 18, 1956.
† Naval Research Lab., Washington, D C.

Introduction

THIS PAPER will be concerned principally with the mixing properties of the circuit of Fig. 1 (next page), where arrows indicate that g and C are functions of the voltage across them. Frequent reference will be made to Torrey and Whitmer[1] and whenever possible the notation used therein will be followed here.

The circuit of Fig. 1 has been widely used, qualitatively at least, as an equivalent circuit for point-contact crystal diodes,[2] particularly for microwave work in which the capacitor is of importance. The part of the crystal diode that Fig. 1 is supposed to represent is shown in Fig. 2. The terminals are at the dotted lines AA' and BB'. The distance from the line AA' to the surface is a small fraction of the shortest wavelength involved, while the line BB' is located so as to include nearly all of the spreading resistance. It can be shown that the latter requirement will be fulfilled if BB' is several times the contact diameter away from the contact region.

The validity of the circuit of Fig. 1 as a representation of Fig. 2 is open to question. It has been verified in the

[1] H. C. Torrey and C. A. Whitmer, "Crystal Rectifiers," McGraw-Hill Book Co., Inc., New York, N. Y.; 1948.
[2] *Ibid.*, p. 24.

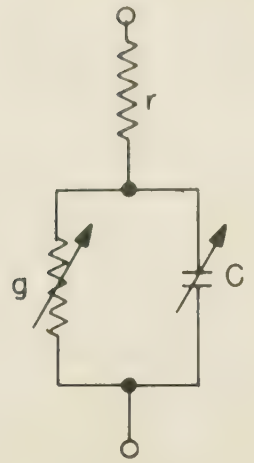

Fig. 1—Small-signal equivalent circuit.

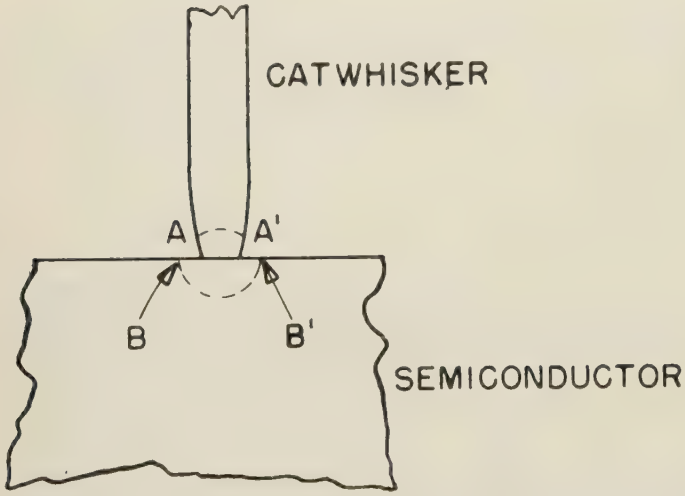

Fig. 2—Point-contact crystal diode.

several megacycle range for silicon point-contact crystals. Analysis of the mixer properties of this circuit yields negative IF conductance under certain conditions. This has been observed in H. Q. North's welded-contact crystals.[3] The actual equivalent circuit is probably at least as complicated as Fig. 1.

The region under consideration is clearly only part of the crystal diode; in addition, there is the rest of the whisker and semiconductor and various components necessary for proper support and protection. These components, however, are nearly lossless and are certainly linear so that the effect is simply that of an impedance transformer and need not be explicitly considered. In choosing the terminals discussed above we have included the region of the nonlinearity and the region of the important losses. The use of the "low-frequency" concepts of voltage, current, and lumped components is justified, if, to put it roughly, the distance between AA' and BB' is small compared with a wavelength. For commercial crystals designed for a minimum wavelength of about 4 cm, the contact diameter is less than 0.001 inch, so that the condition is well met.

The central engineering problem of a microwave mixer is to relate the small-signal parameters to quantities of interest when the crystal is operated as a mixer —decidedly a large-signal nonlinear problem. The behavior (except for noise considerations) of the mixer is completely specified when values are obtained for the elements of the mixer admittance matrix. The situation is much like that encountered in the theory of linear n poles, except that each terminal pair is associated with a different low-power-level frequency. Since an infinite number of these frequencies exists in the mixer, the admittance matrix is an infinite one. Once the admittance matrix is known, the conversion loss, IF admittance, etc., can be calculated when specified admittances terminate each pair except the IF terminal pair.

The complete circuit of Fig. 1 has not (to the author's knowledge) been quantitatively treated in the literature. The case in which C is assumed linear has been treated rather thoroughly.[4] The case in which r is zero but both g and C are nonlinear has been partially treated,[5] but only with respect to the spectacular effect of negative IF conductance which the nonlinear C makes possible; there is in this reference no calculation of conversion loss and no quantitative information on the effect of spreading resistance. Only the broadband (signal and image admittances equal) case was treated by Torrey and Whitmer. One of the purposes of this paper is to point out that at sufficiently high frequencies, the nonlinear capacitance in Fig. 1 can have an important effect on the properties of the mixer even though negative IF conductance does not appear. Negative IF conductance may not appear for one or both of the following reasons: C is not sufficiently nonlinear, or the spreading resistance is too large. The properties of the barrier conductance also have some influence.

Treatment of Spreading Resistance

In a mixer there are an infinite number of frequencies at low power levels. It is customary to consider only three of these: the signal, intermediate, and image frequencies.[6] This approximation becomes increasingly poor for low-loss mixers. Since the inclusion of nonlinear capacitance can result in a mixer with zero conversion loss, the general treatment will be for any number of low-level signals.

A generalization of Fig. 1 may easily be made (in principle) as follows: the spreading resistance r may be considered complex and may be different for each low-level frequency of interest. he t"spreading impedance" will therefore be denoted by z_n, where n denotes the frequency.

[3] *Ibid.*, p. 398.

[4] *Ibid.*, p. 157.
[5] *Ibid.*, p. 406.
[6] *Ibid.*, p. 111.

This might be useful if, for example, one wished to include the catwhisker (which has a different impedance at signal than at IF frequencies because of its inductance and skin effect) in the spreading impedance.

Assume that the admittance matrix Y of the mixer not including the z_n's, is known. Now, Y may be anything, and will at first be kept general, but the case of most interest at present is that in which Y is the admittance matrix of the circuit of Fig. 1 with $r=0$. The latter is given by Torrey and Whitmer[7] for the most general case (arbitrary number of terminal pairs, arbitrary LO voltage waveform) and specialized to a consideration of signal, image, and intermediate frequencies only,[8] and with the local oscillator voltage (LO) waveform restricted to even functions.

The frequencies of interest can be expressed as $\beta+n\omega$ where β is the intermediate frequency, n is a positive or negative integer, and ω is the LO frequency. Current and voltage at the frequency $\beta+n\omega$ will be denoted by i_n and v_n, respectively. Then $I=YV$, where I and V are column matrices formed from the i_n's and the v_n's.

If i_n' and v_n' are the new values after the addition of z_n, then $i_n'=i_n$ and $v_n'-i_n'z_n=v_n$. These equations are substituted into $I=YV$ and the i_n''s are solved for in terms of the v_n''s. The coefficients of the v_n''s are the elements of the new admittance matrix Y' which describes the original matrix with the spreading impedance added.

The calculation is straightforward and the results can be given as follows: form the diagonal matrix Z whose elements along the diagonal are the z_n's. Next form the matrix $B=ZY+1$, where 1 denotes the unit matrix. Calculate b, the determinant of B, and all of its cofactors b_{rc}, where r and c denote row and column. Then, y_{rc}', a typical element of Y', will be given by

$$y_{rc}' = \left(\sum_i b_{ir} y_{ic} \right) \Big/ b,$$

where the unprimed y's are the elements of Y.

To illustrate the procedure, and for future reference, the equations will be worked out for the case of the signal, image, and intermediate frequencies in the notation of Torrey and Whitmer.

At this point Y is arbitrary and can be written

$$Y = \begin{bmatrix} y_{\alpha\alpha} & x_{\alpha\beta} & y_{\alpha\gamma} \\ y_{\beta\alpha} & y_{\beta\beta} & y_{\beta\gamma} \\ y_{\gamma\alpha} & x_{\gamma\beta} & y_{\gamma\gamma} \end{bmatrix}. \tag{1}$$

Assume, as is customary, that the z_n's are all real and equal. Then

$$Z = \begin{bmatrix} r & 0 & 0 \\ 0 & r & 0 \\ 0 & 0 & r \end{bmatrix} \tag{2}$$

$$B = ZY + 1 = \begin{bmatrix} 1 + y_{\alpha\alpha} r & y_{\alpha\beta} r & y_{\alpha\gamma} r \\ y_{\beta\alpha} r & 1 + y_{\beta\beta} r & y_{\beta\gamma} r \\ y_{\gamma\alpha} r & v_{\gamma\beta} r & 1 + y_{\gamma\gamma} r \end{bmatrix} \tag{3}$$

and

$$Y' = \begin{bmatrix} y_{\alpha\alpha}' & y_{\alpha\beta}' & y_{\alpha\gamma}' \\ y_{\beta\alpha}' & y_{\beta\beta}' & y_{\beta\gamma}' \\ y_{\gamma\alpha}' & y_{\gamma\beta}' & y_{\gamma\gamma}' \end{bmatrix} \tag{4}$$

where

$$\begin{aligned}
b y_{\alpha\alpha}' &= y_{\alpha\alpha} b_{11} + y_{\beta\alpha} b_{21} + y_{\gamma\alpha} b_{31} \\
b y_{\alpha\beta}' &= y_{\alpha\beta} b_{11} + y_{\beta\beta} b_{21} + y_{\gamma\beta} b_{31} \\
b y_{\alpha\gamma}' &= y_{\alpha\gamma} b_{11} + y_{\beta\gamma} b_{21} + y_{\gamma\gamma} b_{31} \\
b y_{\beta\alpha}' &= y_{\alpha\alpha} b_{12} + y_{\beta\alpha} b_{22} + y_{\gamma\alpha} b_{32} \\
b y_{\beta\beta}' &= y_{\alpha\beta} b_{12} + y_{\beta\beta} b_{22} + y_{\gamma\beta} b_{32} \\
b y_{\beta\gamma}' &= y_{\alpha\gamma} b_{12} + y_{\beta\gamma} b_{22} + y_{\gamma\gamma} b_{32} \\
b y_{\gamma\alpha}' &= y_{\alpha\alpha} b_{13} + y_{\beta\alpha} b_{23} + y_{\gamma\alpha} b_{33} \\
b y_{\gamma\beta}' &= y_{\alpha\beta} b_{13} + y_{\beta\beta} b_{23} + y_{\gamma\beta} b_{33} \\
b y_{\gamma\gamma}' &= y_{\alpha\gamma} b_{13} + y_{\beta\gamma} b_{23} + y_{\gamma\gamma} b_{33}.
\end{aligned} \tag{5}$$

It is usually assumed that $y_{\beta\beta}$ is real and that there are no circuits *in* the mixer which can discriminate between the signal frequency and the image frequency, *i.e.*, $y_{\gamma\beta}=y_{\alpha\beta}^*$, $y_{\beta\gamma}=y_{\beta\alpha}^*$, $y_{\gamma\alpha}=y_{\alpha\gamma}^*$, and $y_{\gamma\gamma}=y_{\alpha\alpha}^*$, where the asterisks denote complex conjugates. If the preceding four conditions are all met, one says, by definition, that the mixer, or the mixer admittance matrix, is "low Q."[9] Then,

$$Y = \begin{bmatrix} y_{\alpha\alpha} & y_{\alpha\beta} & y_{\alpha\gamma} \\ y_{\beta\alpha} & g_{\beta\beta} & y_{\beta\alpha}^* \\ y_{\alpha\gamma}^* & y_{\alpha\beta}^* & y_{\alpha\alpha}^* \end{bmatrix}.$$

It can then be shown that $b_{33}=b_{11}^*$, $b_{31}=b_{13}^*$, $b_{32}=b_{12}^*$, $b_{21}=b_{23}^*$, and b_{22} is real. From these relations and (5), it follows that $y_{\alpha\beta}'=y_{\gamma\beta}'^*$, $y_{\alpha\alpha}'=y_{\gamma\gamma}'^*$, $y_{\gamma\alpha}'^*=y_{\alpha\gamma}'$, $y_{\beta\alpha}'=y_{\beta\gamma}'^*$, and $by_{\beta\beta}'$ is real. Since b is not, in general, real, $y_{\beta\beta}'$ is not real and the mixer is not low Q. A mixer which meets all the requirements of a low Q mixer except that $y_{\beta\beta}'$ be real will be termed "nearly low Q." If the time zero is properly chosen,[10] $y_{\beta\alpha}'$ can be made real and then

$$Y' = \begin{bmatrix} y_{\alpha\alpha}' & y_{\alpha\beta} & y_{\alpha\gamma}' \\ g_{\beta\alpha}' & y_{\beta\beta}' & g_{\beta\alpha}' \\ y_{\alpha\gamma}'^* & y_{\alpha\beta}'^* & y_{\alpha\alpha}'^* \end{bmatrix}.$$

There would seem to be little point in presenting the long expressions for the y''s but, since each b_{ij} appears several times in Y', the following formulas may be

[7] *Ibid.*, p. 165.
[8] *Ibid.*, p. 408.
[9] *Ibid.*, p. 115.
[10] *Ibid.*, p. 117.

useful

$$\begin{aligned} b_{11} &= (1 + g_{\beta\beta}r)(1 + y_{\alpha\alpha}{}^{*}r) - r^2 y_{\alpha\beta}{}^{*} y_{\beta\alpha}{}^{*} \\ b_{13} &= r^2 y_{\beta\alpha} y_{\alpha\beta}{}^{*} - y_{\alpha\gamma}{}^{*} r(1 + g_{\beta\beta}r) \\ b_{12} &= r^2 y_{\beta\alpha}{}^{*} y_{\alpha\gamma}{}^{*} - r y_{\beta\alpha}(1 + y_{\alpha\alpha}{}^{*}r) \\ b_{21} &= r^2 y_{\alpha\gamma} y_{\alpha\beta}{}^{*} - r y_{\alpha\beta}(1 + y_{\alpha\alpha}{}^{*}r) \\ b_{22} &= \left| 1 + y_{\alpha\alpha}r \right|^2 - r^2 \left| y_{\alpha\gamma} \right|^2 \\ b &= (1 + y_{\alpha\alpha}r)b_{11} + y_{\alpha\beta}r b_{12} + y_{\alpha\gamma}r b_{13}. \end{aligned} \tag{6}$$

Finally, in order to compute Y' for the circuit of Fig. 1, one uses for Y the formulas in Torrey and Whitmer[11] for the general case (LO waveform arbitrary), or those for the case of LO waveform "even."[12]

At microwave frequencies the terminals to which Y' refers are not available for measurement. If for example, one is dealing with a waveguide mixer, impedance measurements must be made in the waveguide at some distance (so that higher modes will die out) from the terminals to which Y' refers. In addition, there will be "parasitic" impedances associated with the mechanical mounting of the point on the crystal. This problem may be present to a lesser extent for the intermediate frequency. One can formally handle this by connecting a four-pole (usually nearly lossless) on each of the terminal pairs. A new admittance matrix will result, Y'', which describes the mixer at terminals which are actually available for measurement. It is intuitively clear that if all the four-poles are linear and if the four-poles connected to the signal and image terminals cannot discriminate between these two frequencies, Y'' will be nearly low Q. The proof would be quite similar to the above proof that Y' is nearly low Q and has been given in essence by Peterson and Llewellyn.[13] The fact that these authors were treating the case of the linear capacitance is immaterial.

Qualitative Statements Concerning the Effect of Finite Spreading Resistance

There is a frequently employed argument that for good high-frequency performance, ωCr should be much less than one. In the first place, since the barrier capacitance is a function of bias, it is not clear what is meant by C in the above expression. Presumably one is to assume that the barrier capacitance is linear. Even so, the above criterion does not appear to be useful or accurate. Consider the two extreme instances, the first in which ωCr is small because r is very small while ωC is finite, and the second in which ωCr is small because ωC is very small, while r is finite. If the above criterion is correct, these two cases should give about the same high-frequency performance. In the first case, the low-frequency conversion loss will be low (assume that in both cases the barrier conductance is sufficiently nonlinear), and the high-frequency conversion loss will be identically low. This is true because of the general theorem that a reactive network placed in tandem with a four-pole does not change its conversion loss. Or, if proof for a particular case is desired, (15) in this paper and (17) in Torrey and Whitmer,[14] may be used to calculate the conversion loss L. It will be noted that ωC_0, where C_0 is the linear capacitance, appears only in the combination $\omega C_0 + b_a$ and since b_a is arbitrary, L will be independent of frequency. In the second instance, however, L will be very high for both the low-frequency and the high-frequency case.

The case of the linear capacitor is treated in Torrey and Whitmer,[15] and the equations for the elements of Y' are also given.[16] The quantity ωCr does appear repeatedly, but this is not the whole story by any means since r appears in other ways also. This must be so, because obviously, in the low-frequency case, in which ωC_0 is negligible, large r will impair the performance.

One would like to enunciate a rule or rules of thumb for low L for the circuit of Fig. 1 at all frequencies. It is clear that the requirement on r is that the elements of Y' be nearly equal to the elements of Y. Eq. (5) indicates that the requirements on b and the b_{ij}'s are that b and b_{11} be close to one and that b_{13}, b_{21}, and b_{12} be nearly zero. Eq. (6) shows that the only conditions which will simultaneously satisfy the above conditions are that $y_{ij}r$ be small compared with one. Using (6), one obtains the result that $g_i r \ll 1$ and $\omega C_i r \ll 1$. Since g_1 and g_2 must be equal to or less than g_0, and C_1 and C_2 must be equal to or less than C_0, it is sufficient to require that $g_0 r$ and $\omega C_0 r$ be small compared with one. Adding conditions for nonlinearity, one can say that at low frequencies the requirements are $g_1 g_2 / g_0{}^2 \cong 1$ and $g_0 r \ll 1$ while for high frequencies the *additional* requirements are $C_1 C_2 / C_0{}^2 \cong 1$ and $\omega C_0 r < 1$. Perhaps it is not too far fetched to propose, for an over-all wideband figure of merit, that $g_1 g_2 C_1 C_2 / g_0{}^3 C_0{}^3 r^2$ be large compared to one.

For the point-contact geometry, r increases as the diameter of contact decreases while the C_i's and g_i's decrease with the area of contact.[17] This is a possible explanation for the well-known fact that, particularly for high frequencies, small contacts are necessary for low L. It is worth pointing out that this is due completely to the geometry of the point contact which is roughly planar for the C_i's and g_i's but three-dimensional for r. In a completely planar geometry, for example, L would be independent of the cross-sectional area.

[11] *Ibid.*, p. 166.
[12] *Ibid.*, p. 408.
[13] L. C. Peterson, and F. B. Llewellyn, "The performance and measurement of mixers in terms of linear-network theory," Proc. IRE, vol. 33, pp. 458–476; July, 1945.
[14] Torrey and Whitmer, *op. cit.*, p. 409.
[15] *Ibid.*, p. 157.
[16] *Ibid.*, p. 160.
[17] *Ibid.*, p. 98.

Operational Meaning of the Elements of Y''

Probably the most straightforward and elegant way to measure and express the properties of a mixer is by means of the elements of Y''. This information, after all, completely describes the properties of the mixer at a given bias and *LO* drive, just as the elements of the admittance matrix of any linear n pole described its properties. Equipped with this information the engineer can calculate the conversion loss, the IF impedance, and other properties as a function of the signal and image termination.

In Torrey and Whitmer[18] there is a discussion of what is called the Phenomenological Theory of Conversion (PTC). According to this theory, one can calculate the elements of Y'' for the case of signal, image, and intermediate frequencies from a series of measurements of the rectifying properties of the crystal made at *LO* power levels; the theory does not appear to be applicable to the mixer which includes a nonlinear capacitance. During the war almost all the measurements of the elements of Y'' were based on the PTC, and at the present time the JAN specifications are based on this method. Nevertheless, the method is highly questionable, particularly if the capacitance is nonlinear. It would therefore seem pertinent to outline a general method for measuring the elements of Y'', regardless of the equivalent circuit of the mixer. The equations for mixer IF admittance y_β and for mixer conversion loss L are[19]

$$y_\beta = Y_{\beta\beta} - \frac{Y_{\alpha\beta}Y_{\beta\alpha}}{Y_{\alpha\alpha} + y_a} \tag{7}$$

and

$$L = Wg_\beta \tag{8}$$

where

$$W = \frac{|\, y_a + Y_{\alpha\alpha}\,|^2}{g_a\,|\, Y_{\beta\alpha}\,|^2}. \tag{9}$$

As before, α, β, and γ refer to the signal, intermediate, and image frequencies, respectively; the Y_{ij}'s are the elements of the 2×2 admittance matrix Y_2, which is formed from the 3×3 matrix Y'' by specifying a termination at the image terminals; y_a is the signal admittance; g_a is the real part of y_a; and g_β is the real part of y_β. The relationships between the elements of Y'' and Y_2 are[20]

$$Y_{\alpha\alpha} = y_{\alpha\alpha} - \frac{y_{\alpha\gamma}y_{\alpha\gamma}^*}{y_{\alpha\alpha}^* + y_c^*} \tag{10}$$

$$Y_{\alpha\beta} = y_{\alpha\beta} - \frac{y_{\alpha\gamma}y_{\alpha\beta}^*}{y_{\alpha\alpha}^* + y_c^*} \tag{11}$$

$$Y_{\beta\alpha} = y_{\beta\alpha} = \frac{y_{\alpha\gamma}^* y_{\beta\alpha}^*}{y_{\alpha\alpha}^* + y_c^*} \tag{12}$$

$$Y_{\beta\beta} = y_{\beta\beta} - \frac{y_{\beta\alpha}^* y_{\alpha\beta}^*}{y_{\alpha\alpha}^* + y_c^*} \tag{13}$$

where y_c is the admittance at the image terminals. Note that the capital letters indicate the elements of Y_2 and the small letters indicate the elements of Y''. For convenience, the elements of Y'' are not primed.

It is known[21] that $y_{\beta\alpha}$ can be made real by a proper choice of the origin of time. If $\boldsymbol{y}_{\beta\alpha}$ is a particular value of $y_{\beta\alpha}$ for some particular choice of time zero, then the general form of $y_{\beta\alpha}$ is: $y_{\beta\alpha} = \exp(-jwt_0)\boldsymbol{y}_{\beta\alpha}$ where t_0 is arbitrary. In the same way, $y_{\alpha\gamma} = \boldsymbol{y}_{\alpha\gamma}\exp(2jwt_0)$ and $\boldsymbol{y}_{\alpha\alpha} = y_{\alpha\alpha}$. By substituting into (12), the following general expression for $Y_{\beta\alpha}$ is obtained: $Y_{\beta\alpha} = \exp(-jwt_0)\boldsymbol{Y}_{\beta\alpha}$, where $\boldsymbol{Y}_{\beta\alpha}$ is a value of $Y_{\beta\alpha}$ for some choice of time zero. Now $\boldsymbol{Y}_{\beta\alpha}$ is in general complex, but by proper choice of t_0, $Y_{\beta\alpha}$ can be made real. In what follows it is assumed that $Y_{\beta\alpha}$ is real and it will be denoted by $G_{\beta\alpha}$.

The parameters to be measured are the elements of Y''. The general procedure is as follows: first, set y_c at some known value, $y_c{}^I$. Second, measure y_β for three different known values of y_a. Eq. (7) can now be used to solve for $Y_{\beta\beta}{}^I$, $Y_{\alpha\alpha}{}^I$, and $Y_{\alpha\beta}{}^I G_{\beta\alpha}{}^I$, the I's corresponding to the value of y_c. Third, L and g_β are measured for any known value of y_a, and from (8) and (9), $G_{\beta\alpha}{}^I$ is obtained. L can be measured by any reliable method such as the heterodyne method[22] using either a cw or noise signal, and g_β can be measured with an rf bridge. Thus, a complete set of Y_{ij}'s is obtained. The above procedure is repeated for a different value of y_c and a second set of Y_{ij}'s is obtained. This is more than enough information to solve for the elements of Y'' by using (10) through (13) twice.

The practical measurement is complicated by the fact that y_a and y_c are not easily varied independently. This is because the waves associated with the two admittances are located physically in the same transmission line. Thus one must resort to frequency-sensitive terminations in order to vary y_a and y_c independently. It appears that an excellent pair of choices for y_c would be infinity and zero, for then $Y_{ij}{}^I = y_{ij}$ and the only remaining unknown would be $y_{\alpha\gamma}$. Then from (11)

$$Y_{\alpha\beta}{}^{II} = y_{\alpha\beta} - \frac{y_{\alpha\gamma}y_{\alpha\beta}^*}{y_{\alpha\alpha}^*}$$

$y_{\alpha\gamma}$ can be obtained. The above method would appear to be practical. The values infinity and zero for y_c can be approximated by inserting a transmission type cavity in the line tuned to the signal frequency. Variation of y_a could be accomplished either by varying a termina-

[18] *Ibid.*, p. 119.
[19] *Ibid.*, p. 136.
[20] *Ibid.*
[21] *Ibid.*, p. 116.
[22] *Ibid.*, p. 200.

tion on the far side of the cavity, or by detuning the cavity (y_a would have to be measured with, for example, a standing-wave machine). In the case of y_c, it could probably be assumed that the corresponding standing-wave ratio would be infinite. Note that no microwave impedance measurements at the microwatt level are necessary. Since the author has never made measurements of this type, he cannot vouch for the success of the above method. Nevertheless, it clearly demonstrates the operational meaning of the elements of Y''.

Calculations of L, y_β, and g_β

Once the admittance matrix Y' has been calculated by the procedure given under the section on "Treatment of Spreading Resistance," (7), (8), and (9) can be used to calculate L, y_β, and g_β. It is clear that for the general case, these equations will be extremely complicated. There is an additional complication owing to the fact that, in general, one wishes these quantities as a function of y_a and y_c. It would appear quite feasible, however, to make numerical calculations, particularly if a computer is available, and it is planned to do so. However, if one chooses highly idealized cases some manageable equations can be obtained.

Case 1

Assume that $r=0$, and that the image and signal are terminated with equal admittances (broadband case). Insofar as g_β is concerned, this case is treated in Torrey and Whitmer.[23] For convenience, Y, which in this case is equal to Y', is reproduced here:

$$Y' = \begin{bmatrix} g_0 + j\omega C_0 & g_1 + j\omega C_1 & g_2 + j\omega C_2 \\ g_1 & g_0 & g_1 \\ g_2 - j\omega C_2 & g_1 - j\omega C_1 & g_0 - j\omega C_0 \end{bmatrix}. \quad (14)$$

There are some additional relationships which are not mentioned in Torrey and Whitmer: $C_1 \leqq C_0$, $C_2 \leqq C_0$, and $2C_1^2/C_0 \leqq C_0 + C_2$. These relations hold for the same reasons that the equivalent ones hold for g_0, g_1, and g_2.[24]

The statement is frequently made that when the frequency is high, the area of the point contact must be made small in order to reduce the capacitance. This is not true, however, when $r=0$. The C_i's and the g_i's are so intimately related to each other that a decrease in contact area, which would reduce the C_i's would reduce the g_i's by the same factor. In other words, g_i/C_i depends only on the character of the potential barrier and not on the geometry. Now L is a dimensionless quantity which depends on the g_i's, the C_i's, and y_a which is arbitrary. Assume that for some geometry, y_a is adjusted for minimum conversion loss, L_1. Now assume that the geometry is changed (*e.g.*, the contact area is reduced) so as to halve the C_i's and the g_i's. Then assuming that one readjusts y_a to minimize the conversion loss again to the value L_2, L_1 and L_2 will be equal.

Torrey and Whitmer point out that for negative g_β the barrier capacitance must be strongly nonlinear, *i.e.*, C_1/C_0 or C_2/C_0 must be large. It should be noted, however, that L depends on all the elements of the admittance matrix and that therefore as long as C_1 and C_2 are finite there will be some high frequency at which the nonlinearity of the barrier capacitance will play a role in determining L. For example, from $y_{a\beta}$, (14), no matter how small C_1 is there will be some frequency at which ωC_1 will be of the same order of magnitude as g_1.

It is clear that Y', (14), leads to absurd results if g_1 or g_0 are set equal to zero. This is a result of the assumption in Torrey and Whitmer that the intermediate frequency β is such that $\beta C_i \ll g_i$. This restriction, which is usual in microwave mixers, may be removed if desired. This has been done in some recent work at the Bell Telephone Laboratories.[25] Only the case of the pure nonlinear capacitance is considered, but some new effects show up which are not in evidence when βC_i is assumed negligibly small compared with g_i. Throughout this paper it is assumed that $\beta C_i \ll g_i$.

As Torrey and Whitmer point out, the region on the y_a plane corresponding to negative g_β adjoins regions of either arbitrarily large g_β and/or arbitrarily small g_β. In the latter case, since W remains finite, it is clear that L is arbitrarily small in the same region. One would like to know the behavior of L in the region in which g_β is arbitrarily large. The condition for $g_\beta = \infty$ is $B_0^2 + G_0^2 = g_2^2 + \omega^2 C_2^2$, where $G_0 = g_0 + g_a$, $B_0 = b_0 + \omega C_0$.[26] Since Torrey and Whitmer do not give an equation for W, it is presented here.

$$W = \frac{1}{g_a} \frac{[1 - (g_2^2 + \omega^2 C_2^2)/(G_0^2 + B_0^2)]^2 (G_0^2 + B_0^2)^2}{g_1^2[(G_0 - g_2)^2 + (B_0 - \omega C_2)^2]}. \quad (15)$$

It is seen that W goes to zero for the same condition. If, however, one calculates the product $g_\beta W$ the following expression is obtained:

$$L = W g_\beta = MN \frac{G_0^2 + B_0^2 - (g_2^2 + \omega^2 C_2^2)}{(G_0^2 + B_0^2)^2} \quad (16)$$

where

$$M = g_0 \left\{ \left[b_a + \omega \left(C_0 - \frac{g_1 C_1}{g_0} \right) \right]^2 + \left[g_a + g_0 \left(1 - \frac{g_1^2}{g_0^2} \right) \right]^2 - G^2 \right\}. \quad (17)$$

$$N = \frac{(G_0^2 + B_0^2)^2}{g_a g_1^2 [(G_0 - g_2)^2 + (B_0 - \omega C_2)^2]} \quad (18)$$

[23] *Ibid.*, p. 408.
[24] *Ibid.*, p. 409.
[25] M. C. Waltz, A. E. Bakanowski, and A. Uhlir, "Second Interim Technical Report on Crystal Rectifiers," Bell Telephone Labs., Task 8, Signal Corps Contract DA 36-039 sc-5589; January 15, 1955.
[26] Torrey and Whitmer, *op. cit.*, p. 409. See (15).

and G is defined in Torrey and Whitmer.[27] Thus, the condition in question gives an infinite g_β but a conversion loss of zero. One can now make the statement that for the broad-band case, negative g_β regions are always associated with arbitrarily high gain, regardless of whether g_β goes to infinity or to zero at the boundary of the negative g_β region. Note the use of the term "arbitrarily small." The mere fact of conversion gain, *i.e.*, $L<1$, is not particularly significant since mixers are not connected in tandem to obtain a large over-all gain. The quantity of interest is the over-all receiver noise figure which is given by $F_r=L(t+F_i-1)$, where F_r is the over-all receiver noise figure, t is the noise temperature ratio of the mixer, and F_i is the noise figure of the IF amplifier. It is clear that a mixer with $L=1.05$ is very little worse than one with $L=0.95$ in spite of the fact that the latter mixer shows conversion gain. A mixer which can have an arbitrarily small L is quite a different matter however. The important question is then what happens to t when L is small. At present this question cannot be answered without resorting to experiment.

Case 2

Assume that r is finite, but that the image can be shorted at the barrier. This is impossible in principle if r is frequency independent, since $1/r$ would be the largest admittance which could be connected to the image terminals. The requirements for approximating the above are given by (92)–(95) in Torrey and Whitmer,[28] and it can be shown that these requirements are reasonable if $1/r \gg \omega C_0$. Obviously at sufficiently high frequencies this condition will not be met. Assume that the frequency is such that $g_i \ll \omega C_i$. The above two assumptions are not mutually exclusive. Assume the maximum nonlinearity, $g_1=g_0=g$, $C_1=C_0=C$. Finally, assume that $gr \ll 1$. The last condition is almost always met. Then[29,30]

$$Y = \begin{bmatrix} Y_{\alpha\alpha} & Y_{\alpha\beta} \\ Y_{\beta\alpha} & Y_{\beta\beta} \end{bmatrix} = \begin{bmatrix} j\omega C & j\omega C \\ g & g \end{bmatrix} \tag{20}$$

$$B = \begin{bmatrix} 1+j\omega Cr & j\omega Cr \\ rg & 1 \end{bmatrix}. \tag{21}$$

$$\left.\begin{aligned} b &= 1 - j\omega Cr; \\ b_{11} &= 1; \\ b_{12} &= -rg; \\ b_{21} &= -j\omega Cr; \\ b_{22} &= 1 + j\omega Cr. \end{aligned}\right\} \tag{22}$$

$$Y' = (1/b)Y. \tag{23}$$

$$L = g_\beta W \tag{24}$$

where

$$W = \frac{1}{g_a} \frac{|y_a + y_{\alpha\alpha}'|^2}{|y_{\beta\alpha}'|^2} \tag{25}$$

$$W = \frac{1}{g_a} \frac{|by_a + j\omega C|^2}{g^2} \tag{26}$$

$$W = \frac{1}{g_a} \frac{g_a^2[1+(\omega Cr)^2] + b_a^2[1+(\omega Cr)^2] - g_a(2\omega^2C^2r) + b_a(2\omega C) + (\omega C)^2}{g^2}. \tag{27}$$

$$y_\beta = \frac{g}{b} - \frac{i\omega Cg/b^2}{y_a + \frac{j\omega C}{b}} \tag{28}$$

$$y_\beta = \frac{1}{b}\left(g - \frac{j\omega Cg}{by_a + j\omega C}\right). \tag{29}$$

For zero spreading resistance

$$W^0 = \frac{1}{g_a g^2}\left[g_a^2 + (b_a + \omega C)^2\right] \tag{30}$$

$$y_\beta{}^0 = g\left(1 - \frac{j\omega C}{y_a + j\omega C}\right) \tag{31}$$

$$g_\beta{}^0 = \mathrm{Re}\,(y_\beta{}^0) = g\left[1 - \frac{(\omega C)^2 + \omega C b_a}{g_a^2 + b_a^2 + 2b_a\omega C + (\omega C)^2}\right]. \tag{32}$$

If we are interested in small values of L, we can focus our attention on g_β since W cannot approach zero or infinity for any nontrivial case. Consider the condition for $g_\beta=0$:

$$g_a^2 + (b_a - 0.5\omega C)^2 = 0.25(\omega C)^2. \tag{33}$$

On the y_a plane, this is the equation of a circle with center at 0, $-0.5\ \omega C$ and radius $0.5\ \omega C$. If W does not approach zero, and it does not, then points outside the circle and arbitrarily close to the circle will give arbitrarily small conversion loss. Points inside the circle yield negative IF conductance which presumably is to be associated with IF oscillations, and the equation for L does not apply. The situation is quite similar to the broad-band case.[30] It is presented here because to the author's knowledge it has not appeared in the literature and yet the equations are shorter and it is a simpler case to understand than the broad-band one. A consideration of L as a function of frequency will yield some interesting results. Suppose that one considers C and g to be fixed and ω and y_a to be such that the point y_a is a considerable distance away from the circle. Then L will be given by Wg_β and will be large if y_a is far enough away from the circle. However, as the frequency is increased while y_a is held constant, the conversion loss will de-

[27] *Ibid.*, p. 409.
[28] *Ibid.*, p. 136.
[29] *Ibid.*, (92)–(95); and also, p. 408 (11).
[30] *Ibid.*, p. 409. Note that in the narrow-band high-frequency case presented above, the region of negative g_β is adjacent only to a region of small g_β and not to a region of large g_β. Note also that W possesses no nontrivial singularities.

crease, approaching zero as the circle approaches y_a. Thus, we have a conversion loss that decreases as the frequency increases. It is quite clear that one pays for small L in terms of bandwidth. For y_a must be reasonably close to the circle for small L, but a change in frequency will in general move y_a with respect to the circle, not only because the circle moves but also because in general y_a is also a function of frequency. These two effects could conceivably cancel over a small-frequency band. If y_a moves inside the circle then the oscillatory condition holds and if y_a moves too far away from the circle, L increases.

Returning to the case $r \neq 0$, let us set $y_a' = y_a b$ and define a function

$$f(y) = g - \frac{j\omega C g}{y + j\omega C}. \tag{34}$$

Then from (31),

$$y_\beta^0(y_a) = f(y_a), \qquad r = 0 \tag{35}$$

while from (29),

$$y_\beta = \frac{1}{b} f(y_a'), \qquad r \neq 0. \tag{36}$$

Note that y_β^0 is considered a function, while y_β is not. Then

$$y_\beta = \frac{1 + j\omega C r}{1 + (\omega C r)^2} g \left[1 - \frac{j\omega C}{g_a' + j(b_a' + \omega C)} \right]. \tag{37}$$

Of course, y_a is arbitrary; *i.e.*, we assume y_a is under the control of the circuit engineer and can be made to assume any value. The question arises as to whether or not y_a' is also arbitrary, for if it is, the effect of the spreading resistance on y_β is simply multiplication by the factor $1/b$. Now

$$\begin{aligned} y_a' &= g_a' + j b_a' = (1 - j\omega r C)(g_a + j b_a); \\ g_a &= \frac{g_a' - \omega C r b_a'}{1 + (\omega C r)^2}; \end{aligned} \tag{38}$$

$$b_a = b_a' + \omega C r \left[\frac{g_a' - \omega C r b_a'}{1 + (\omega C r)^2} \right]. \tag{39}$$

From (38), some values of b_a' will require a negative g_a for solution. This is not physically acceptable; however, if b_a' is limited to negative values, a positive g_a will always satisfy (38). Assuming that b_a' is limited to negative values, (29) gives

$$y_\beta = \frac{1}{1 + (\omega C r)^2} (1 + j\omega C r) [g_\beta^0(g_a', b_a') + j b_\beta^0(g_a', b_a')] \tag{40}$$

and

$$g_\beta = \frac{1}{1 + (\omega C r)^2} [g_\beta^0(g_a', b_a') - \omega C r b_\beta^0(g_a', b_a')] \tag{41}$$

where

$$y_\beta^0(y_a') = g_\beta^0(g_a', b_a') + j b_\beta^0(g_a', b_a') = f(y_a'). \tag{42}$$

The factor $1/[1+(\omega C r)^2]$ affects the magnitude of g_β but is not a factor in determining whether or not g_β becomes negative. From (31)

$$g_\beta = \frac{1}{1 + (\omega C r)^2} \left[g_\beta^0(g_a', b_a') + \frac{(\omega C)^2 g g_a' r}{g_a'^2 + (b_a' + \omega C)^2} \right]. \tag{43}$$

This equation shows, and it is quite clear intuitively, that the presence of finite spreading resistance always decreases the possibility of obtaining negative g_β, and shows precisely the condition for negative g_β with finite spreading resistance in terms of the value of g_β without spreading resistance. Of course, g_β is given by (32). Eqs. (8), (27), and (43) can be used to calculate L when g_β is positive.

Case 3

Suppose $r = 0$ and the image is shorted. Then[31]

$$Y = Y' = \begin{bmatrix} g_0 + j\omega C_0 & g_1 + j\omega C_1 \\ g_1 & g_0 \end{bmatrix} \tag{44}$$

and, from (7)

$$\frac{g_\beta}{g_0} = 1 - \frac{(g_1^2/g_0)(g_0 + g_a) + (\omega C_1 g_1/g_0)(\omega C_0 + b_a)}{(g_0 + g_a)^2 + (\omega C_0 + b_a)^2}. \tag{45}$$

To investigate the conditions for $g_\beta = 0$, the numerator and denominator of the fraction are set equal, and with a little manipulation the following equation is obtained:

$$\left[g_a + \left(g_0 - \frac{g_1^2}{2g_0} \right) \right]^2 + \left[b_a + \left(\omega C_0 - \frac{\omega C_1 g_1}{2g_0} \right) \right]^2 = \frac{g_1^2}{4g_0^2} (g_1^2 + \omega^2 C_1^2). \tag{46}$$

This is the equation of a circle in the y_a plane with center at

$$\left(\frac{g_1^2}{2g_0} - g_0 \right), \qquad \left(\frac{\omega C_1 g_1}{2g_0} - \omega C_0 \right)$$

and radius squared of

$$\frac{g_1^2}{4g_0^2} (g_1^2 + \omega^2 C_1^2).$$

Note that both coordinates of the center of the circle are always negative. The general condition for g_β to be negative with a physically realizable y_a is that the radius be greater in magnitude than the x coordinate of the center of the circle. Thus a low-frequency cutoff for negative g_β can be calculated by setting the radius of the circle equal to the x coordinate of the center of the circle. Some special cases are of interest. For the case of a linear capacitor, $C_1 = 0$, the center of the circle is at $(g_1^2/2g_0) - g_0$; $-\omega C_0$ and the radius squared is

[31] *Ibid.*, p. 408.

$$\frac{g_1^4}{4g_0^2}.$$

Since $g_1 \leqq g_0$, all points inside the circle can be shown to correspond to negative g_a, and this is physically inacceptable. Just as in the broad-band case, then[32] negative IF conductance is not obtained with a linear capacitor. Note, however, that one of the conditions, which is certainly not met in practice, is that the *LO* voltage waveform be symmetrical. To the author's knowledge, the more general case has not been investigated, although there is experimental evidence[33] that relaxation of this restriction will not change the picture.

[32] *Ibid.*
[33] H. Q. North, *et al.*, "Welded Germanium Crystals," GE Rep., Contract OEMsr-262, Order No. DIC 178554; September 20, 1945.

If one sets $g_0 = g_1 = g$ and $C_0 = C_1 = C$, *i.e.*, maximum nonlinearity for both the barrier capacitance and conductance, the center of the circle is at $-0.5\ g$, $-0.5\ \omega C$ and the radius is $0.5\sqrt{g^2+\omega^2C^2}$. Thus, in this special case there is no low-frequency cutoff for negative IF conductance.

When g_β is not negative, W is of interest and is given by

$$W = \frac{(g_0 + g_a)^2 + (b_a + \omega C_0)^2}{g_a g_1^2}. \tag{47}$$

Acknowledgment

The author wishes to thank A. Brodzinsky for his encouragement and helpful discussions.

Resonance Properties of Ring Circuits*

FRIEDRICH J. TISCHER†

Summary—**The ring guide or ring circuit, a microwave device consisting of a waveguide having the ends connected to form an annular ring, has properties similar to those of ordinary resonant cavities. Wave propagation within the ring guide, its interaction with a waveguide to which it is coupled, and its resonant circuit properties are investigated in this report. The properties of a prototype circuit consisting of a ring guide of rectangular cross section were found to agree with theory.**

Introduction

CAVITIES with conducting walls have, at wavelengths of the order of their geometrical sizes, the same electromagnetic properties as resonant circuits consisting of capacitances and inductances at lower frequencies. Therefore, cavities are useful as resonant circuits and filter elements at microwave frequencies. They can also be considered as waveguide sections short circuited at each end. The electromagnetic energy oscillates between the electric and magnetic states. Standing waves and an imaginary Poynting vector are of significance at any point in the cavity.

A new type of microwave circuit[1] consists of a waveguide having the ends connected to form a ring in which waves progressing in one direction only are excited. This circuit is characterized by a real Poynting vector within the ring guide cavity. Properties of the circuit, including the form of wave propagation within the ring, interaction with a waveguide to which it is coupled, and its *Q*-value, are investigated. Circuit performance when excited to produce traveling waves in one direction is compared with that obtained when excited to produce waves in both directions.

* Manuscript received by the PGMTT, June 14, 1956. The reported work was performed under Contract Tu1-9004.
† Dept. of Elec. Eng., Ohio State Univ., Columbus, Ohio. Formerly at Res. Labs., Redstone Arsenal, Huntsville, Ala.
[1] F. J. Tischer, Swedish Patent No. 152,491; August 26, 1952.

Wave Propagation in the Ring Circuit When Coupled to a Waveguide

The system under investigation consists of a waveguide to which a ring guide is coupled as shown schematically in Fig. 1. In order to obtain waves progressing in one direction only in the ring, directional coupling is used. When nondirectional coupling is applied, waves progressing in both directions are obtained. These two types of coupling are shown in Fig. 2, *i.e.*, directional coupling by two holes spaced a distance of $\lambda_g/4$ apart and nondirectional coupling by a single hole.

In the following derivation based on the wave concept, h indicates the waves progressing toward the coupling element, while r corresponds to waves reflected and traveling from the coupling element. The symmetry plane AA', Fig. 2, is used as phase reference. The ports of the main waveguide are 1 and 2, while those of the secondary guide which will be connected to form a ring are 3 and 4. The other parameters which describe the wave propagation in the region of the junction are the reflection coefficients ρ_{nn} at the four ports and the transmission coefficients T_{nm} between the different ports with reference to plane AA'.

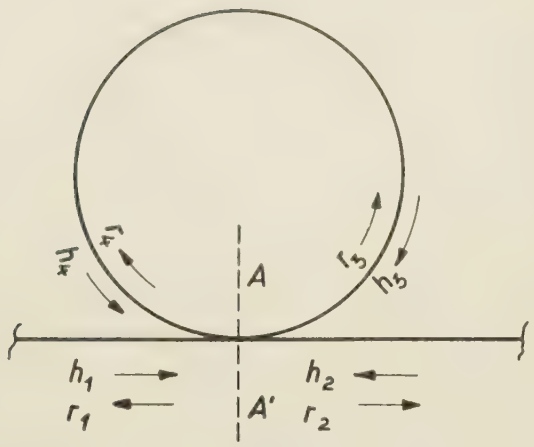

Fig. 1—Ring circuit.

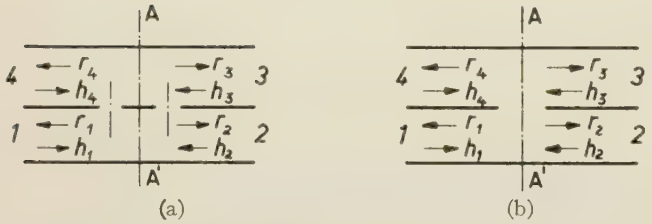

Fig. 2—Coupling conditions. (a) Directional coupling. (b) Non-directional coupling.

The wave propagation in the region of the junction can be described in general by the following equation systems:

$$\begin{aligned} r_1 &= \rho_{11}h_1 + T_{12}h_2 + T_{13}h_3 + T_{14}h_4 \\ r_2 &= T_{21}h_1 + \rho_{22}h_2 + T_{23}h_3 + T_{24}h_4 \\ r_3 &= T_{31}h_1 + T_{32}h_2 + \rho_{33}h_3 + T_{34}h_4 \\ r_4 &= T_{41}h_1 + T_{42}h_2 + T_{43}h_3 + \rho_{44}h_4. \end{aligned} \tag{1}$$

The assumption of symmetry of the coupling elements yields

$$\rho_{11} = \rho_{22} = \rho_{33} = \rho_{44} = \rho_0,$$
$$T_{nm} = T_{mn}$$

and

$$T_{12} = T_{34} = T, \quad T_{13} = T_{24} = k_h, \quad T_{14} = T_{23} = k_r$$

where k_h and k_r are coupling factors for the waves traveling in the two directions from the coupling element in the secondary guide. One obtains with these values

$$\begin{aligned} r_1 &= \rho_0 h_1 + k_h h_3 + k_r h_4 \\ r_2 &= T h_1 + k_r h_3 + k_h h_4 \\ r_3 &= k_h h_1 + \rho_0 h_3 + T h_4 \\ r_4 &= k_r h_1 + T h_3 + \rho_0 h_4 \end{aligned} \tag{2}$$

where h_2 is made 0 by reflectionless termination of port 2.

The ring guide is formed by connecting ports 3 and 4 with a length of guide so that:

$$\begin{aligned} h_3 &= r_4 \cdot e^{-\phi} \\ h_4 &= r_3 \cdot e^{-\phi}. \end{aligned} \tag{3}$$

ϕ is a complex quantity, the imaginary part being the phase delay around the ring guide and the real part the attenuation along this path in nepers. Thus,

$$\phi = (\alpha + i\beta)L \tag{4}$$

where L is the circumference and α and β are the attenuation and phase constants of the ring guide, respectively. Combining (3) and (2) yields:

$$\begin{aligned} r_3(1 - Te^{-\phi}) &= k_h h_1 + \rho_0 r_4 e^{-\phi} \\ r_4(1 - Te^{-\phi}) &= k_r h_1 + \rho_0 r_3 e^{-\phi}. \end{aligned} \tag{5}$$

Solving for r_3 and r_4,

$$r_3 = h_1 \frac{k_h(1 - Te^{-\phi}) + k_r\rho_0 e^{-\phi}}{(1 - Te^{-\phi})^2 - \rho_0^2 e^{-2\phi}} \tag{6}$$

and

$$r_4 = h_1 \frac{k_r(1 - Te^{-\phi}) + k_h\rho_0 e^{-\phi}}{(1 - Te^{-\phi})^2 - \rho_0^2 e^{-2\phi}} \tag{7}$$

are obtained. Similarly, r_1 and r_2 may be found. From these values, the reflection coefficient ρ_{in} and the transmission coefficient T_{12} in the main guide are

$$\rho_{in} = \frac{r_1}{h_1} = \rho_0 + \frac{2k_r k_h(1 - Te^{-\phi})e^{-\phi} + (k_r^2 + k_h^2)\rho_0 e^{-2\phi}}{(1 - Te^{-\phi})^2 - \rho_0^2 e^{-2\phi}} \tag{8}$$

and

$$T_{12} = \frac{r_2}{h_1} = T + \frac{2k_r k_h \rho_0 e^{-2\phi} + (k_r^2 + k_h^2)(1 - Te^{-\phi})e^{-\phi}}{(1 - Te^{-\phi})^2 - \rho_0^2 e^{-2\phi}}. \tag{9}$$

These relations describe the properties of the ring circuit as a resonant filter.

It is necessary to distinguish between two cases of wave propagation, namely, waves progressing in only one direction, and standing waves. These conditions depend on the coupling. They can be expressed by $k_r = 0$ for directional coupling and $k_h = k_r = k$ for nondirectional coupling.

For directional coupling,

$$R_D = \frac{r_3}{h_1 k_h} = \frac{1}{1 - Te^{-\phi}} \tag{10}$$

describes the complex wave in the ring guide. This relation is obtained for $k_r = 0$ and $\rho_0 = 0$ which follow from the properties of a directional coupling element. Therefore,

$$r_4 = 0, \qquad \rho_{in} = 0 \tag{11}$$

and

$$T_{12} = T + \frac{k_h^2 e^{-\phi}}{1 - Te^{-\phi}}. \tag{12}$$

Consideration of the nondirectional case ($k_h = k_r = k$) gives

$$R_N = \frac{r_3}{h_1 k} = \frac{r_4}{h_1 k} = \frac{1}{1 - (\rho_0 + T)e^{-\phi}} \tag{13}$$

and

$$\rho_{in} = \rho_0 + 2k^2 e^{-\phi} \frac{1}{1 - (\rho_0 + T)e^{-\phi}} \tag{14}$$

$$T_{12} = T + 2k^2 e^{-\phi} \frac{1}{1 - (\rho_0 + T)e^{-\phi}} . \tag{15}$$

From (10) through (15), it can be seen that the relations for the amplitude of the ring wave represented by R_D and R_N are the most important. They appear in all relations for the over-all reflection and transmission coefficients. This is expected since a part of the energy in the ring is coupled back into the main guide. This energy adds to the energy in the main guide, and the resultant interaction determines the properties of the circuit.

Frequency Dependence of the Wave Amplitude in the Ring Guide

The resonance characteristics can be obtained by representing the wave amplitude in the ring guide as a function of frequency. Accordingly, the absolute values $|R_D|$ and $|R_N|$ must be determined. Introduction of the attenuation and phase constants, α and $\beta = 2\pi/\lambda_g$ into (10) and (13) gives

$$R_D = \frac{1}{1 - Te^{-\alpha L} e^{-i\frac{2\pi_L}{\lambda_g}}} \tag{16}$$

and

$$R_N = \frac{1}{1 - (\rho_0 + T)e^{-\alpha L} e^{-i\frac{2\pi_L}{\lambda_g}}} . \tag{17}$$

The equations show that near resonance, variation of the frequency results mainly in a rotation of the complex terms T and $\rho_0 + T$ in the denominators of both relations. The frequency dependence follows the same law for both coupling conditions. This dependence can be represented in a normalized form valid for both coupling conditions by

$$R = \frac{1}{1 - \alpha e^{-ix}} . \tag{18}$$

Plotting the absolute value $|R|$ vs frequency deviation gives a resonance curve as I in Fig. 3. Resonance occurs when x equals a multiple of 2π, the circumference L then being a multiple of the guide wavelength λ_g.

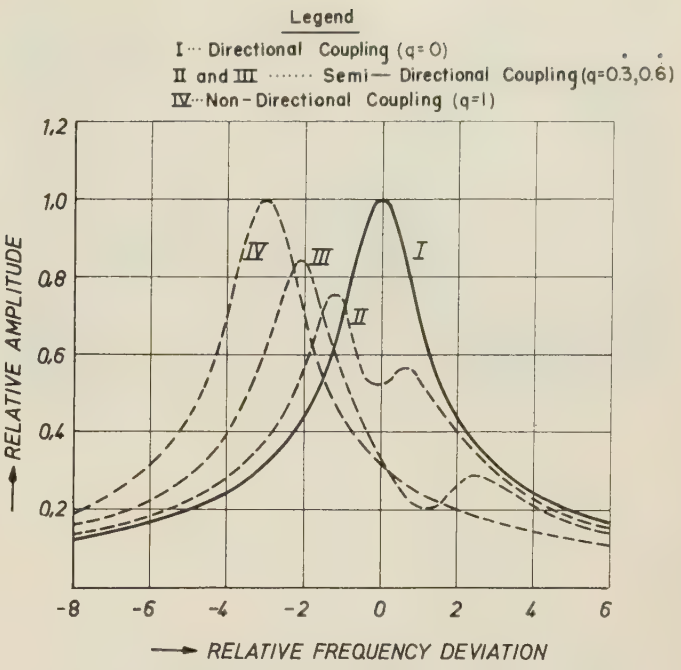

Fig. 3—Frequency response.

Calculation of the reflection coefficient ρ_0 in the nondirectional case for small and lossless coupling shows that it is small in magnitude and approximately a pure imaginary. R_D and R_N were found to differ mainly in their resonant frequencies.

The Case of Semidirectional Coupling

Interesting relations are obtained if the coupling in the two directions, defined by the coupling factors k_h and k_r, is unequal. This type of coupling is called semidirectional. If $k_r/k_h = q$ is introduced in (6),

$$r_3 = h_1 k_h \frac{1 - \left(T - \frac{k_r}{k_h}\rho_0\right)e^{-\phi}}{[1 - (T + \rho_0)e^{-\phi}][1 - (T - \rho_0)e^{-\phi}]} \tag{19}$$

is obtained. Eq. (19) has two poles and a zero between them in the complex plane. Therefore, the frequency response of a ring circuit with semidirectional coupling has a form which is analogous to that of band-pass filters containing two resonant circuits.

Eq. (19) is plotted in Fig. 3 for $q = 0, 0.3\dot{3}, 0.6\dot{6}, 1$, for curves I through IV, respectively, under the condition $|\rho_{0_{max}}| = 3(1 - |T|)$. Ordinary resonance curves for directional and nondirectional coupling and the double peak response for semidirectional coupling are shown.

A similar double peak response is observed when a discontinuity is introduced in a directionally coupled ring circuit with waves traveling in only one direction. To analyze this case, the assumption is made wherein a symmetrical discontinuity with a reflection coefficient ρ_1 is placed opposite to the coupling element (Fig. 4). The discontinuity can be taken into account by introducing

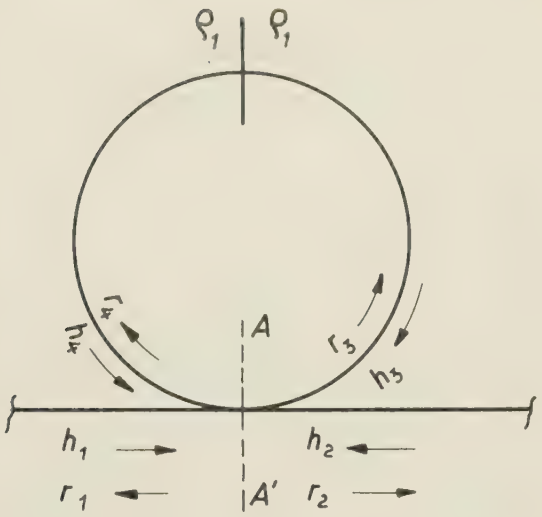

Fig. 4—Ring circuit with discontinuity (ρ_1).

terms of a Taylor's series for frequencies near resonance. This yields

$$\frac{1}{R} \approx 1 - a + iae^{-ix}\frac{dx}{d\lambda}\Delta\lambda. \tag{25}$$

Use of this simplified relation allows determination of $\Delta\lambda_{1,2}$ by equating real and imaginary parts of (25). Therefore,

$$\pm\Delta\lambda_{1,2} \approx \frac{1-a}{a}\,\frac{1}{\dfrac{dx}{d\lambda}} \tag{26}$$

where $e^{-ix}=1$ at resonance.

Introduction of $x=2\pi L/\lambda_g$ and differentiation gives

$$\pm\frac{\Delta\lambda_{1,2}}{\lambda_{res}} \approx \frac{1-a}{a}\left(\frac{\lambda_{res}}{\lambda_{g\,res}}\right)^2\frac{1}{\beta L} \tag{27}$$

$$h_3 = [r_3\rho_1 + r_4(1+\rho_1)]e^{-\phi}$$
$$h_4 = [r_4\rho_1 + r_3(1+\rho_1)e^{-\phi} \tag{20}$$

$$r_3 = h_1\frac{k_h[1-\rho_0\rho_1e^{-\phi} - T(1+\rho_1)e^{-\phi}] + k_r[\rho_0(1+\rho_1)e^{-\phi} + T\rho_1e^{-\phi}]}{[1-\rho_0\rho_1e^{-\phi} - T(1+\rho_1)e^{-\phi}]^2 - [\rho_0(1+\rho_1)e^{-\phi} + T\rho_1e^{-\phi}]^2}. \tag{21}$$

The corresponding relation for r_4 can be obtained by interchanging k_h and k_r in (21). For the case of directional coupling where $k_r=0$ and $\rho_0=0$, (21) can be simplified to:

$$r_3 = h_1k_h\frac{1-T(1+\rho_1)e^{-\phi}}{[1-Te^{-\phi}][1-T(1+2\rho_1)e^{-\phi}]}. \tag{22}$$

Comparison of (22) and (19) shows that both relations have characteristics similar to those of a band-pass filter with two resonant circuits. A difference exists, since (22) gives a symmetrical response having equal frequency deviations from the zero to the poles while (19) is nonsymmetrical.

The Q-Value of Resonant Ring Circuits

When the ring circuit is used as a resonator, the quality factor can be obtained by finding the frequency deviations $\Delta\lambda_{1,2}$ from resonance for which the amplitude of the ring waves decreases by a factor $1/\sqrt{2}$. Starting from the normalized frequency response, according to (18), the reciprocal value of R is

$$\frac{1}{R} = 1 - ae^{-ix}. \tag{23}$$

For resonance, $x=2\pi,\ 4\pi,\ \cdots\ n2\pi$,

$$\frac{1}{R_{res}} = 1 - a \tag{24}$$

is obtained where $a=|T|e^{-\alpha L}$ or $|T+\rho_0|e^{-\alpha L}$. For small attenuation in the ring guide and loose coupling $(1-a)\ll 1$, (23) can be approximated by the first two which is valid for both coupling conditions of the ring circuits at resonance. If a is replaced by the values corresponding to the coupling conditions, the following results are obtained:

Directional coupling: $a=|T|e^{-\alpha L}\approx|T|(1-\alpha L)$

$$a = |T|e^{-\alpha L} \approx |T|(1-\alpha L)$$
$$\pm\frac{\Delta\lambda_{1,2}}{\lambda_{res}} \approx \left(\frac{1+\alpha L}{|T|}-1\right)\left(\frac{\lambda_{res}}{\lambda_{g\,res}}\right)^2\frac{1}{\beta L}. \tag{28}$$

Nondirectional coupling: $a=|T+\rho_0|e^{-\alpha L}$

$$\pm\frac{\Delta\lambda_{1,2}}{\lambda_{res}} \approx \left(\frac{1+\alpha L}{|T+\rho_0|}-1\right)\left(\frac{\lambda_{res}}{\lambda_{g\,res}}\right)^2\frac{1}{\beta L}, \tag{29}$$

where β is the resonant phase constant. The relative wavelength deviations (28) and (29) are measures of the Q values. The unloaded values are obtained by reducing the coupling zero ($\rho_0\to 0$, $|T|\to 1$). Under this condition,

$$\pm\frac{\Delta\lambda_{1,2}}{\lambda_{res}} \approx \frac{\alpha}{\beta}\left(\frac{\lambda_{res}}{\lambda_{g\,res}}\right)^2 \tag{30}$$

is valid for both types of coupling, giving for the Q value

$$Q = \frac{\lambda_{res}}{2\Delta\lambda_{1,2}} \approx \frac{\beta}{2\alpha}\left(\frac{\lambda_{g\,res}}{\lambda_{res}}\right)^2. \tag{31}$$

This unloaded Q value can also be obtained directly by use of the energy concept applied to the definition of the Q value. According to this definition

$$Q = \frac{\omega W_{tot}}{P_d} \tag{32}$$

where $\omega = 2\pi f$, W_{tot} corresponds to the total energy content of the circuit, and P_d to the power dissipated. The power dissipated in a guide of length L is

$$P_d = P_{in} - P_{out} = P_{in}(1 - e^{-2\alpha L}) \approx 2\alpha L P_{in} \quad (33)$$

for small αL, where P_{in} and P_{out} are the powers passing through the input and output cross sections. The power transported by the waves through the input cross section can be expressed as the product of the energy contained per unit length in the guide w_{tot} and the group velocity v_{gr}. Thus

$$P_{in} = w_{tot} \cdot v_{gr} = w_{tot} \frac{v_0^2}{v_{ph}} \quad (34)$$

introducing

$$\lambda_0 = \frac{v_0}{f}, \qquad \lambda_g = \frac{v_{ph}}{f}$$

gives

$$W_{tot} = w_{tot} \cdot L = \frac{P_{in} \cdot L \cdot v_{ph}}{v_0^2}$$

from which

$$Q = \frac{1}{2\alpha} \frac{2\pi}{\lambda_g} \left(\frac{\lambda_g}{\lambda_0}\right)^2. \quad (35)$$

By introduction of $\beta = 2\pi/\lambda_g$, (31) may be obtained. In both derivations, the assumption was made that the attenuation varies insignificantly in the region of resonance.

Experimental Investigation of a Ring Circuit with Rectangular Waveguide

The ring guide permits design of a circuit with variable resonant frequency without use of sliding shorts and capacity plungers. One type of ring circuit comprising a rectangular waveguide of variable width is shown in Fig. 5. The waveguide in the form of a ring consists of two grooves of rectangular cross section machined into adjacent walls of two thick metallic disks. Each groove forms half of the guide in which TE_{01} waves with radial E vector are excited. One of the disks is movable in the axial direction. The movement is obtained by rotation of a micrometer head to which one disk is attached, thus permitting a change of the width of the guide. The change of width results in a variation of the wavelength in the guide λ_g, and of the resonant wavelength. The resonant wavelength can be expressed by

$$\lambda_{res} \approx \frac{1}{\sqrt{\frac{n^2}{L^2} + \frac{1}{4a^2}}}$$

where a is the width, L the circumference of the guide, and n the number of wavelengths per circumference. Normalization with respect to L yields

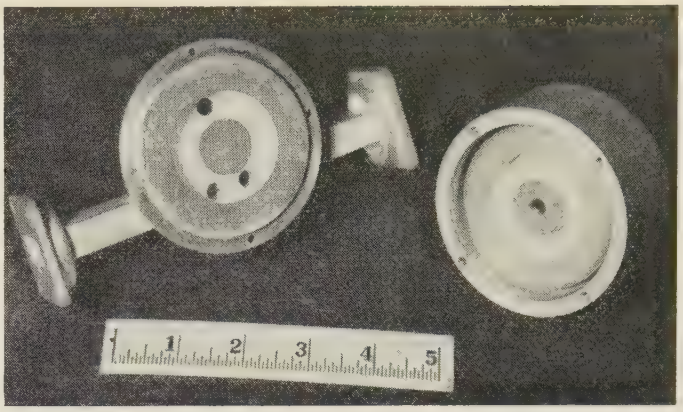

Fig. 5—Prototype of a ring circuit with rectangular waveguide and variable resonance frequency.

$$\frac{\lambda_{res}}{L} \approx \frac{1}{\sqrt{n^2 + \left(\frac{L}{2a}\right)^2}} \quad (36)$$

which relates resonant wavelength to the dimensions of the ring guide. Eq. (33) is an approximation in which the bending of the guides and the influence of the slots are neglected.

The Q value of a ring guide is given by (31). The values of α and β for a rectangular waveguide are

$$\alpha = \frac{(6.9)10^{-6}\sqrt{f^{[c/s]}}}{\lambda_0^{[m]}} \frac{\frac{\lambda_0}{b} + 4\left(\frac{\lambda_0}{\lambda_c}\right)^3}{\sqrt{1 - \left(\frac{\lambda_0}{\lambda_c}\right)^2}} \sqrt{\frac{\sigma}{\sigma_{cu}}} \quad (37)$$

and

$$\beta = \frac{2\pi}{\lambda_g},$$

where a is the variable width, b the constant height of the guide, and σ/σ_{cu} the conductivity related to that of copper. Introduction in (31) yields

$$\frac{2\Delta f}{f_{res}} = \frac{2\Delta f}{\lambda_{res}} = (2.2) \cdot 10^{-10} m \sqrt{f} \sqrt{\frac{\sigma_{cu}}{\sigma}},$$

$$m = \frac{\lambda_0}{b} + 4\left(\frac{\lambda_0}{\lambda_c}\right)^3, \quad (38)$$

the form factor m showing the dependence of Q on the geometry of the ring guide. In Fig. 6, m is shown as a function of the normalized wavelength in the guide λ_0/λ_g with λ_0/b as the parameter. The diagram permits the choice of dimensions to obtain a high Q value which is inversely proportional to Δf. It should be noted that the half-power bandwidth of a comparable circular cavity in the case of optimized dimensions corresponds to a form factor $m = 1.5$ for low loss TE_{01} waves. The measured Q values of the ring circuit shown in Fig. 5 are compared with those obtained using (38) in Fig. 7. Taking into account the fact that the measured values

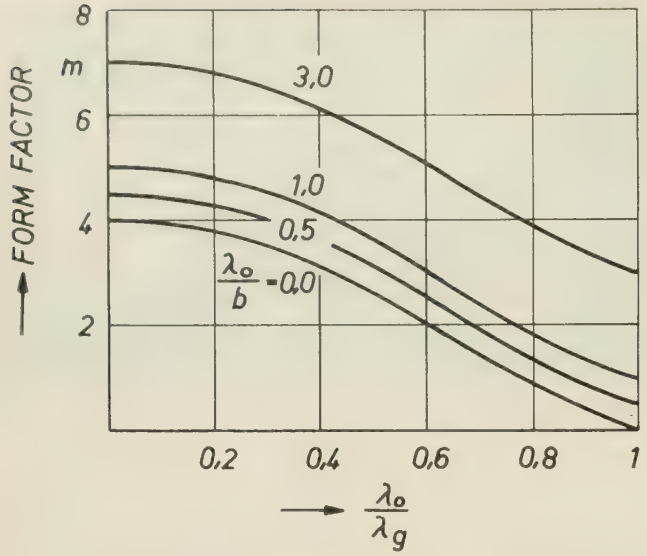

Fig. 6—Dependence of the form factor m on the geometry of rectangular waveguide.

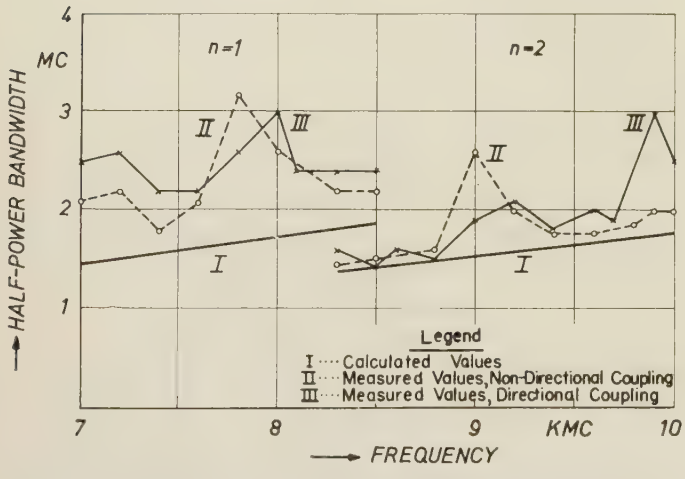

Fig. 7—Calculated and measured values of the half-power bandwidth for prototype shown in Fig. 5.

of Δf correspond to the loaded Q while the calculation is based on the unloaded Q, the agreement is considered satisfactory.

Conclusion

The essential difference between the ring circuit and the conventional microwave cavity lies in its capacity to resonate with unidirectional progressive waves in the ring when directionally coupled to the main guide. When nondirectionally coupled, the circuit assumes the behavior of an ordinary cavity with standing waves. The resonance curves are similar in either case, the Q values differing by only a small amount due to the coupling effects.

Interesting properties result from semidirectional coupling or the introduction of a small discontinuity into the directionally coupled ring. In either instance, the circuit is characterized by a double-peaked resonance. Accordingly, it is useful as a microwave filter.

The device has immediate application as a tunable resonant circuit. Tuning is accomplished by any means whereby the electrical length of the ring is changed. Thus a phase shifter may be employed, permitting a variation in the phase of the guide wavelength around the ring so that its electrical length can be made a multiple of a wavelength at resonance. An adjustable width ring, which allows adjusting the guide wavelength uniformly over the circumference of the ring, is a means of performing simple, low-loss tuning. Since increasing the ring width reduces the attenuation, higher modes of resonance will have higher Q values. Multiple resonance occurs when the guide is adjusted for two or more guide wavelengths.

Possible fields of application for the ring circuit are the same as those of commonly used standing-wave type cavities. The high Q values of the adjustable width circuit favor its application for frequency measurement and stabilization. The geometrical form permits easy fabrication, especially for use at extremely high frequencies.

Acknowledgment

The author wishes to express his thanks to Capt. W. J. Lindberg for his help in the composition of this paper, in checking the derived relations, and in the experimental work. J. Copeland designed and tested the experimental model.

Frequency Stabilization of a Microwave Oscillator with an External Cavity*

IRVING GOLDSTEIN†

Summary—**This paper describes a procedure by which a cavity stabilizer may be designed for a microwave oscillator. Formulas are derived for the following essential design parameters: 1) stabilization factor; 2) stabilization range; 3) vswr of the stabilizer circuit with cavity tuned; 4) vswr of the stabilizer circuit with the cavity detuned; and 5) insertion loss of the cavity assembly.**

The validity of designing with the derived relations has been experimentally confirmed.

Introduction

IN MANY applications, the need arises for a microwave oscillator having a stable frequency characteristic both on a long and short-time basis. The addition of an external cavity and associated microwave circuitry to an ordinary magnetron or klystron transforms these tubes into frequency stabilized oscillators. The general scheme has been investigated by many.[1] Although this paper concerns itself with a stabilizer configuration which has been previously studied,[2] a more than cursory survey of the literature does not show a precise analysis and quantitative development such as is here described.[3] The validity of the results justifies their collation. The configuration in Fig. 1 is one in which the external cavity and damping resistor[4] are either in series or parallel with the oscillator output line. The damping resistor consists of a matched load and an inductive or capacitive susceptance placed so that there is a conductance in series with the stabilizing cavity. The purpose of the damping resistor is to suppress unwanted modes in the tube, the transmission line, and stabilizing cavity assembly. The resistor also increases the stabilization range.

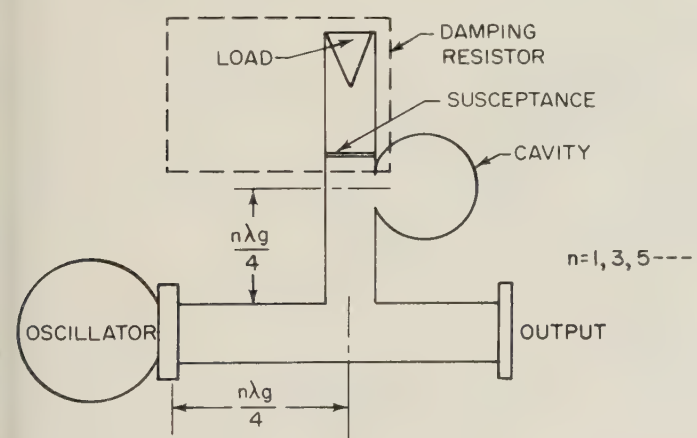

Fig. 1—Cavity stabilized oscillator.

List of Symbols

S = stabilization factor.
m = junction transformer ratio.
G_T = damping resistor (normalized).
Q_{EC} = external Q of the cavity.
Q_{OC} = unloaded Q of the cavity.
Q_{EM} = external Q of the oscillator.
ρ_{off} = vswr into assembly with cavity detuned.
ρ_{on} = vswr into assembly with cavity tuned.
L = insertion loss of the stabilizing system.
f_0 = system frequency.
ΔF = stabilization frequency range.
PF = pulling figure for the oscillator.

The design relations are given below (their derivation will be presented in the Appendix):

$$S = m^2\left[\frac{(G_T)^2}{\left(G_T + \frac{Q_{EC}}{Q_{OC}}\right)^2}\,\frac{Q_{EC}}{Q_{EM}}\right] + 1 \tag{1a}$$

$$L = 20\log\left[1 + \frac{m^2 G_T \frac{Q_{EC}}{Q_{OC}}}{2\left(G_T + \frac{Q_{EC}}{Q_{OC}}\right)}\right] \tag{1b}$$

$$\rho_{\text{on}} = \left[1 + \frac{m^2 G_T \frac{Q_{EC}}{Q_{OC}}}{G_T + \frac{Q_{OC}}{Q_{OC}}}\right] \tag{1c}$$

$$\rho_{\text{off}} = m^2 G_T + 1 \tag{1d}$$

$$\text{PF} = \frac{0.417 f_0}{Q_{EM}} \tag{1e}$$

$$\Delta F = f_0\left(\frac{G_T}{Q_{EC}} + \frac{1}{Q_{OC}}\right), \tag{1f}$$

* Manuscript received by the PGMTT, June 14, 1956.
† Raytheon Manufacturing Co., Bedford, Mass.

[1] F. F. Rieke, "Microwave Magnetrons," M.I.T. Rad. Lab. Ser. No. 6, McGraw-Hill Book Co., Inc., New York, N. Y., 1948. See Ch. 16.
W. V. Smith, "Magnetron Tuning and Stabilization," M.I.T. Rad. Lab. Rep. No. 567, July 13, 1944.
W. M. Preston and J. B. Platt, "Magnetron Stabilizer Tuner," Rad. Lab. Group Rep. No. 473, 1943.
W. M. Preston, "Magnetron Stabilizing Tuner," Rad. Lab. Group Rep. No. 71, May 31, 1944.
E. Shelton, "Stabilization of microwave oscillators," IRE Trans., vol. ED-1, pp. 30–40; December, 1954.

[2] Preston and Platt, *op. cit.*

[3] The results developed have been independently derived by E. Shelton of Raytheon in a private communication.

[4] Rieke, *op. cit.*

Before the actual design of the stabilizer circuit can be undertaken, there are some fundamental requirements of the oscillator and system to be considered.

For the oscillator, the starting characteristic is important. Upon start of oscillation, the tube is exposed to the mismatch of the stabilizer cavity detuned from resonance. The maximum value of this vswr ρ_{off}, must be known for the tube. In the case of pulse tubes electrical breakdown in the cavity is an important consideration. The resonator dimensions must be such that the voltage gradient in the cavity is safely below the breakdown level.

For the system, the following listed properties are important:

1) Stabilization factor required;
2) The insertion loss that can be tolerated in the stabilized circuit;
3) Stabilization range:
   a) This range must be large enough to prevent unlocking the stabilized tube by external match variations at the tube output;
   b) The range must also be sufficiently large to allow for an automatic frequency control loop either from the cavity to tune in the oscillator or from the oscillator to control the cavity.

The procedure for determining all the necessary quantities in design relations (1) is given in the following paragraphs.

1) The transformer ratio m of the junction can be determined from a vswr measurement of the oscillator input to the junction by itself with matched loads on the other two arms.

2) Q_{EC} the cavity external Q, and Q_{OC}, the cavity unloaded Q, can be determined by standard methods. The cavity must be of the line terminating absorption type.

3) Q_{EM}, the oscillator external Q, can be determined from a pulling figure measurement. The pulling figure is defined as the maximum excursion in frequency for a vswr of 1.5 moved through a wavelength. From (1c), Q_{EM} can be computed.

4) For a value of ρ_{off} (known for the oscillator) and a measured junction transformer ratio m the value of damping resistor G_T is determined from (1d).

$$G_T = \frac{\rho_{off} - 1}{m^2}.$$

The location and value of the susceptance necessary to yield the computed value of G_T at the cavity is then determined in the manner illustrated by the following example (see Fig. 2).

For $\rho_{off}=3$ and $m^2=0.7$ using (1d) we obtain $G_T=2.86$. The remaining problem is to determine the value and position of the admittance that will yield the computed value of G_T at the cavity. Using the Smith chart in Fig. 3 (opposite) and moving from $G_T=2.86$ toward the load to $1-jb$ point yields the value and position of inductive susceptance necessary; namely, $-j$ 1.1 at a distance of 0.416 λg from the center of the cavity input.

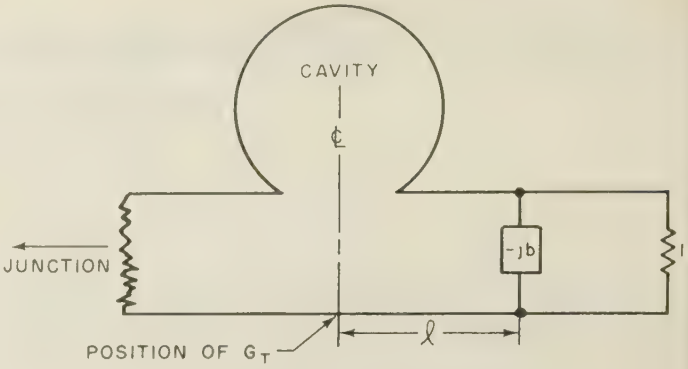

Fig. 2—Circuit for computing susceptance.

Now with all the quantities known, one can determine the necessary characteristics of the stabilized oscillator. The calculated values are compared to the experimental results on Figs. 4–6 (p. 60). The data was obtained on a cw magnetron.

Appendix

The analysis to follow is based on the equivalent circuit of oscillator and cavity combination shown in Fig. 7.

Expressing the admittance of a tuned circuit as $Y=G(1+jQ_0\epsilon)$ and also defining the other relations as shown below.

$$Q_E = p^2 y \qquad y = \sqrt{\frac{C}{L}}$$

$$Q_O = Ry \qquad \omega_0 = \frac{1}{\sqrt{LC}}$$

$$\epsilon = \frac{\omega}{\omega_0} - \frac{\omega_0}{\omega} \approx \frac{2\Delta\omega}{\omega_0}$$

$$Y_{(4-4)} = p^2(Y_C) \tag{2}$$

where

$$Y_C = G_C(1 + jQ_{0C}\epsilon)$$

$$Y_{(4-4)} = p^2 G_C(1 + jQ_{0C}\epsilon) \tag{3}$$

$$Y_{(4-4)} = \frac{Q_{EC}}{Q_{OC}}(1 + jQ_{0C}\epsilon) \tag{4}$$

$$Z_{(4-4)} = \frac{1}{\frac{Q_{EC}}{Q_{OC}}[1 + jQ_{0C}\epsilon]} \tag{5}$$

$$Z_{(4-5)} = \frac{1}{\frac{Q_{EC}}{Q_{OC}}[1 + jQ_{0C}\epsilon]} + \frac{1}{G_T}. \tag{6}$$

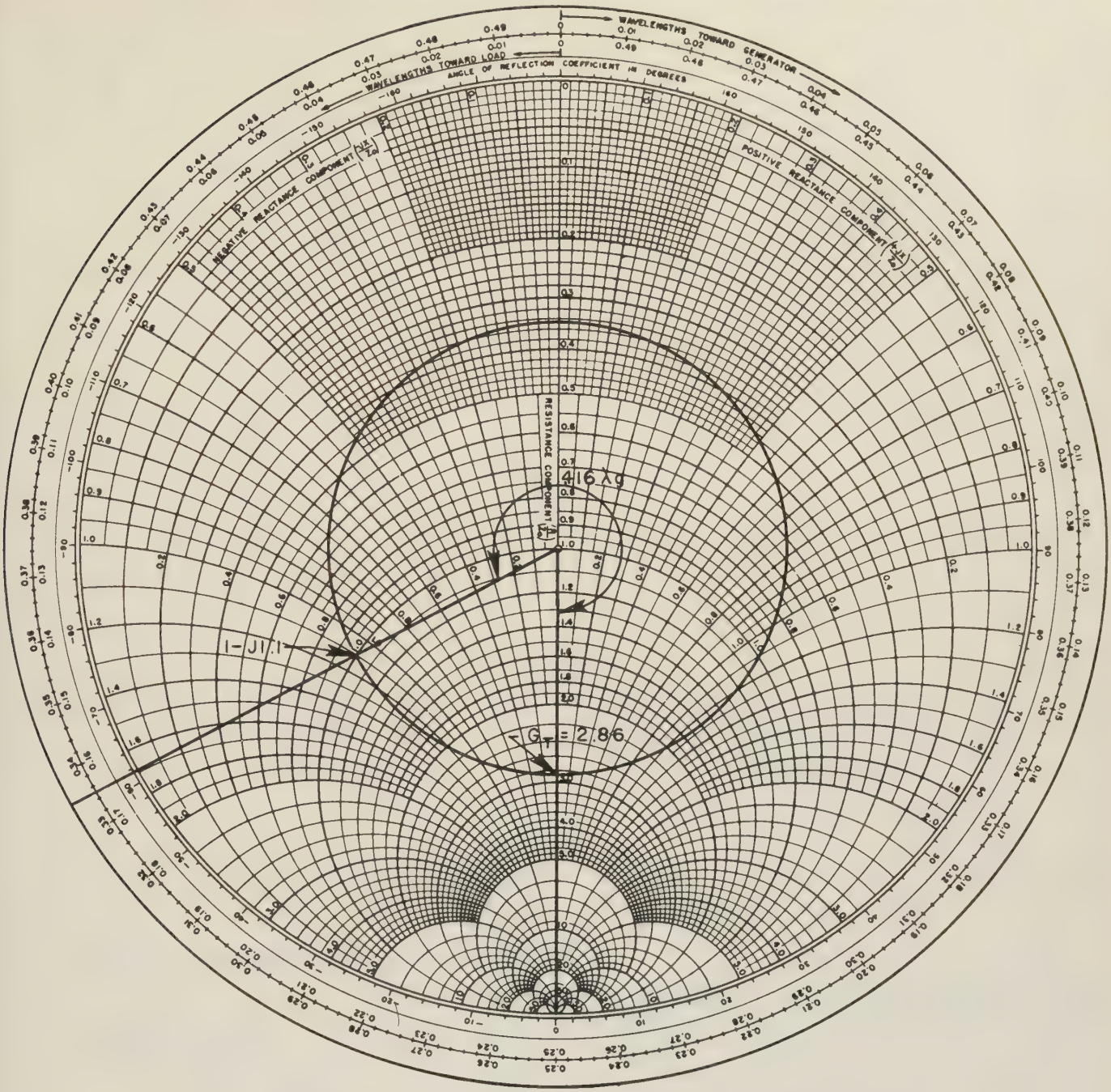

Fig. 3—Determination of the susceptance to yield the correct value of damping resistor.

Let

$$V = \frac{Q_{EC}}{Q_{OC}}$$

and recombining the terms of (6)

$$Z_{(4-5)} = \frac{G_T + (V + jQ_{EC}\epsilon)}{(V + jQ_{EC}\epsilon)G_T} \tag{7}$$

but because of

$$\frac{n\lambda g}{4} \qquad n = 1, 3, 5 \cdots$$

$$Z_{(2-2)} = \frac{m^2}{Z_{(4-5)}} = \frac{m^2 G_T(V + jQ_{EC}\epsilon)}{G_T + (V + jQ_{EC}\epsilon)} \tag{8}$$

$$Z_{(2-3)} = \frac{m^2(V + jQ_{EC}\epsilon)G_T}{G_T + (V + jQ_{EC}\epsilon)} + 1 \tag{9}$$

$$Z_{(1-1)} = \frac{1}{Z_{(2-3)}} \qquad Y_{(1-1)} = Z_{(2-3)}$$

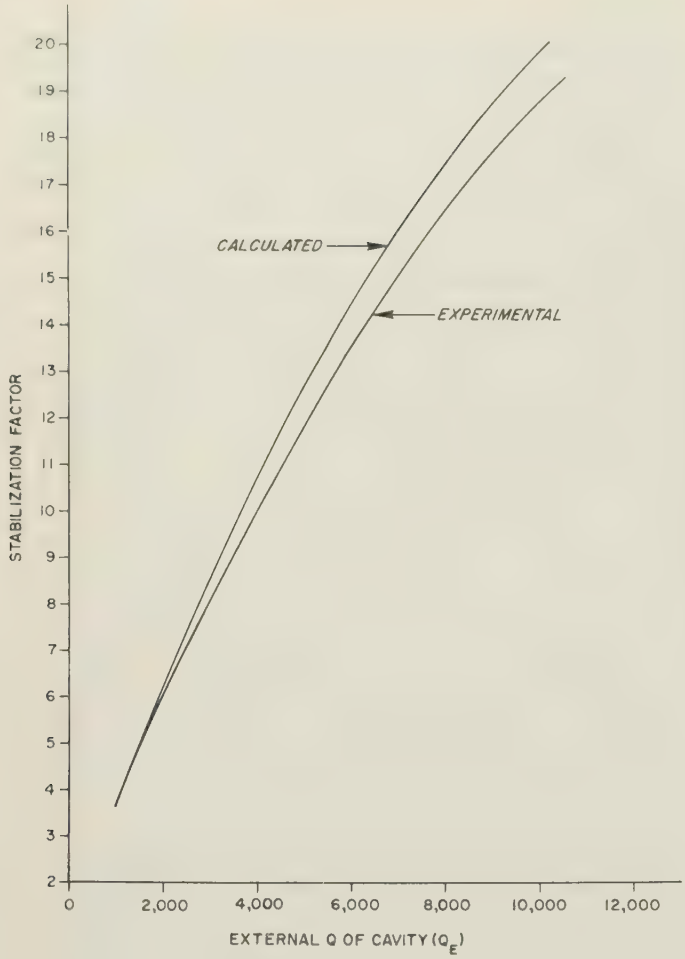

Fig. 4—Stabilization factor characteristic.

again because

$$\frac{n\lambda g}{4} \qquad n = 1, 3, 5 \cdots$$

$$Y_{(1-1)} = Z_{(2-3)} = \frac{(m^2VG_T + G_T + jm^2Q_{EC}\epsilon G_T + jQ_{EC}\epsilon)(G_T + jVQ_{EC}\epsilon)}{(G_T + V)^2 + (Q_{EC}\epsilon)^2} \cdot \quad (10)$$

Finding the imaginary part of $Y_{(1-1)}$ yields

$$B_{(1-1)} = \frac{m^2Q_{EC}\left(\frac{2\Delta\omega}{\omega_0}\right)G_T^2}{(G_T + V)^2 + \left(Q_{EC}\,\frac{2\Delta\omega}{\omega_0}\right)^2} \cdot \quad (11)$$

Differentiating (11) with respect to $\Delta\omega$ yields

$$\frac{dB_{(1-1)}}{d\Delta\omega} = \frac{\left[m^2(G_T + V)^2 + 4Q_{EC}^2\left(\frac{\Delta\omega}{\omega_0}\right)^2\right]\left[\frac{2Q_{EC}^2G_T^2}{\omega_0}\right]}{\left[(G_T + V)^2 + 4Q_{EC}^2\left(\frac{\Delta\omega}{\omega_0}\right)^2\right]^2} \cdot \quad (12)$$

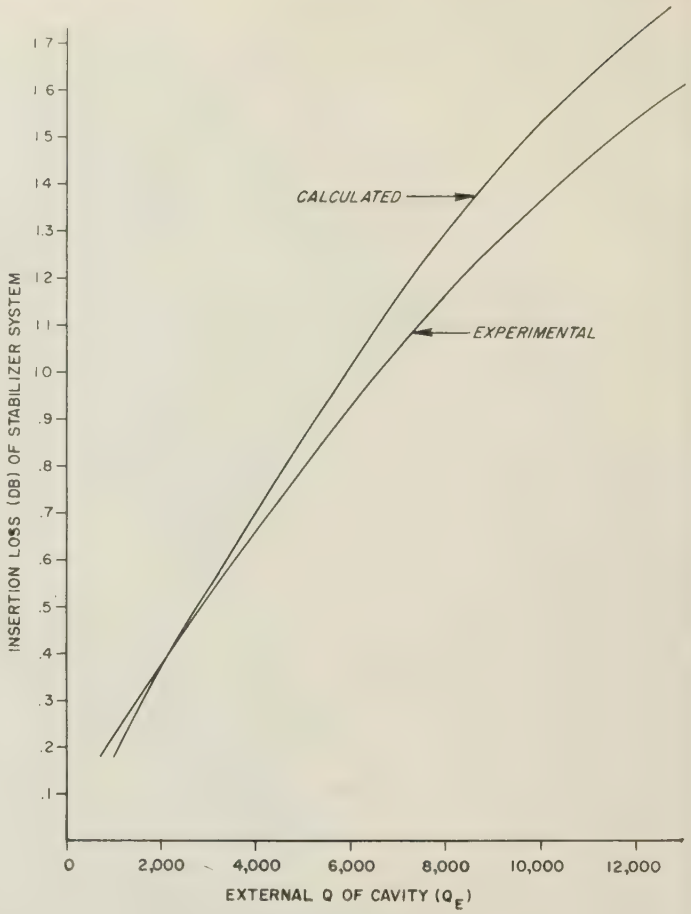

Fig. 5—Insertion loss characteristic.

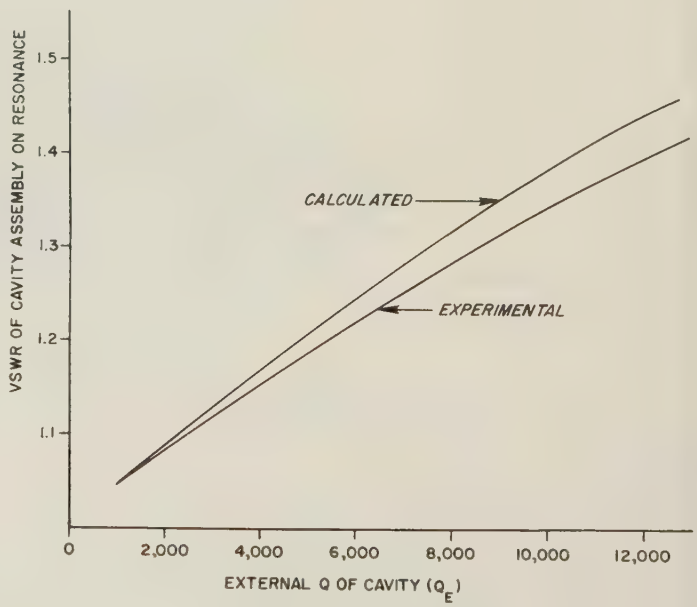

Fig. 6—Input vswr characteristic.

Let $\Delta\omega \rightarrow 0$

$$\frac{dB_{(1-1)}}{d\Delta\omega} = \frac{2m^2Q_{EC}(G_T)^2}{\left(G_T + \frac{Q_{EC}}{Q_{OC}}\right)^2\omega_0} \cdot \quad (13)$$

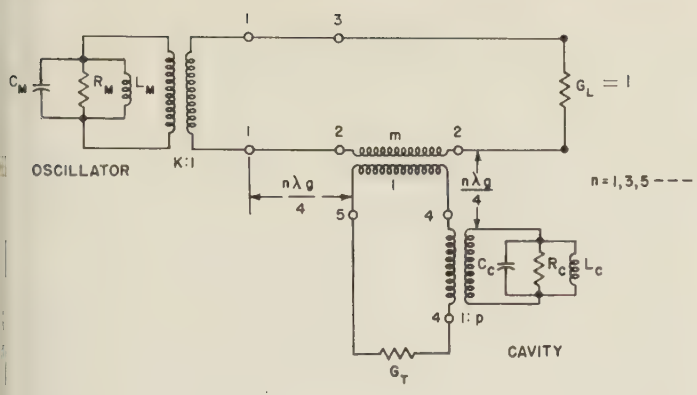

Fig. 7—Oscillator and cavity equivalent circuit.

Consideration of the oscillator circuit yields

$$Y_{(1-1)M} = K^2 G_M[1 + jQ_{OM}\epsilon]. \tag{14}$$

In a manner similar to operation of (4)

$$Y_{(1-1)M} = \frac{Q_{EM}}{Q_{OM}}\,[1 + jQ_{OM}\epsilon] \tag{15}$$

$$B_{(1-1)M} = Q_E\epsilon = 2Q_{EM}\,\frac{\Delta\omega}{\omega_0} \tag{16}$$

$$\frac{dB_{(1-1)M}}{d\Delta\omega} = \frac{2Q_{EM}}{\omega_0}\,. \tag{17}$$

The stabilization factor is defined as

$$S = \frac{\dfrac{dB_{(1-1)}}{d\Delta\omega}}{\dfrac{dB_{(1-1)M}}{d\Delta\omega}} + 1. \tag{18}$$

Substituting (13) and (17) into (18) yields the relation for stabilization factor.

$$S = m^2\,\frac{Q_{EC}}{Q_{EM}}\left[\frac{G_T}{G_T + \dfrac{Q_{EC}}{Q_{EC}}}\right]^2 + 1. \tag{19}$$

The stabilization range is defined as the frequency spread between the peaks of the transformed cavity susceptance at the oscillator terminals. Fig. 8 illustrates the curve. Stabilization depends upon the transformed cavity and magnetron susceptance having the same slope.

Since at the peaks of the transformed susceptance curve

$$\frac{dB_{(1-1)}}{d\Delta\omega} = 0, \tag{20}$$

we can obtain an expression for the frequency spread by setting (12) equal to zero and solving for ΔF.

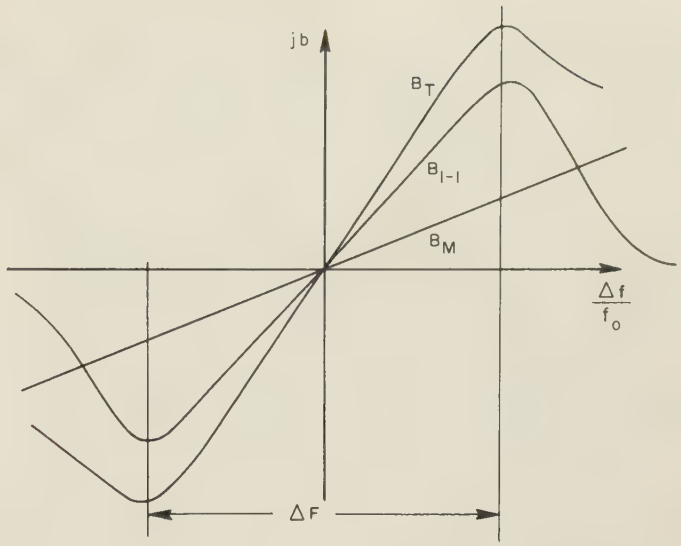

Fig. 8—Cavity and magnetron susceptance characteristics.

The solution yields the total stabilization range namely

$$\Delta F = f_0\left[\frac{G_T}{Q_{EC}} + \frac{1}{Q_{OC}}\right]. \tag{21}$$

The off resonance vswr looking in the stabilizing cavity assembly is derived from the following:

Using (9) off resonance $\epsilon \rightarrow \infty$

$$Z_{(2-3)} = \frac{\left[\dfrac{m^2V}{\epsilon} + jQ_{EC}G_T\right]}{\left[\dfrac{G_T}{\epsilon} + \dfrac{V}{\epsilon} + jQ_{EC}\right]} + 1 \tag{22}$$

$$Z_{(2-3)} = m^2G_T + 1 \tag{23}$$

$$\rho_{\text{off}} = m^2G_T + 1 \tag{24}$$

is the expression for the vswr into the assembly with the cavity detuned. The relation for the expected vswr with the cavity tuned is derived also using (8).

Using (8) and letting $\Delta\omega \rightarrow 0$ yields

$$Z_{(2-2)} = \frac{m^2G_T\,\dfrac{Q_{EC}}{Q_{OC}}}{G_T = \dfrac{Q_{EC}}{Q_{OC}}} \tag{25}$$

$$\rho_{\text{on}} = Z_{(2-2)} + 1 \tag{26}$$

$$\rho_{\text{on}} = \frac{m^2G_T\,\dfrac{Q_{EC}}{Q_{OC}}}{\left(G_T + \dfrac{Q_{EC}}{Q_{OC}}\right)} + 1. \tag{27}$$

The loss in the stabilizer is calculated again with aid of Fig. 8. Using (25), the loss is determined using the

A, B, C, D, matrix[5]

$$\begin{bmatrix} A & B \\ C & D \end{bmatrix} = \begin{bmatrix} 1 & Z_{22} \\ 0 & 1 \end{bmatrix}. \tag{28}$$

The loss is given by

$$|R|^2 = \frac{(A + B + C + D)^2}{4}. \tag{29}$$

Substituting (25) into (29) yields

$$|R|^2 = \left[1 + \frac{m^2 G_T \dfrac{Q_{EC}}{Q_{OC}}}{2\left(G_T + \dfrac{Q_{EC}}{Q_{OC}}\right)} \right]^2 \tag{30}$$

but $L = 20 \log R$.

Substituting (30) in (31)

$$L = 20 \log \left[1 + \frac{m^2 G_T \dfrac{Q_{EC}}{Q_{OC}}}{2\left(G_T + \dfrac{Q_{EC}}{Q_{OC}}\right)} \right]. \tag{31}$$

[5] E. A. Guillemin, "Communication Networks," John Wiley and Sons, Inc., New York, N. Y., vol. 2, ch. 4, pp. 132–180; 1947.

Cooling of Microwave Crystal Mixers and Antennas*

GEORGE C. MESSENGER†

Summary—**The development of low-noise mixer crystals has reached the point where the noise figure is approaching fundamental, theoretical limits. The desire for still greater sensitivity has led to the consideration of other possible means for noise reduction. This paper will discuss two possibilities: physically cooling the mixer crystal, and using an antenna directed toward background noise which is lower than room temperature. The improvement which can be realized increases rapidly as the room-temperature noise figure is reduced.**

Receiver Sensitivity Improvement from "Cold Antenna"

THE IMPROVEMENT ratio of receiver sensitivity as the antenna looks at free space, to the sensitivity as it looks at a room temperature background, increases hyperbolically as the noise figure is improved.

$$\frac{(N_0)T_0}{(N_0)T_s} = \frac{F}{F + \dfrac{T_s}{T_0} - 1} = [\mathrm{SR}]_A. \tag{1}$$

Here $(N_0)T_0$ is the output noise in the receiver as it looks at a room-temperature source, T_0, and $(N_0)T_s$ is the output noise in the receiver as it looks at the free-space background T_s. F represents the receiver noise figure. $[\mathrm{SR}]_A$ is the receiver sensitivity improvement ratio due to the cold antenna.

Because of the rapidity with which this ratio improves as F approaches its theoretical limit 1, it becomes economical to think of cooling the mixer *if* it has a very low F to begin with. X-band receivers using narrow-band techniques and low-noise germanium mixer crystals have noise figures low enough to make this improvement in sensitivity important and feasible.

Receiver Sensitivity Improvement from Cooling Mixer

The noise figure of a receiver using a crystal is given by

$$F = L_x[t_x + F_{\mathrm{if}} - 1] \tag{2}$$

where F is the receiver noise figure, L_x is crystal conversion loss, t_x is crystal noise temperature, and F_{if} is the IF noise figure. This formula is not convenient for discussing improvements due to cooling because t_x is a function of L_x.[1] The functional relationship is

$$t_x = \begin{cases} \bar{t}\left(1 + \dfrac{1}{L_x}\right) + \dfrac{1}{L_x} & \text{narrowband} \\ \bar{t}\left(1 - \dfrac{2}{L_x}\right) + \dfrac{2}{L_x} & \text{broadband.} \end{cases} \tag{3}$$

Here $\bar{t}$ is the noise temperature due only to the crystal. Substituting back in (2)

$$F = [L_x\bar{t} - (1, 2)]\bar{t} + (1, 2) + L_x(F_{\mathrm{if}} - 1) \tag{4}$$

where the 1 and 2 pertain to narrowband and broadband, respectively. Now

* Manuscript received by the PGMTT, June 14, 1956.
† Philco Corp., Research Div., Philadelphia, Pa.

[1] The harmonics of the local oscillator are assumed to be all shorted.

$$[\mathrm{SR}]_M = \frac{(L_x - 1, 2)\bar{t} + (1, 2) + L_x(F_{\mathrm{if}} - 1)}{(L_x - 1, 2)\bar{t}\,\frac{T}{T_0} + (1, 2) + L_x(F_{\mathrm{if}} - 1)} \quad (5)$$

where T is the mixer temperature and T_0 is room temperature and SR_M is the receiver-sensitivity-improvement-ratio due to cooling the mixer.

Now $\bar{t}$ is proportional to temperature if it is composed of any combination of shot and thermal noise. Theoretically, at least, it should decrease linearly with temperature. Cooling to 70°K without increasing L_x[2] should be practical. Therefore $\bar{t}$ can be cut by approximately a factor of four. Table I shows how the operation of a

TABLE I

Improvement in Sensitivity by Cooling the Mixer and Antenna

		F at 300°K		SR by cooling Mixer to 70°K		Additional SR by Antenna Temp. of 10°K	
		Ratio	db	Ratio	db	Ratio	db
BB	$F_{\mathrm{if}}=1.3$	3.9	5.9	1.15	0.6	1.41	1.5
NB		3.5	5.4	1.60	2.0	1.84	2.6
BB	$F_{\mathrm{if}}=1.0$	3.0	4.7	1.20	0.8	1.67	2.2
NB		2.75	4.4	1.90	2.8	3.2	5.0

1N263 diode could be improved by cooling and looking at a cold target area, under the assumption of an ideal F_{if} and of an F_{if} of 1.3 which is presently obtainable. Using selected 1N263 diodes the following room temperature values were measured:

$$L_x(BB) = 3.0 \qquad t_x(BB) = 1.0$$
$$L_x(NB) = 2.5 \qquad t_x(NB) = 1.1.$$

For the obtainable broad-band mixer with a 1.3 F_{if} and a 5.9 db room-temperature noise figure, an improvement of 0.6 db comes from cooling the mixer and another improvement of 1.5 db by looking at a background temperature of 10°K. The cumulative effect is a 2.1 db improvement. The equivalent total improvement for the obtainable narrow-band mixer would be 4.6 db. If the F_{if} could be cut to 1.0, the total improvement could be increased to 7.8 db, for a narrow-band mixer.

Experimental Results

The results of noise-figure measurements on an experimental broad-band X-band receiver using germanium crystals are plotted as a function of absolute temperature in Fig. 1. The theoretical curves are computed using the room-temperature noise figure as a basis. The crystals were not rematched at either the high or low temperature which may explain why the discrepancies are all on the high side.

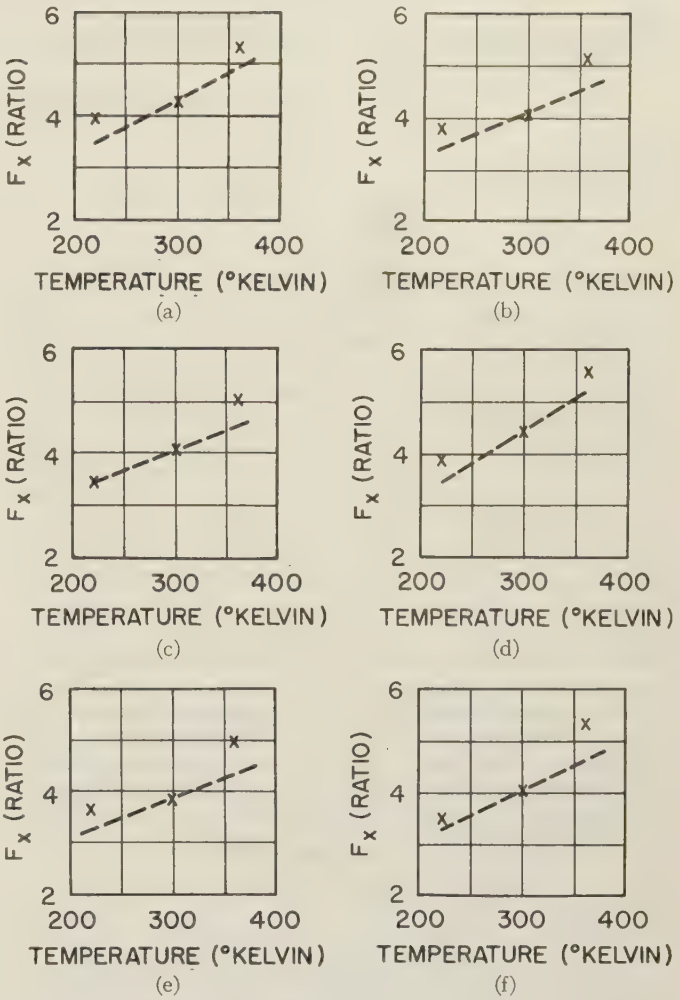

Fig. 1—Noise figure vs temperature. This figure shows the comparison between theoretical and experimental noise figures obtained for six 1N263 mixer crystals. The crystals were matched at room temperature but were not rematched at the other temperatures. Failure to rematch may account for the discrepancies which are all on the high side.

Experiments at liquid-air temperatures are not feasible at the present time because the entire receiver front end would require redesign in order to permit operation at these temperatures. The crystal package would also require redesign with operation at low temperature in mind.

Conclusion

The nature of both (1) and (5) is such that the amount of improvement possible increases greatly as the room-temperature noise figure is reduced. In receivers where sensitivity is of paramount importance the low-noise figures already attainable in narrow-band receivers using low-noise germanium crystals makes further refinement, such as cooling the mixer, practical and worthwhile.

In the present narrow-band mixer the cumulative improvement in sensitivity of cooling the mixer and of looking at a cold background could be as much as 4.6 db,

[2] The resistivity of the germanium would increase slightly and the log slope of the iv characteristic would increase. The net effect on L_x would be small.

Measurement and Control of Microwave Frequencies by Lower Radio Frequencies*

R. C. MACKEY† AND W. D. HERSHBERGER†

Summary—From the fields of nuclear and paramagnetic resonance comes a relation between precession frequency and magnetic field strength for nuclei and unpaired electrons. The relation is such that $f_n = K_n H$ for nuclei and $f_e = K_e H$ for electrons. Thus if the frequency of one oscillator is set for f_n and the frequency of another oscillator is adjusted so that simultaneous nuclear and electronic resonance occurs in the same magnetic field, the frequency ratio of the oscillators is given by the ratio of K_e to K_n. Values of K_e and K_n have been tabulated for many substances and therefore allow frequency comparisons to be made. For example, protons in mineral oil and electrons in hydrogen have a precession frequency ratio of 658.228; hence for an f_e in x band, f_n is about 14 mc when the magnetic field is 3300 Gauss. Changing the value of H causes the frequencies to move up or down the frequency scale but their ratio is always constant. By this method microwave frequencies may be measured with equipment of a much lower frequency range. The precision of measurement is limited by the widths of the nuclear and electronic resonance curves and runs between one part in 10^4 to 10^5. This frequency measurement method may be made the basis of automatic control of microwave frequencies by quartz crystals or very stable lower frequency oscillators. An experimental model of such a system has been constructed and operated.

Introduction

THE most well-known method of accurately measuring, generating, or controlling microwave frequencies today is that of frequency multiplication. This method usually multiplies the frequency of a stable crystal controlled oscillator in several steps, utilizing lumped constant circuits, distributed constant circuits, and finally klystron or crystal multiplier stages depending upon the final microwave power required. Many stages are required to reach the microwave region as small multiplication factors must be used in each stage if sufficient power is to be available for driving a succeeding stage. The result is a complex device composed of many circuits, each of which requires careful tuning and adjustment. The maintenance of a multiplier chain usually requires auxillary test equipment capable of covering the frequency spectrum from the crystal oscillator to final microwave output.

The Nuclear-Electronic method of measurement and control to be described here avoids many of the difficulties of the multiplier chain, but is perhaps no less complex. Its attractiveness lies in the ability to perform a frequency multiplication of some 650 times in one stage. This means that, for example, one crystal controlled oscillator circuit at 14 mc can permit measurement or control of a klystron oscillator at approximately 9300 mc. This is accomplished by comparing the precession frequencies of atomic nuclei and electrons in a magnetic field. The comparison is made visually for measurement purposes and automatically for frequency control purposes.

* Manuscript received by the PGMTT, June 15, 1956. Supported in part by contract N6-onr-27519.

† University of California, Los Angeles, Calif.

Magnetic Resonance

The method of frequency comparison to be described makes use of some of the properties of matter at the subatomic level. In fact, it is the properties of electrons and atomic nuclei that are of interest. The field of study concerned with the interaction of these particles and electromagnetic fields is known as magnetic resonance. When nuclei are studied, the term nuclear magnetic resonance or nuclear magnetism is used; when electron interactions are studied the term paramagnetic or ferromagnetic resonance may be used. Since electrons and nuclei are predominantly found combined to form matter, material substances may be expected to, and indeed do perform magnetic resonance.

Resonance implies a tuning or a matching between an applied frequency and a frequency either actually or potentially present in the substance in question. A violin string, a cymbal, the air column in an organ pipe, an electrical circuit comprising capacity and inductance, all resonate to the frequency which is that of their own natural vibrations. There is a frequency peculiar to electrons and some nuclei which is matched by an applied frequency when magnetic resonance occurs. This natural frequency is not, however, one of vibration, but is a frequency of precession. The mechanism of precession may be recalled by considering the spinning top or gyroscope of Fig. 1. The top has angular momentum along its axis of rotation. Gravity will apply a force to the spinning top through the center of gravity, and the floor the equal and opposite reaction. The result of this torque is a precession about lines of gravitational force.

A similar situation exists for electrons and some nuclei when placed in a magnetic field. Electrons and some nuclei have rotation about an axis through their centers and therefore have angular momentum. Because nuclei are composed of several spinning particles (protons and neutrons) it is possible that the resultant angular momentum may be zero. In fact, only about half of the known nuclei have a rotation of the nucleus as a whole about an axis which passes through its center of gravity. Since electrons and protons are charged particles they are in effect a small current by virtue of their motion. This current may be considered to cause a magnetic field to exist along the axis of rotation. The nucleus or electron is thus said to possess a magnetic moment

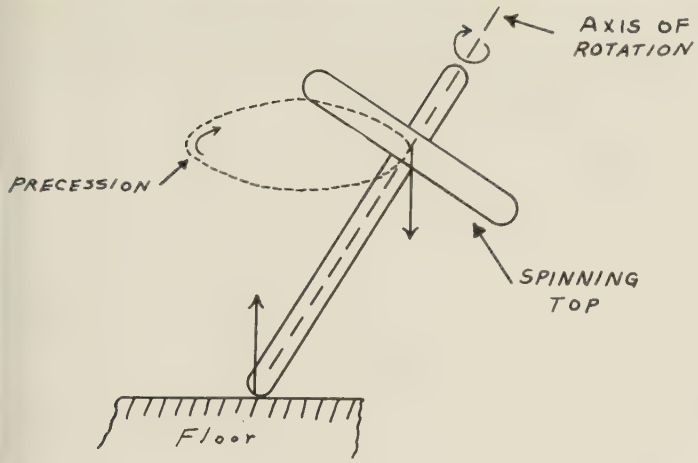

Fig. 1—Top spinning in a gravitational field.

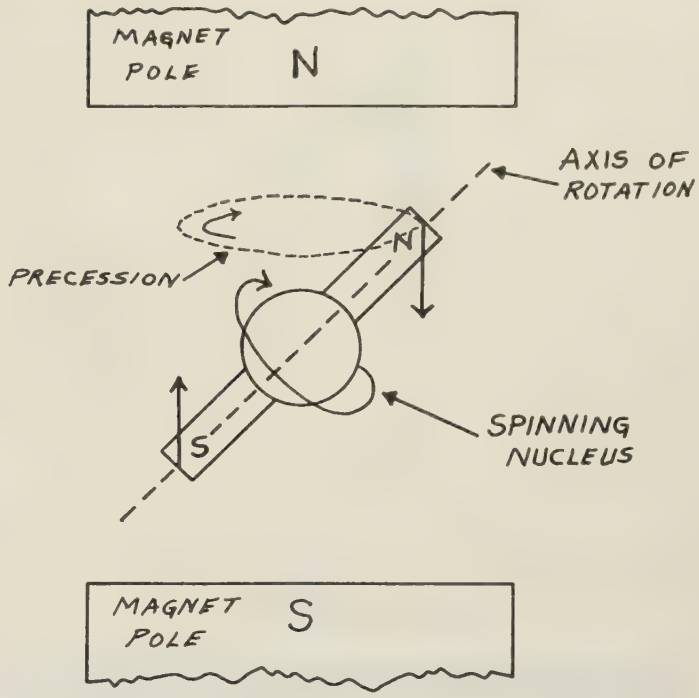

Fig. 2—Nucleus spinning in a magnetic field.

much the same as a small bar magnet. Consider a single nucleus located between the poles of a magnet. The essential features of the situation are illustrated in Fig. 2. Because of its magnetic moment, the spinning nucleus behaves as if a small bar magnet were rigidly attached to it and oriented in the direction of the axis of rotation. The north pole of this equivalent bar magnet will be repelled from the north pole of the magnet by a downward force, and the south pole will be repelled from the south pole of the magnet by an upward force. These two equal and opposite forces result in a torque upon the nucleus. The result is a precession of the axis of the spinning nucleus and the magnetic moment. The rate at which this precession occurs is proportional to the strength of the magnetic field existing at the nucleus. The factor of proportionality is characteristic of the material containing the nuclei as the field at a nucleus is the resultant of the applied external field and the internal field due to neighboring atoms. The same situation exists for an electron placed in a magnetic field except that for the same field strength the precession frequency is greater, resulting in a larger constant of proportionality.

Electrons are the commonest of particles found in the universe, but they display magnetic resonance only in certain special substances. The spin and magnetic moment properties are elusive and not commonly observed because most matter is made up of electrons that pair off two by two in such a way that, as far as external measurements are concerned, their effects are cancelled out. The exceptional cases are those of certain free atoms, ferromagnetic substances, and some paramagnetic substances which usually contain an odd number of electrons. The odd number means that at least one electron must be unpaired and its undiminished magnetic properties may be detected by external measurements.

When a material containing nuclei having a magnetic moment or unpaired electrons is placed in a magnetic field, all of these particles precess about the field lines at the gyromagnetic frequency but in random phase so that the net effect external to the sample is zero. If the precessing particles are, in addition, placed in an alternating magnetic field of the same frequency, they may be made to fall in step with the alternating field. This is the magnetic resonance condition—external applied field of the same frequency as the precessing magnetic moment For maximum effect, the oscillating field must lie in a plane perpendicular to the lines of magnetic force about which the magnetic moments are precessing. Changing the random phase precession to a coherent one takes some energy from the applied alternating magnetic field. This loss of energy in the applied alternating field is a means by which magnetic resonance of the particles is detected.

Nuclear Resonance

The components necessary in a system for detecting nuclear resonance absorption will now be described in general (see Fig. 3). The basic requirement is that of a strong steady magnetic field and a comparatively weak oscillating magnetic field of the proper frequency oriented perpendicular to one another. The steady field may be supplied by either a permanent magnet or an electromagnet. In the experimental setup a surplus 10 cm magnetron magnet was used at a field strength of about 3300 Gauss. The sample consisted of hydrogen nuclei or protons in water which resonate in the above field at about 14 mc. The coil which supplied the alternating rf field to the sample is the tank coil of an oscillator operating at the precession frequency. The amplitude of the oscillations decreases when resonance occurs due to the energy absorption of the sample. To facilitate observation of the resonance condition the steady mag-

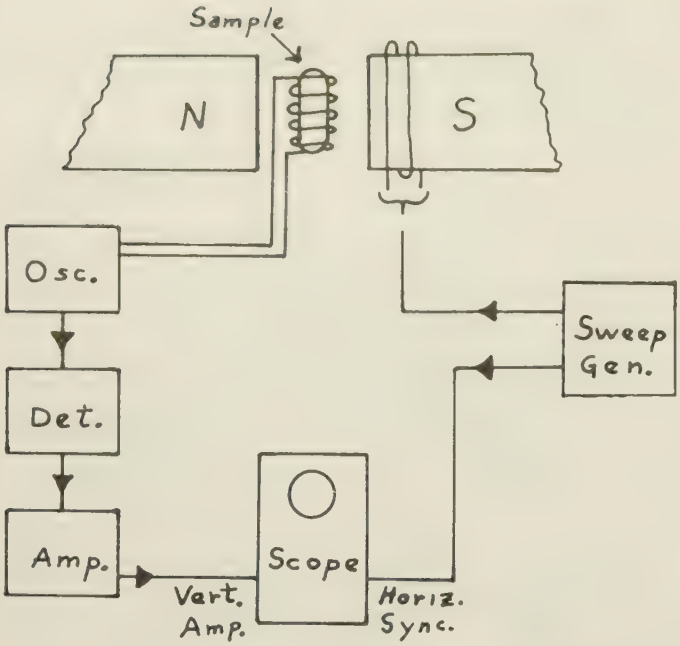

Fig. 3—System for detecting nuclear resonance.

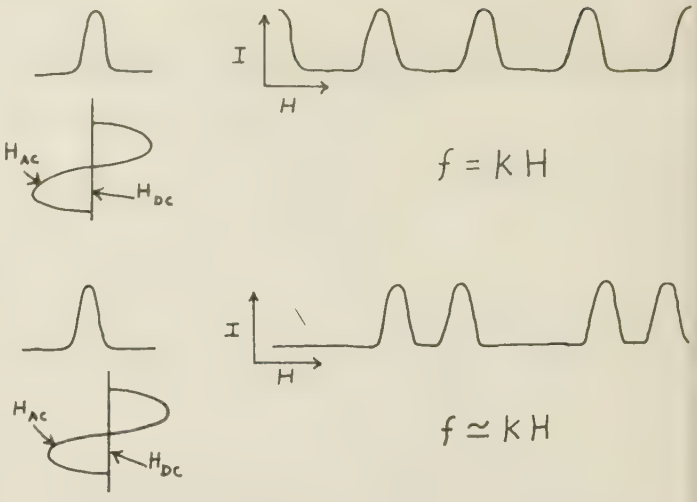

Fig. 4—Oscilloscope pattern of magnetic resonance.

netic field is amplitude modulated by an audio frequency about 15 Gauss from its steady resonance value. This causes the magnetic resonance to be swept through twice each audio cycle. The resonance may be observed visually if the oscillator amplitude is displayed on the vertical axis of an oscilloscope when the horizontal sweep is locked in synchronism with the magnetic field sweep frequency. The resonance condition is easier to observe if the horizontal sweep frequency is just half of the magnet sweep frequency. Fig. 4 shows how the scope pattern arises for H_{DC} exactly at resonance and for H_{DC} slightly above resonance. At resonance the four peaks will be equally spaced.

Electronic Resonance

The magnetic resonance of electrons requires the same perpendicular relation between the steady magnetic field and the oscillating rf field. For the same magnetic field as in the nuclear resonance case (3300 Gauss) the required frequency for electronic resonance is in the X-band microwave region at 9300 mc. This requires that the sample containing unpaired electrons be placed in a microwave cavity resonant to 9300 mc. The general picture is shown in Fig. 5. The sample must be placed in the cavity at a position of maximum rf magnetic field, and the cavity must be oriented so the oscillating microwave magnetic field is perpendicular to the steady magnetic field. If the cavity is of the transmission type, detection of the energy passing through it will give the resonance information. Again this signal is applied to the vertical axis of an oscilloscope with horizontal sweep synchronized to the magnetic sweep frequency. The resonance display is the same as in the nuclear case.

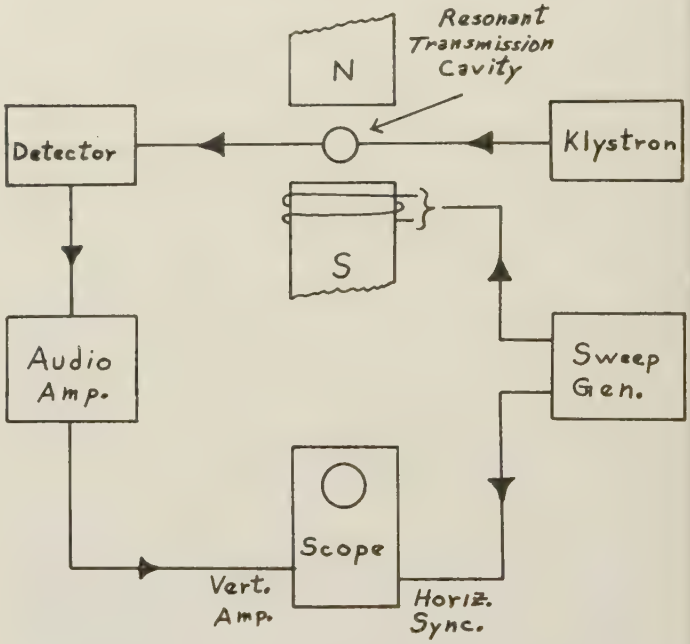

Fig. 5—System for detecting electron resonance.

Field-Frequency Relation

As was previously stated, the precession frequency is proportional to the field existing at the particle in question. This is simply expressed here for our purposes as

$$f = kH. \tag{1}$$

The constant of proportionality is characteristic of the particle, nucleus or electron, and its environment, *i.e.*, fields due to surrounding particles. For protons in water $k \simeq 4.3$ kc/Gauss and for almost free electrons $k \simeq 2.8$ mc/Gauss. Values of k have been tabulated for many nuclei and for electrons in many substances. The fact that k is accurately known for many nuclei has led to the use of nuclear resonance for magnetic field measurement.

Note that (1) allows considerable freedom in the value of frequency or field at resonance. If for some reason the field available is limited, the frequency may be adjusted according to (1) to cause resonance within the range of available field strength. However, the resonance signal increases with increasing field strength and this factor may place a lower limit on H_{DC}. Values of H_{DC} range in practice from a few to ten thousand Gauss. Fields of good homogeneity stronger than 10^4 Gauss are difficult to achieve.

Simultaneous Resonance

Consider now a nuclear and electron resonance taking place in the same magnet. The following relations exist

$$f_n = k_n H \quad \text{nuclear resonance} \tag{2}$$

$$f_e = k_e H \quad \text{electron resonance} \tag{3}$$

$$f_e = \frac{k_e}{k_n} f_n \quad \text{simultaneous resonance.} \tag{4}$$

Eq. (4) states that the ratio of the two oscillator frequencies is the same as the ratio of the two proportionality constants. Thus if simultaneous resonance is observed and one frequency is measured, the other frequency can be computed. Using the aforementioned values of k_e and k_n, (4) becomes

$$f_e = \frac{2.8\,\text{mc/g}}{4.3\,\text{kc/g}} f_n, \text{ or, } f_e \backsimeq 650 f_n. \tag{5}$$

Thus in this one comparison stage frequencies differing by a factor of some 650 times may be measured and compared. Again using the aforementioned values for k_e, k_n, and H, a radio frequency of 14 mc simultaneously resonates with a microwave frequency of 9300 mc. If the magnet field strength is doubled—raised to 6600 Gauss—then 28 mc will resonate with 18.6 kmc. Thus by changing the magnetic field strength a considerable range of frequencies may be covered. Further range extension may be obtained by choosing a ratio of k_e/k_n to be greater or smaller as needed.

The implication here is that frequencies in the microwave range may be measured or controlled by lower radio frequencies by simultaneous nuclear and electronic resonance in the same magnetic field. The accurate measurement of radio frequencies in the 1–50 mc range no longer presents a problem. A block diagram of a system for observing simultaneous resonance is shown in Fig. 6. Fig. 7 shows an oscillograph display of simultaneous resonance of protons in water (upper trace) and electrons in diphenyl-trinitrophenyl-hydrazyl (lower trace). The exact frequency ratio between the two traces is 658.66.

The reverse procedure is used to determine the proportionality constant of a material; the two frequencies are measured and knowing the constant for one material, the unknown constant is computed.

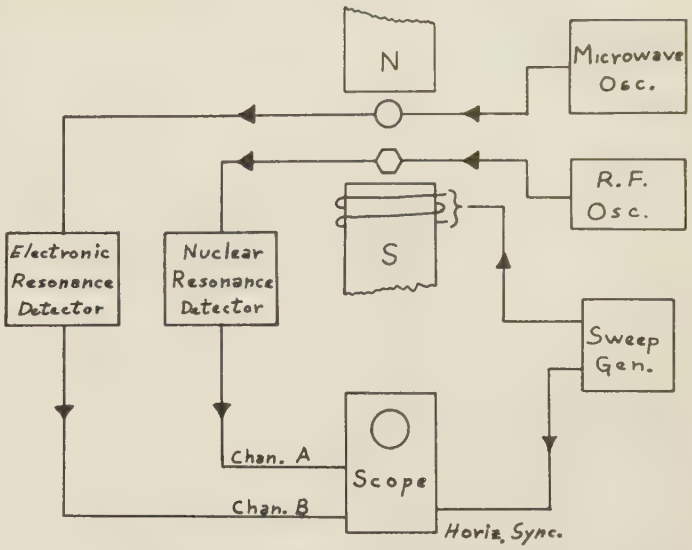

Fig. 6—Setup for observing simultaneous nuclear and electronic resonance.

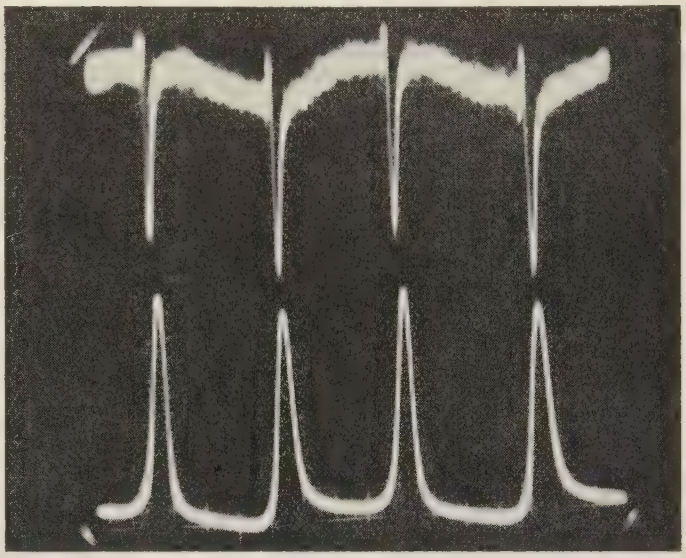

Fig. 7—Oscillographic display of simultaneous resonance. Upper trace—nuclear resonance of protons in water. Lower trace—electronic resonance of hydrazyl.

Automatic Frequency Control

Automatic frequency control of a microwave signal is possible with the simultaneous comparison stage. The general method is as follows (see Fig. 8): a crystal controlled or otherwise very stable oscillator operating at 14 mc causes nuclear resonance of protons in a magnetic field at about 3300 Gauss. A klystron oscillator causes an electron resonance at 9300 mc in the same magnet. The two resonance signals are fed into an electronic circuit which checks simultaneity and produces an output voltage of one sign for microwave frequency too high and a voltage of opposite sign for microwave frequency too low. This error signal is fed to a klystron control electrode, preferably the reflector, so as to cor-

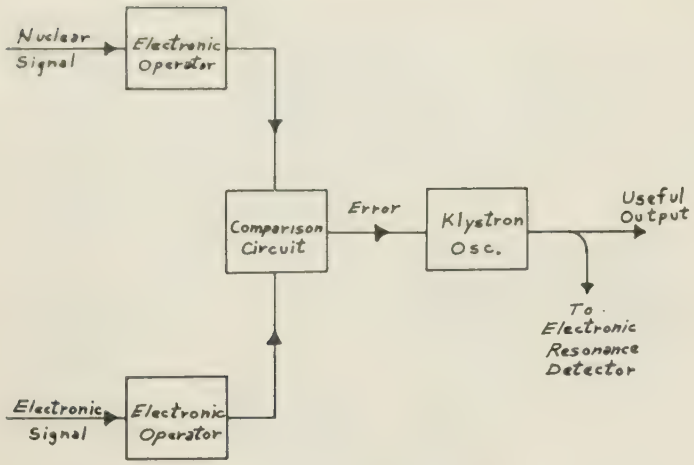

Fig. 8—AFC system using simultaneous resonance.

rect the microwave frequency for simultaneity. A strong electronic resonance signal may be observed with only 100 microwatts of microwave power leaving the major portion of the klystron power for useful output. The blocks marked electronic operator prepare the resonance signals so they may be fed into a phase detector and thus give rise to an error signal.

Limitations

The major limitation on the accuracy of measurement or control is the natural resonance line width of the electron resonance. One of the substances giving the strongest electron resonance is diphenyl-trinitrophenyl-hydrazyl with a line width of 2.7 Gauss. On the assumption that the center one tenth of this curve could be located, an accuracy of 1 part in 10^4 could be obtained. Another factor contributing to inaccuracy is magnetic field homogeneity. All of the sample must see the same field strength else the resonance line will be broadened beyond its natural width. Good field homogeneity may be insured by careful alignment of the pole faces and by using a large ratio of pole diameter to gap distance. Careful shimming of the pole face will also improve field homogeneity. Fields more homogeneous than one part in 10^6 over a square centimeter are difficult to attain because of local inhomogeneities in the magnetic properties of the pole face material.

Narrow electron resonance lines may be obtained from the electrons in an electron beam which is made to interact with the microwave field. Line widths of the order of 0.5 Gauss have been reported by this method giving a frequency ratio accurate to one part in 10^5. The narrowest electron resonance to come to our attention is that of a solution of sodium in ammonia with a half maximum width of 0.08 Gauss. This electron resonance used with a water proton resonance might give rise to control accuracies of one part in 10^6, depending on the signal to noise ratio for the electron resonance and the field homogeneity.

The observed width of the proton resonance in water is usually due to the magnetic field inhomogeneity as it has been possible to obtain in fields of 7000 Gauss proton resonance curves with a line width of 0.001 Gauss. This corresponds to a resolution of one part in 7 million.

Discontinuities in a Rectangular Waveguide Partially Filled with Dielectric*

CARLOS M. ANGULO†

Summary—The modal spectrum for a rectangular waveguide with a dielectric slab at the bottom of the guide is obtained following the Characteristic Green's Function method developed by Marcuvitz. Then a four-terminal network is found as equivalent to the junction of the partially filled waveguide and an empty rectangular waveguide.

An integral equation is written for the electric field at the plane of the junction and variational expressions are derived for the parameters of the four-terminal network connecting the transmission line equivalent to the partially filled waveguide to the transmission line equivalent to the empty guide.

A reasonable guess for the electric field at the discontinuity gives approximate values for the parameters of the four-terminal network. These values agree with experiment.

The parameters of the network are plotted vs frequency and thickness of the slab.

* Manuscript received by PGMTT, June 20, 1956.
† Brown University, Providence, R. I.

Introduction

A CONSIDERABLE AMOUNT of literature has been devoted recently to surface waves. The reader is referred to van Bladel and Higgins[1] for an introduction to the effect of dielectrics in rectangular waveguides and to Barlow and Cullen[2] for surface waves in dielectric slabs. The main purpose of this paper is to obtain a four-terminal network equivalent to the junction of an empty rectangular waveguide and a rectangular waveguide partially filled with dielectric. The Schwinger variational principle combined with the

[1] J. van Bladel and T. J. Higgins, "Cut-off frequency in two-dielectric layered rectangular wave guides," *J. App. Phys.*, vol. 22, p. 329; March, 1951.

[2] H. M. Barlow and A. L. Cullen, "Surface waves," *Proc. IEE*, Part III, vol. 100, p. 329; November, 1953.

modal analysis and synthesis technique developed by Marcuvitz give excellent results in our problem and encouraged the author to extend the method to the open-dielectric slab as reported in another paper.[3] In the methods used in this paper it is important to know the mode spectrum in the partially-filled guide as well as to be sure of the completeness of the mode spectrum. Therefore a systematic method of finding the modes is also given in this paper. This is the Characteristic Green's Function method given by Marcuvitz[4] which yields the modes he gave in his communication to the annual meeting of the Physical Society in 1952.

The geometry of the partially-filled waveguide allows us to separate the characteristic modes into two groups (see Fig. 1):

E_y modes, for which $H_y = 0$ and

H_y modes, for which $E_y = 0$.

Let us assume that the launching of energy in one or both of the waveguides of Fig. 1 is such that only E_y modes are excited. Under these circumstances only E_y modes will be present in both guides. We will not mention this fact again and it will be understood that we refer only to E_y modes throughout this paper.

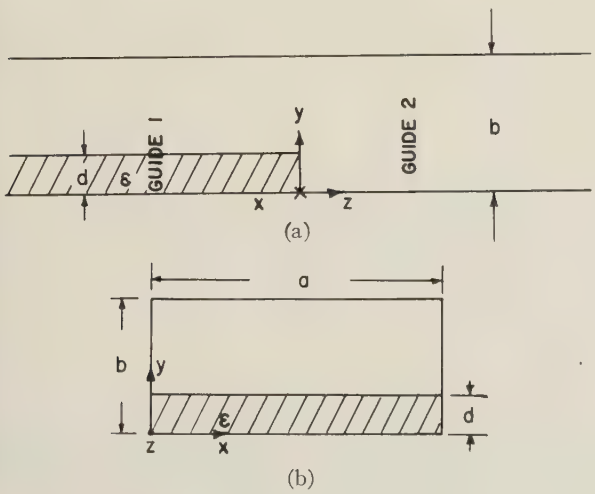

Fig. 1—(a) Longitudinal section of the junction; (b) cross section of waveguide 1.

The Characteristic Modes of the Partially-Filled Guide

The direction of propagation is OZ. We will refer to the projection of each field on the XOY plane as the transverse component and we will represent it with the subscript t.

The transversal component of the fields can be represented as follows:

$$\vec{E}_t(x, y, z) = \sum_{n,m} V_{n,m}(z)\vec{e}_{n,m}(x, y) \tag{1}$$

$$\vec{H}_t(x, y, z) = \sum_{n,m} I_{n,m}(z)\vec{h}_{n,m}(x, y). \tag{2}$$

The set of characteristic E_y modes is a complete orthonormal set. In order to satisfy Maxwell's equations, the following relations should hold:

$$\vec{h}_{n,m}(x, y) = \phi_n(x)\psi_m(y)\vec{x}_0 \tag{3}$$

$$0 = \left(\frac{d^2}{dx^2} + \zeta_n^2\right)\phi_n(x) \tag{4a}$$

$$\phi_n(0) = \phi_n(a) = 0 \tag{4b}$$

$$0 = \left[\epsilon(y)\frac{d}{dy}\frac{1}{\epsilon(y)}\frac{d}{dy} + \eta_m^2\right]\psi_m(y) \tag{5a}$$

$$\left[\frac{d\psi_m}{dy}\right]_{y=0} = \left[\frac{d\psi_m}{dy}\right]_{y=b} = 0 \tag{5b}$$

$$\vec{e}_{n,m} = -\frac{1}{\omega Z_{n,m}\mathcal{K}_{n,m}}\left[\frac{K^2 - \eta_m^2}{\epsilon(y)}\vec{y}_0 + \frac{1}{\epsilon(y)}\frac{\partial^2}{\partial x \partial y}\vec{x}_0\right]\phi_n(x)\psi_m(y) \tag{6}$$

$$\frac{dV_{n,m}(z)}{dz} = -jZ_{n,m}\mathcal{K}_{n,m}I_{n,m}(z) \tag{7a}$$

$$\frac{dI_{n,m}(z)}{dz} = -jY_{n,m}\mathcal{K}_{n,m}V_{n,m}(z) \tag{7b}$$

where $\vec{x}_0$ and $\vec{y}_0$ are the unit vectors in the OX and OY directions; ζ_n, η_m, $\mathcal{K}_{n,m}$ are the propagation wave-number in the OX, OY and OZ directions; $\epsilon(y)$ is the relative permittivity; $K^2 = \omega^2\mu_0\epsilon_0\epsilon(y)$ is the propagation wave-number of a plane wave in the direction perpendicular to the front wave; μ_0 and ϵ_0 are the permeability and permittivity of vacuum. Finally

$$Z_{n,m} = \frac{1}{Y_{n,m}} = \frac{\mathcal{K}_{n,m}}{\omega\epsilon_0} \tag{8}$$

is defined as the characteristic impedance of the waveguide for the n, m mode.

It is clear that for one given mode the propagation wave numbers ζ_n and $\mathcal{K}_{n,m}$ are the same in both media. However, η_m will have different values in the dielectric and in the air.

The solutions of (4) are obviously proportional to

$$\sin\frac{n\pi_x}{a}. \tag{9}$$

The solution of (5) is more complicated because of the variation of $\epsilon(y)$. We proceed to find the function $\psi_m(y)$ by the Characteristic Green's Function method. This method is most advantageous, since it leads directly to the completeness relation

$$\epsilon(y)\delta(y - y') = \sum_m \psi_m(y)\psi_m(y'). \tag{10}$$

For an explanation of the method in general, see Marcuvitz.[4] In our case we have to solve

[3] C. M. Angulo, "Diffraction of surface waves by a semi-infinite dielectric slab," IRE Trans., vol. AP-5, no. 1; January, 1957.
[4] N. Marcuvitz, "Field Representations in Spherically Stratified Regions," N.Y.U. Res. Rep. No. En-29, 1951.

$$\left[\frac{d}{dy}\frac{1}{\epsilon(y)}\frac{d}{dy}+\frac{p(y)}{\epsilon(y)}\right]G(y, y', p) = -\delta(y-y') \quad (11a)$$

$$\left[\frac{dG}{dy}\right]_{y=0} = \left[\frac{dG}{dy}\right]_{y=b} = 0 \quad (11b)$$

where $\delta(y-y')$ is the Dirac's delta function and G is the Characteristic Green's Function. $p(y)$ is equal to the square of the propagation wave number in the OY direction; *i.e.*, $p(y)=\eta^2$.

Since

$$\epsilon(y) = \begin{cases}\epsilon & d<y<b \\ 1 & 0<y<d\end{cases} \quad (12)$$

$p(y)$ will also take two constant values.

For one mode

$$\omega^2\mu_0\epsilon_0 = K_0{}^2 = \zeta_n{}^2+\eta^2{}_{m(\text{air})}+\mathcal{K}^2{}_{n,m} \quad (13a)$$

$$\omega^2\mu_0\epsilon_0\epsilon = K^2 = \zeta_n{}^2+\eta^2{}_{m(\text{diel})}+\mathcal{K}^2{}_{n,m}. \quad (13b)$$

Therefore the two values that $p(y)$ takes are

$$p(y) = \begin{cases}p' = p+K_0{}^2(\epsilon-1) & d<y<b \\ p & 0<y<d.\end{cases} \quad (14)$$

The solution for (11) is

$$G(y, y', p) = -\frac{\left[\cos\sqrt{p'}(y_>-d)+\epsilon\frac{\sqrt{p}}{\sqrt{p'}}\tan\sqrt{p}(b-d)\sin\sqrt{p'}(y_>-d)\right]\frac{\cos\sqrt{p'}y_<}{\cos\sqrt{p'}d}}{\sqrt{p}\tan\sqrt{p}(b-d)+\frac{\sqrt{p'}}{\epsilon}\tan\sqrt{p'}d} \quad \text{for } \begin{matrix}0<y<d\\0<y'<d\end{matrix} \quad (15)$$

and

$$G(y, y', p) = -\frac{\left[\cos\sqrt{p}(y_<-d)-\frac{\sqrt{p'}}{\epsilon\sqrt{p}}\tan\sqrt{p'}d\sin\sqrt{p}(y_<-d)\right]\frac{\cos\sqrt{p}(y_>-b)}{\cos\sqrt{p}(b-d)}}{\sqrt{p}\tan\sqrt{p}(b-d)+\frac{\sqrt{p'}}{\epsilon}\tan\sqrt{p'}d} \quad \text{for } \begin{matrix}d<y<b\\d<y'<b.\end{matrix} \quad (16)$$

The symbol $y_<$ stands for y or y', whichever is smaller, and $y_>$ for whichever is larger.

If we consider now the constant p as a complex variable, we have

$$\epsilon(y)\delta(y-y') = -\frac{1}{2\pi j}\int G(y, y', p)dp. \quad (17)$$

The integration must be done counterclockwise around all the singularities of $G(y, y', p)$ in the p plane.

In the present situation the singularities are only an infinite discrete set of poles along the real axis (Fig. 2).

These poles are the values of p for which

$$\sqrt{p}\tan\sqrt{p}(b-d)+\frac{\sqrt{p'}}{\epsilon}\tan\sqrt{p'}d = 0 \quad (18a)$$

$$p'-p = K_0{}^2(\epsilon-1). \quad (18b)$$

These values of p give the resonances of the system or the characteristic modes of the partially-filled guide.

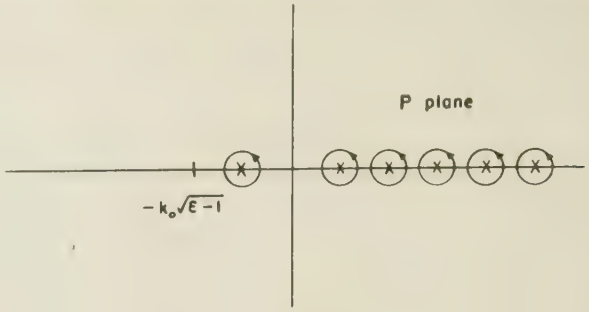

Fig. 2

The normalized mode spectrum in the y direction is then given as minus the summation of all the residues of $G(y, y', p)$. The residues of (15) give the $\psi_m(y)$ for $0<y<d$ and the residues of (16) give the functions $\psi_m(y)$ for $d<y<b$ (Fig. 1).

Eq. (18) has solutions for which

$$K_0 < p < K_0\sqrt{\epsilon}. \quad (19)$$

These modes have sinusoidal variation in the dielectric ($0<y<d$) and hyperbolic variation in the air. They are the surface waves and the number of them that the partially-filled guide can support depends on the frequency and thickness of the slab. The lowest of these surface waves has no cut-off frequency. We will assume in this paper that the frequency is such that the structure has only one surface wave among its characteristic modes. Fig. 3 plots $\eta_{(\text{diel})}$ and $j\eta_{(\text{air})}$ vs K_0d for different values of the relative permittivity ϵ for the only surface wave in our case. Fig. 4 is the plot of $\mathcal{K}$.

Eq. (18) has also solutions for which

$$K_0 < K_0\sqrt{\epsilon} < p. \quad (20)$$

These modes have sinusoidal variation in the OY direction in both regions, dielectric and air. For the wavelength of the excitation in this paper ($\lambda=3.2$ cm) these are nonpropagating modes. Figs. 5 to 8 (p. 72) are the plots for $\eta_{(\text{air})}$ and $\eta_{(\text{diel})}$ for the first five modes of this type and $\epsilon=2.49$.

Finally, the mode functions are obtained as follows:

$$\overrightarrow{h}{}^{\{\text{air}\}}_{\{\text{diel}\}}{}_{n,m}(x, y) = \overrightarrow{x}_0B^{\{\text{air}\}}_{\{\text{diel}\}}{}_{n,m}\sin\frac{n\pi}{a}x\cos\eta^{\{\text{air}\}}_{\{\text{diel}\}}{}_m\begin{Bmatrix}y-b\\ y\end{Bmatrix} \quad (21a)$$

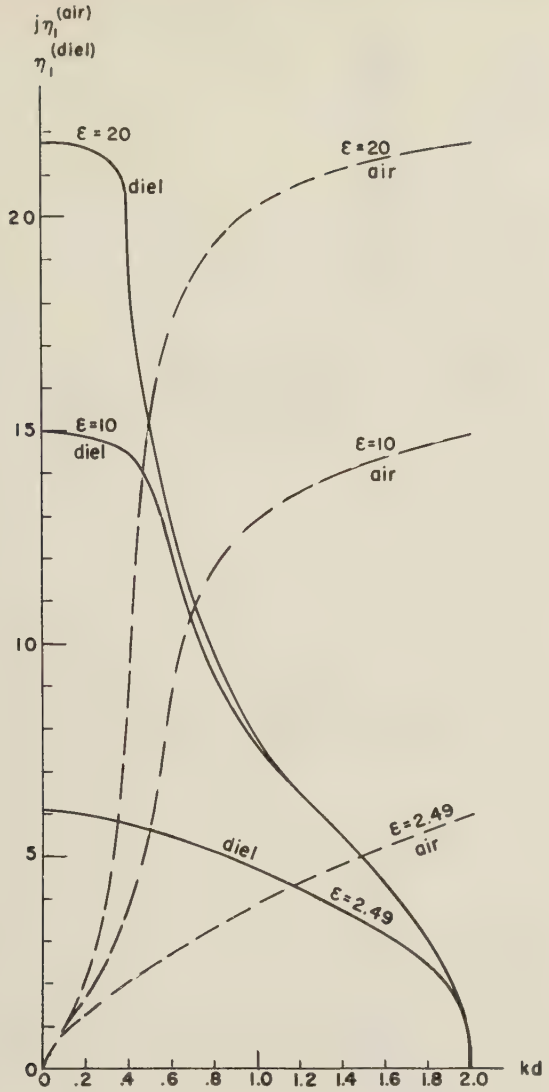

Fig. 3—Propagation wave number in the OY direction for the propagating mode (slow wave).

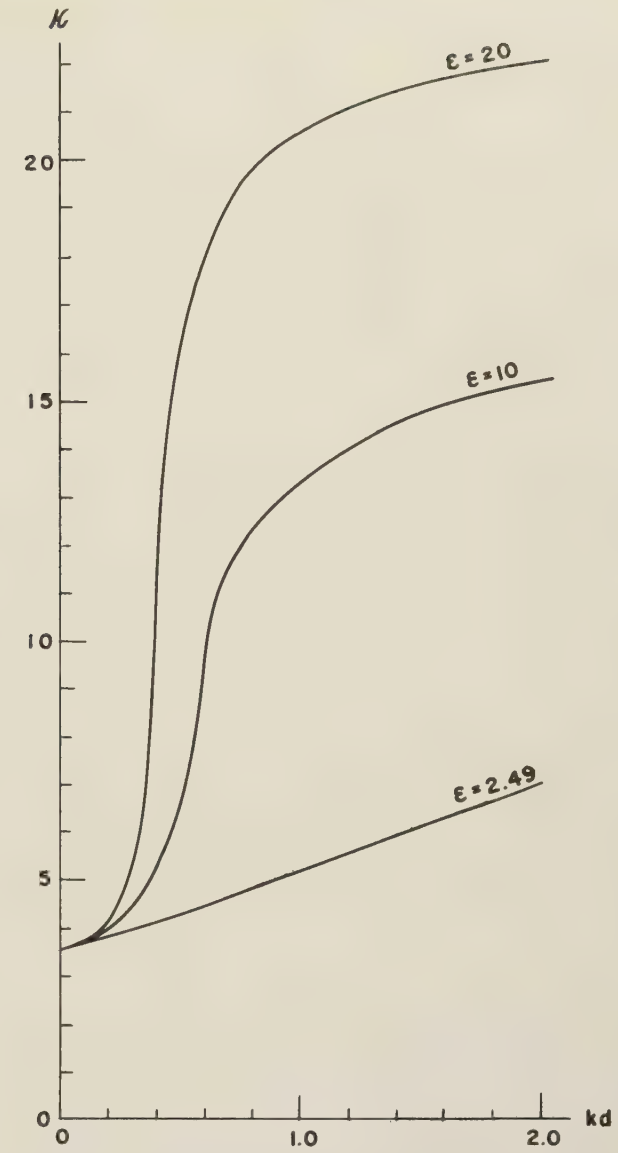

Fig. 4—Propagation wave number in the OZ direction for the propagating mode (slow wave).

$$\vec{e}_{n,m}^{\{\substack{\text{air}\\\text{diel}}\}}(x, y) = \frac{-B_{n,m}^{\{\substack{\text{air}\\\text{diel}}\}}}{\omega Z_{n,m}\mathcal{K}_{n,m}}\left[\frac{\mathcal{K}_{n,m}^2 + \left(\frac{n\pi}{a}\right)^2}{\begin{Bmatrix}1\\ \epsilon\end{Bmatrix}}\vec{y}_0 \sin\frac{n\pi}{a}x\cos\eta_m^{\{\substack{\text{air}\\\text{diel}}\}}\begin{Bmatrix}y-b\\ y\end{Bmatrix} - \frac{\frac{n\pi}{a}\eta_m^{\{\substack{\text{air}\\\text{diel}}\}}}{\begin{Bmatrix}1\\ \epsilon\end{Bmatrix}}\vec{x}_0\cos\frac{n\pi}{a}x\sin\eta_m^{\{\substack{\text{air}\\\text{diel}}\}}\begin{Bmatrix}y-b\\ y\end{Bmatrix}\right]. \quad (21b)$$

The normalization constant is chosen such that

$$\int_0^b dy\int_0^a \vec{z}_0 \times \vec{e}_{n,m}(x, y)\cdot\vec{h}_{n,m}(x, y)dx = 1 \quad (22)$$

and its value is

$$2\sqrt{\frac{\epsilon}{ad}}\,\frac{\mathcal{K}_{n,m}}{\sqrt{\mathcal{K}_{n,m}^2 + \left(\frac{n\pi}{a}\right)^2}}$$

$$B_{n,m}^{(\text{diel})} \doteq \frac{}{\left\{1 + \frac{\sin 2\eta_m^{(\text{diel})}d}{2\eta_m^{(\text{diel})}d} + \frac{\cos^2\eta_m^{(\text{diel})}d}{\cos^2\eta_m^{(\text{air})}(b-d)}\epsilon\frac{b-d}{d}\left[1 + \frac{\sin 2\eta_m^{(\text{air})}(b-d)}{2\eta_m^{(\text{air})}(b-d)}\right]\right\}^{1/2}} \quad (23a)$$

$$B_{n,m}^{(\text{air})} = \frac{\eta_m^{(\text{diel})}}{\eta_m^{(\text{air})}}\quad\frac{\cos\eta_m^{(\text{diel})}d}{\cos\eta_m^{(\text{air})}(b-d)}B_{n,m}^{(\text{diel})}. \quad (23b)$$

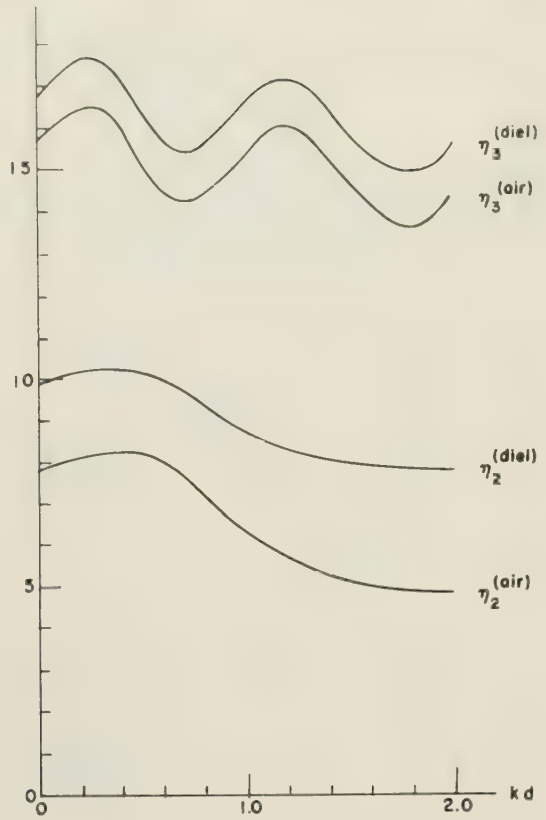

Fig. 5—Propagation wave number in the OY direction for the first two nonpropagating modes.

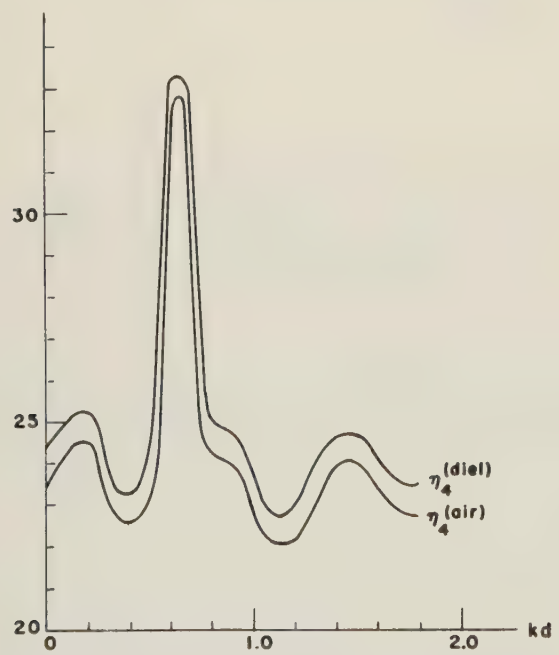

Fig. 6—Propagation wave number in the OY direction for the third nonpropagating mode.

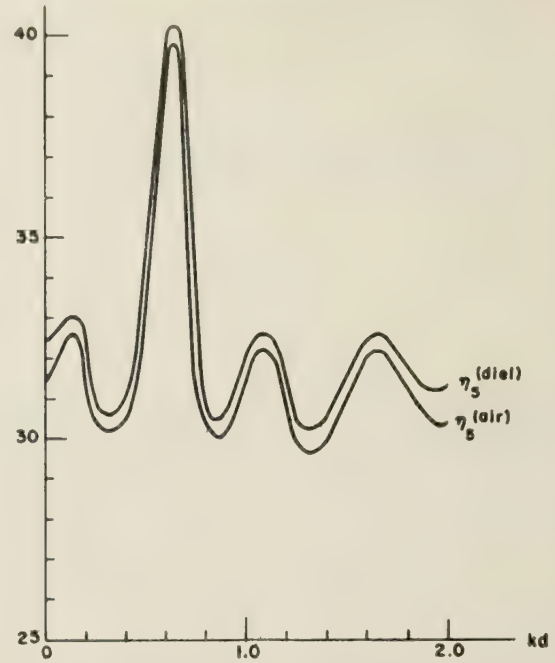

Fig. 7—Propagation wave number in the OY direction for the fourth nonpropagating mode.

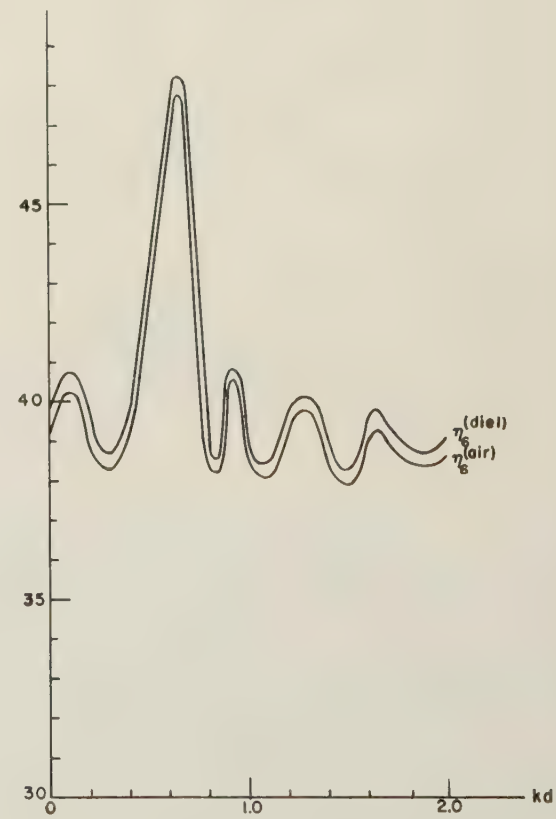

Fig. 8—Propagation wave number in the OY direction for the fifth nonpropagating mode.

The Four-Terminal Network Equivalent to the Discontinuity

In the empty rectangular waveguide we use a representation similar to the one described previously. It is well known and we will not write any details here.

Let us represent the transversal magnetic field $\vec{H}_t$ at the junction of the two guides in terms of the characteristic modes of guide 1 and in terms of those of guide 2. We can equate the two representations, since the transversal magnetic field is continuous at $z=0$. Therefore:

$$I_1^{(1)}(0)\vec{h}_1^{(1)}(x, y) - \sum_n{}' Y_n^{(1)} V_n^{(1)}(0)\vec{h}_n^{(1)}(x, y)$$

$$= -I_1^{(2)}(0)\vec{h}_1^{(2)}(x, y) + \sum_m{}' Y_m^{(2)} V_m^{(2)}(0)\vec{h}_m^{(2)}(x, y) \quad (24)$$

where the upper index refers to waveguide 1 or 2 in Fig. 1, the summations are actually double summations and only for convenience we have indicated the mode with only one subindex. In (24) we have also assumed that each guide propagates only the lowest mode and we have separated these modes from the summations and indicated them with the subindex 1. The prime in the summations indicates that the first or lowest mode is excluded.

In view of the orthogonality properties (22) and of (1) and (2) we can write (24) as follows:

$$I_1^{(1)}(0)\vec{h}_1^{(1)}(x, y) + I_1^{(2)}(0)\vec{h}_1^{(2)}(x, y) = \int_0^b dy' \int_0^a \overleftrightarrow{\mathcal{Y}}(x, y; x', y') \times \vec{z}_0 \cdot \vec{E}_t(x', y')dx'. \quad (25)$$

In (25) we have written the dyadic $\overleftrightarrow{\mathcal{Y}}$ which has the following meaning

$$\overleftrightarrow{\mathcal{Y}}(x, y; x', y') = \sum_n{}' Y_n^{(1)}\vec{h}_n^{(1)}(x, y)\vec{h}_n^{(1)}(x', y') + \sum_m Y_m^{(2)}\vec{h}_m^{(2)}(x, y)\vec{h}_m^{(2)}(x', y'). \quad (26)$$

Eq. (25) is the integral equation for the electric field at the discontinuity. We cannot solve it exactly but we can use the Schwinger variational principle for the unknown electric field.

If the unknown field is written as follows:

$$\vec{E}_t(x, y) = I_1^{(1)}(0)\vec{\mathcal{E}}_1(x, y) + I_1^{(2)}(0)\vec{\mathcal{E}}_2(x, y). \quad (27)$$

One arrives at the following relations

$$V_1^{(1)}(0) = Z_{11}I_1^{(1)}(0) + Z_{12}I_1^{(2)}(0) \quad (28a)$$

$$V_1^{(2)}(0) = Z_{21}I_1^{(1)}(0) + Z_{22}I_1^{(2)}(0) \quad (28b)$$

which link the dominant modes in the two guides replacing the effect of the discontinuity by a four-terminal network. The expressions for the impedances are stationary and can be calculated with a small error without knowing the exact field at $z = 0$.

$$\frac{1}{Z_{22}} = \frac{\int_0^b \int_0^a dxdy\vec{z}_0 \times \vec{\mathcal{E}}_2(x, y) \cdot \int_0^b \int_0^a dx'dy' \overleftrightarrow{\mathcal{Y}}(x, y; x', y') \cdot \vec{z}_0 \times \vec{\mathcal{E}}_2(x', y')}{\left[\int_0^b \int_0^a \vec{z}_0 \times \vec{\mathcal{E}}_2(x, y) \cdot \vec{h}_1^{(2)}(x, x)dxdy\right]^2} \quad (29a)$$

$$\frac{1}{Z_{12}} = \frac{\int_0^b \int_0^a dxdy\vec{z}_0 \times \vec{\mathcal{E}}_2(x, y) \cdot \int_0^b \int_0^a dx'dy' \overleftrightarrow{\mathcal{Y}}(x, y; x', y') \cdot \vec{z}_0 \times \vec{\mathcal{E}}_1(x', y')}{\int_0^b \int_0^a z_0 \times \vec{\mathcal{E}}_2(x, y) \cdot \vec{h}_1^{(1)}(x, y)dxdy \int_0^b \int_0^a \vec{z}_0 \times \vec{\mathcal{E}}_1(x', y') \cdot \vec{h}_1^{(2)}(x', y')dx'dy'} \quad (29b)$$

$$\frac{1}{Z_{11}} = \frac{\int_0^b \int_0^a dxdy\vec{z}_0 \times \vec{\mathcal{E}}_1(x, y) \cdot \int_0^b \int_0^a dx'dy' \overleftrightarrow{\mathcal{Y}}(x, y; x', y') \cdot \vec{z}_0 \times \vec{\mathcal{E}}_1(x', y')}{\left[\int_0^b \int_0^a \vec{z}_0 \times \vec{\mathcal{E}}_1(x, y) \cdot \vec{h}_1^{(2)}(x, y)dxdy\right]^2}. \quad (29c)$$

The above expressions are minima for the exact field. Of all the approximations tried one of them gives a very convergent series and the smallest value for the admittance. Two points measured experimentally agree within 5 per cent with the curve for $1/Z_{22}$ vs K_0d. The approximation consists of taking the field of the dominant mode in the empty waveguide as the field at the discontinuity, *i.e.*:

$$\vec{\mathcal{E}}_1(x, y) = \vec{\mathcal{E}}_2(x, y) = \vec{e}_1^{(2)}(x, y). \quad (30)$$

If one substitutes into (29) and performs the necessary integrations one obtains

$$\frac{Z_{1,0}^{(1)}}{Z_{22}} = \sum_{m=2}^{\infty} M_m^2 \quad (31a)$$

$$\sqrt{\frac{Z_{1,1}^{(1)}Z_{1,0}^{(2)}}{Z_{12}}} = \frac{1}{M_1}\sum_{m=2}^{\infty} M_m^2 \quad (31b)$$

$$\frac{Z_{1,1}^{(1)}}{Z_{11}} = \frac{1}{M_1^2}\sum_{m=2}^{\infty} M_m^2 \quad (31c)$$

where

$$M_m = \frac{1}{\sqrt{1 - \left(\frac{\lambda}{2a}\right)^2}} \sqrt{\frac{a}{2b\mathcal{K}_{1,m}^{(1)}}} \frac{B_{1,m}^{(\text{diel})}}{\eta_m^{(\text{diel})}} \left\{1 - \left[\frac{\eta_m^{(\text{diel})}}{\eta_m^{(\text{air})}}\right]^2 \frac{1}{\epsilon}\right\} \sin \eta_m^{(\text{diel})} d. \quad (32)$$

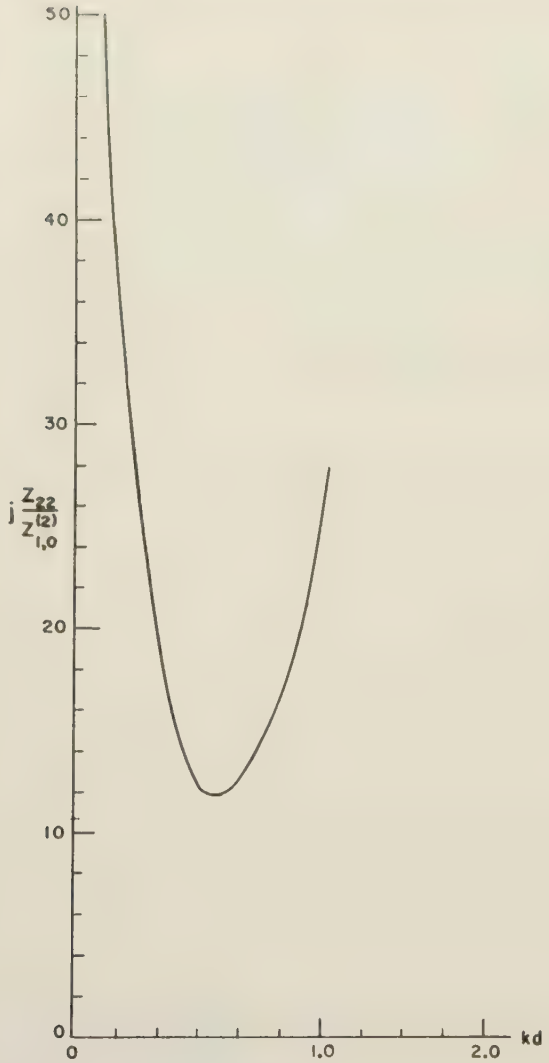

(a)

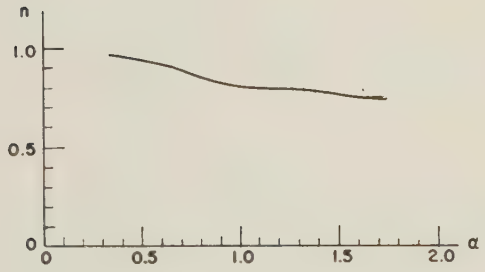

(b)

Fig. 9—(a) Shunt impedance offered by the discontinuity; (b) transformer ratio.

The series converges very rapidly and only five terms are necessary. $B_{1,m(\text{diel})}$ is given in (23a); η_m is plotted in Figs. 5–8 for $m=2$, 3, 4, 5 and in Fig. 3 for $m=1$.

Fig. 9 is a plot of

$$j\frac{Z_{22}}{Z_{1,0}^{(2)}} \text{ and } n=\frac{1}{M_1}\sqrt{\frac{Z_{1,0}^{(2)}}{Z_{1,1}^{(1)}}} \text{ vs } K_0 d$$

for an X-band rectangular waveguide, for $\lambda=3.2$ cm and $\epsilon=2.49$.

Eq. (31) indicates that we can replace the discontinuity by the four-terminal network of Fig. 10, a pure

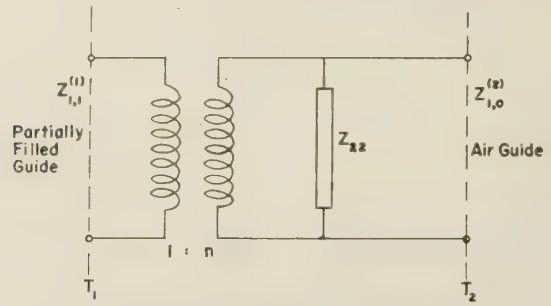

Fig. 10—Circuit equivalent to the discontinuity.

shunt and an ideal transformer with the following transform ratio:

$$n^2=\frac{Z_{22}}{Z_{11}}=\frac{1}{M_1^2}\frac{Z_{1,0}^{(2)}}{Z_{1,1}^{(1)}}.$$

The reference planes are at the plane of the discontinuity $z=0$ in Fig. 1.

Acknowledgment

The main results of this paper were obtained while the author was at the Polytechnic Institute of Brooklyn; the paper was presented as a thesis for the Master's degree in electrical engineering. The guidance of Professor Marcuvitz is gratefully acknowledged. The author wishes also to express his thanks to Professor Ernst Weber for lending the facilities of the Microwave Research Institute for the experimental measurements and computations. Additional computations and the final publication form have been possible through Contract AF 19(604)-1391 between Cambridge Air Force Research Center and Brown University.

Correspondence

Optimum Bandwidth for Waveguide-to-Coaxial Transducers

Mumford[1] has determined a method for optimizing the bandwidth of waveguide-to-coaxial transducers. His equivalent circuit is a coaxial line, of characteristic impedance Z_0, terminated in a resistance R, such that:

$$R = 240\pi \frac{b}{a} \frac{\lambda g}{\lambda} \sin^2 \frac{2\pi l}{\lambda g} \cos^2 \frac{\pi d}{a} \qquad (1)$$

where each of the terms in (1) are as defined by Mumford. After determining the value of l, at center frequency, he adjusts d so that:

$R = Zo$ at center frequency, and achieves bandwidths of the order of 20 per cent for a vswr of 1.10.

Since Zo is invariant with frequency, the vswr varies as the product

$$\frac{\lambda g}{\lambda} \sin^2 \frac{2\pi l}{\lambda}$$

which has a maximum value at center frequency (Fig. 1), for reasons listed here.

$2\pi l/\lambda g$ is usually about 80°, so that $\sin^2 2\pi l/\lambda g$ remains fairly constant for large increases in frequency, but decreases rapidly as frequency is decreased. $\lambda g/\lambda$ increases with decreasing frequency, but at a much slower rate than the decrease of $\sin^2 2\pi l/\lambda g$; $\lambda g/\lambda$ also decreases with increasing frequency.

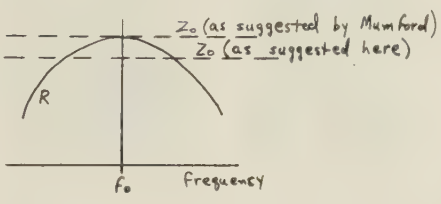

Fig. 1.

From the foregoing, it can readily be seen that even wider bandwidths than those achieved by Mumford are obtainable if R is made greater than Zo at center frequency. In order to determine how much greater than Z_0, R should be, I have found the following equations very useful:

$1.10 = R/Z_0$ at center frequency, f_0, which is obtained by setting vswr at center frequency equal to 1.10, and leads to:

$$\cos^2 \frac{\pi d}{a} = \frac{Z_0}{240\pi b/a} \cdot \frac{1.10}{\left(\frac{\lambda g}{\lambda} \sin^2 \frac{2\pi l}{\lambda g}\right)_{at\, f_0}} \qquad (2)$$

and

$$\left(\frac{R}{Z_0}\right)_{at\, f_0} = \left(\frac{Z_0}{R}\right)_{at\, f_L}$$

where f_L is the low frequency end of the desired band. This yields

$$\cos^2 \frac{\pi d}{a} = \frac{Z_0}{240\pi g/a} \left[\left(\frac{\lambda g}{\lambda} \sin^2 \frac{2\pi l}{\lambda g}\right)_{at\, f_L} \cdot \left(\frac{\lambda g}{\lambda} \sin^2 \frac{2\pi l}{\lambda g}\right)_{at\, f_L}\right]^{-\frac{1}{2}}. \qquad (3)$$

Use of (3) has led me to a design which has a calculated vswr of 1.10 or better over a frequency band in excess of 30 per cent.

David S. Friedman
Westinghouse Electric Corp.
Baltimore 3, Md.

Addendum to Planar Transmission Lines—I*

If it is desired to use fine wires of diameter a instead of these flat strips, an elementary argument shows that the characteristic impedance is given very closely by

$$Z = \frac{120}{Vk} \ln \left(\frac{4h}{\pi a} \tanh \frac{\pi d}{2h}\right).$$

The attenuation is given to sufficient accuracy by the relevant formulas of the paper referred to above.

David Park
Fulbright Lecturer
University of Ceylon
Colombo, Ceylon

[1] W. W. Mumford, "The optimum piston position for wide-band coaxial-to-waveguide transducers," Proc. IRE, vol. 41, p. 256; February, 1953.

* David Park, "Planar transmission lines," vol MTT-3, pp. 8–12; April, 1955.

Contributors

Carlos M. Angulo (S'50–A'52–M'52–SM'56) was born in Pinto (Madrid) Spain, in 1921. He received the degree of Ingeniero de Telecomunicacion from the Escuela Oficial de Telecomunicacion in Madrid, Spain, in 1946; the M.E.E. degree in communication engineering in 1951 and the D.E.E. in electrophysics in 1955, both from the Polytechnic Institute of Brooklyn.

C. M. Angulo

From 1946 to 1948, Dr. Angulo worked as an assistant technical director of Transradio Espanola S.A. in Madrid in radio telegraphy and radio telephony. In 1947 he became a research associate of the Spanish Council of Scientific Research in Madrid and he worked in electroacoustics.

Dr. Angulo joined the Polytechnic Institute of Brooklyn as a research associate in 1949 and as instructor of electrical engineering in 1950; his research during this period was in microwaves. He became an assistant professor of engineering in 1952 and associate professor in 1955, at Brown University, Providence, R. I., where he is at present doing research in antennas and propagation, and teaching.

During the summer of 1956, Dr. Angulo was a visiting research associate professor at the Control Systems Laboratory of the University of Illinois working in propagation problems.

He is a member of Tau Beta Pi, Sigma Xi, and the American Association for the Advancement of Science.

Tsung-Shan Chen (A'48–M'55) was born in Hopei, China, on February 2, 1913. He received the B.S. from Tangshan Chiao-Tung University, China, in 1933, and the M.S. from Purdue University in 1934. He attended M.I.T. and received the S.M. in 1935 and the Sc.D. in 1938, both in electrical engineering.

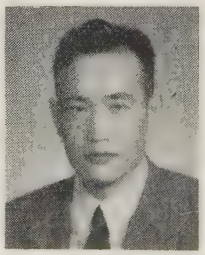

T. S. Chen

He was professor of electrical engineering at the National Central University, China, until 1947. He joined RCA in 1951, and has been working in the Microwave Tube Advanced Development Section of the Tube Division at Harrison, N. J.

Rabindra Ghose (M'53–SM'54) was born in Howrah, India, on September 1, 1925. He graduated in electrical engineering from the College of Engineering and Technology, Bengal, India, 1946. From June, 1946 to February, 1949 he served the College of Engineering and Technology as an instructor of electrical engineering. He received a post-graduate diploma from the Indian Institute of Science in 1948; M.S. in electrical engineering from the University of Washington, Seattle, in 1952; M.A. in mathematics, and Ph.D. in electrical engineering from the University of Illinois in 1954. He was also awarded the professional degree of Electrical Engineer by the University of Illinois in 1956.

R. N. Ghose

Dr. Ghose served the Corps of Signals, India, as a technical officer from 1949 to 1951. During 1951 and 1954 he served the University of Washington and the University of Illinois as a research fellow. From 1954 to 1956 he was a member of the technical staff at RCA. He is now with the Ramo-Wooldridge Corporation in Los Angeles, Calif.

Dr. Ghose is an associate member of the Institute of Electrical Engineers, London, and a member of Sigma Xi, Eta Kappa Nu, and Pi Mu Epsilon.

❖

Richard C. Mackey (S'50–A'53) was born in Los Angeles, Calif., on July 27, 1926. He received the B.S. degree in engineering in 1950 from the University of California, Los Angeles, and the M.S. degree in 1952 from the same institution.

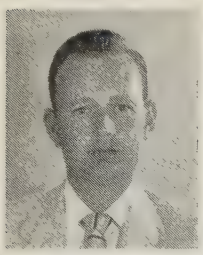

R. C. Mackey

Mr. Mackey has been employed since 1950 at the University of California, Los Angeles, where he is now an assistant engineer and associate in engineering. His work has been in connection with research on the properties of materials at microwave frequencies, including gas spectroscopy and paramagnetic resonance. He has also worked in the fields of electronic instrumentation and microwave frequency standards and stabilization.

Mr. Mackey is a member of Tau Beta Pi and Sigma Xi.

❖

Irving Goldstein (A'48–M'55) was born in Worcester, Mass., on December 19, 1920. He received the B.S. degree in electrical engineering (cum laude) from Worcester Polytechnic Institute in 1947. He served in the Army Signal Corps during World War II.

I. Goldstein

Mr. Goldstein attended Brooklyn Polytechnic Institute in 1943–1944 as a member of ASTP studying electrical engineering. He pursued graduate studies at M.I.T. in 1947–1948, and joined Raytheon Manufacturing Company in 1947 as an electronics engineer. In 1948 he joined the microwave laboratory as a design and development engineer of components used in radar, beacons, countermeasure systems, and relay equipment. In 1954 he transferred to the Missile Systems Division as a senior engineer and then as section head of the microwave components group.

He is a member of the RETMA Subcommittee on Waveguides and Fittings.

❖

W. Delmar Hershberger (A'37–SM'45–F'54) was born on May 10, 1903, in Wellman, Iowa. He received the A.B. degree in 1927 from Goshen College, the A.M. in physics in 1930 from George Washington University, and a Ph.D. in electrical engineering in 1937 from the University of Pennsylvania. From 1927 to 1931 he was employed at the Naval Research Laboratory working on target detection using the pulse-echo ultrasonic method, and from 1931 to 1936 at the Signal Corps Laboratories on target detection employing microwaves. From 1937 to 1949 he was employed by the Radio Corporation of America and worked on the development of a 500 mc pulse-type altimeter and obstacle detection equipment used in 1938.

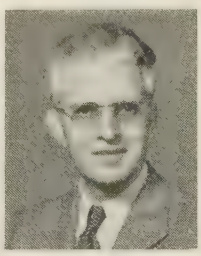

W. Hershberger

During the war Dr. Hershberger worked on various radar system problems and after the war was active in the study of materials using the methods of microwave spectroscopy. Since 1949 he has served as a Professor of Engineering at the University of California, Los Angeles, and he spent the year 1955–1956 at the University of Leiden, Netherlands, as a Fulbright Research Scholar. He served four years as a member of the Board of Directors and in 1954 as Chairman of WESCON.

He is a member of the American Physical Society, the American Association for the Advancement of Science, Sigma Xi, and Tau Beta Pi.

❖

Clarence W. Jones was born in Canton, Me., on August 17, 1918. He received the B.S. degree in electrical engineering from the University of Maine in 1942 and the M.S. degree in electrical engineering from Washington University, St. Louis, Mo., in 1952. He was a member of the staff of the M.I.T. Radiation Laboratory from 1942 through 1945. From 1946 to 1952, he was employed as a radar engineer at the Emerson Electric Mfg. Co., St. Louis, and in 1952 Mr. Jones joined the staff of Lincoln Laboratory where he has been engaged in microwave component and tr tube development.

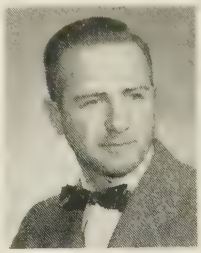

C. W. Jones

Mr. Jones is a member of Tau Beta Pi and Phi Kappa Phi, and an associate member of Sigma Xi.

❖

D. D. King (M'46) was born on August 7, 1919, in Rochester, N. Y. He received the A.B. degree in engineering sciences from Harvard College in 1942 and the Ph.D. degree in physics from Harvard University in 1946. He was a teaching fellow in physics and communication engineering in 1943, serving as a staff member of the pre-radar Officer's Training School at Cruft Laboratory, Harvard University. He was a research associate there during 1945. In 1946 he was appointed research fellow in electronics, and in 1947, assistant professor of applied physics in Harvard.

D. D. King

In 1948, Dr. King was appointed associate professor of physics in the Institute for Cooperative Research of Johns Hopkins University, in 1950, assistant director, and in 1955, director of the Radiation Laboratory. He became vice-president, research, of Electronic Communications, Inc.

Dr. King is a member of Sigma Xi and the American Physical Society.

❖

Alan C. Macpherson was born in Washington, D. C., on December 24, 1920. He received the B.S. degree in physics from the University of Maryland in 1943 and the M.A. degree in physics from George Washington University in 1950. From 1943–1946 he worked on radar, proximity fuse production, and special purpose electronic tubes. In 1947 he joined the NBS where he dealt with precision measurements of power and impedance at microwave frequencies. He is now with the Naval Research Laboratory, Washington, D. C.

A. C. Macpherson

He is a member of Sigma Pi Sigma, RESA, and the American Physical Society.

George C. Messenger (S'51–A'53) was born in Brattleboro Vt., on July 20, 1930. He received the B.S. degree in physics from Worcester Polytechnic Institute in 1951. He has since done graduate work in electrical engineering at the Moore School, University of Pennsylvania.

G. C. Messenger

Mr. Messenger joined Philco Corporation in 1951 where he has been a staff member of the Research Division. He has worked primarily in the field of semiconductor device design, being associated with microwave mixer diodes, and high-frequency transistors.

Mr. Messenger is a member of the American Physical Society.

❖

Herbert G. Pascalar (S'50–A'51) received the Bachelor of Science degree in electrical engineering from Union College in Schenectady, N. Y., and the M.E.E. degree from Syracuse University in 1947 and 1950 respectively.

H. G. Pascalar

From 1951 to 1954 he engaged in radar microwave development at Radio Corporation of America, in Camden, N. J. Since 1954, Mr. Pascalar has been a staff member of Lincoln Laboratory at Massachusetts Institute of Technology.

Henry J. Riblet (M'55) was born July 21, 1913, at Calgary, Canada. He received the Ph.D. from Yale University in 1939 and taught mathematics thereafter for three years at Adelphi College and at Hofstra College. He joined the M.I.T. Radiation Laboratory in 1942 and at the close of the war was in charge of one of the three developmental sections of the Antenna Group. From 1946 to 1948 he headed the vf group at the Submarine Signal Company. He is presently employed by the Microwave Development Laboratories, Inc., of which he was a co-founder.

H. J. Riblet

He is a member of the American Mathematical Society and the American Physical Society.

❖

S. Perry Schlesinger (M'55) was born in New York City on October 9, 1918. He received the B.S. degree from Michigan State in 1941, an M.S.E. from Union College in 1950 and is now working toward a Doctorate at Johns Hopkins University.

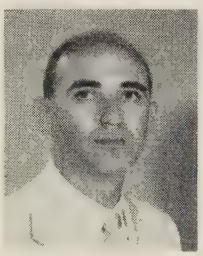

S. P. Schlesinger

In 1946, following war service as a destroyer engineer officer, Mr. Schlesinger joined the General Electric Company, subsequently serving as an assistant professor of electrical engineering on the faculties of Union College and the U. S. Naval Academy. From 1953 through 1956 he was a research associate at the Radiation Laboratory of Johns Hopkins University working on back-scattering studies, millimeter techniques, and, most recently, problems in dielectric image line transmission. He is now on the faculty of electrical engineering at Columbia University.

Mr. Schlesinger is a member of Sigma Xi and Phi Kappa Phi.

❖

Friedrich J. Tischer (SM'55) was born in Plan, Austria, in 1913. He received his preparatory education at the Realgymnasium in Budweis and attended the University of Prague from 1932 to 1938. In 1937 he received the Master's degree in electronics and was awarded the Ph.D. degree in technical sciences from the University of Prague in 1938.

F. J. Tischer

He then joined the Telefunken Laboratories, Berlin, where he worked in the field of television and microwaves. In 1941, he founded the Tischer Physical Research Laboratory at Budweis and Aigen, Austria.

Dr. Tischer joined the staff of the Royal Institute of Technology in Stockholm, Sweden in 1947, where he directed the activities in microwave research. In 1954 he came to the United States and conducted research in microwaves with the Research Division, Ordnance Missile Laboratories, Redstone Arsenal, Army Guided Missile Center until August, 1956, at which time he joined the staff of the department of electrical engineering, Ohio State University, as an associate professor and a research associate in the Antenna Laboratory.

INSTITUTIONAL LISTINGS

The IRE Professional Group on Microwave Theory and Techniques is grateful for the assistance given by the firms listed below, and invites application for Institutional Listing from other firms interested in the Microwave field.

CASCADE RESEARCH CORPORATION, 53 Victory Lane, Los Gatos, Calif.
Res., Dev., & Prod. Microwave Ferrite Devices, Backward Wave Oscillators & Microwave Test Equip.

COLLINS RADIO CO., Cedar Rapids, Iowa
Complete Industrial Microwave, Communication, Navigation and Flight Control Systems

HUGHES AIRCRAFT COMPANY, Culver City, California
Radar Systems, Guided Missiles, Antennas, Radomes, Tubes, Solid State Physics, Computers

MARYLAND ELECTRONIC MANUFACTURING CORPORATION, College Park, Md.
Development and Production of Microwave Antennas and Waveguide Components

(Please see back cover for additional listings.)

INSTITUTIONAL LISTINGS (Continued)

MICROWAVE DEVELOPMENT LABS., INC., 92 Broad St., Babson Park, Mass.
Design, Development & Production of Waveguide Components & Complete RF Assemblies

NATIONAL INSTRUMENT CO., INC., 23 E. 26 St., New York, N. Y.
Wide-Band Microwave Equipment, Simulated Flight Instruments, Lobe Switches, Custom Built Precision Apparatus

RAYTHEON MANUFACTURING CO., 148 California St., Newton, Mass.
Microwave Communications Systems, Radar, Missiles, Cooking Equipment, Tubes & Components

WEINSCHEL ENGINEERING CO. INC., Kensington, Md.
Attenuation Standards, Coaxial Attenuators and Insertion Loss Test Sets

WHEELER LABORATORIES, INC., 122 Cutter Mill Road, Great Neck, N. Y.
Consulting Services, Research & Development, Microwave Antennas & Waveguide Components

The charge for an Institutional Listing is $50.00 per issue or $140.00 for four consecutive issues. Applications for Institutional Listings and checks (made out to the Institute of Radio Engineers) should be sent to Mr. L. G. Cumming, Technical Secretary, Institute of Radio Engineers, 1 East 79th Street, New York 21, N. Y.